DEPARTMENT OF ELECTRICAL ENGINEERING

INVESTIGATION OF SOLID - STATE COOLER BASED ON ELECTROCALORIC EFFECT

Examiners: Professor, D.Sc. Erkki Lähderanta,
Professor, D.Sc. Sergey Karmanenko and
Supervisors: Professor, D.Sc. Erkki Lähderanta,
Professor, D.Sc. Sergey Karmanenko.

Lappeenranta 22.05.2007

Elizaveta Vereshchagina
Karankokatu 4 C3
53810 Lappeenranta
Phone: +358440252632

ABSTRACT

Author: Elizaveta Vereshchagina

Title: **Investigation of solid-state cooler based on electrocaloric effect**

Department: Electrical Engineering

Year: 2007

Place: Lappeenranta

Thesis for the Degree of Master of Science in Technology: 130 pages, 118 figures, 8 tables.

Examiners: Professor, D.Sc. Erkki Lähderanta,

Professor, D.Sc. Sergey Karmanenko.

Keywords: Electrocaloric effect, ferroelectric, cooling.

Electrocaloric cooling based on ability of material to change temperature by applying an electric field under adiabatic conditions is relatively new and challenging direction of ferroelectrics research. In this work we report about analytical, simulation and experimental data for $BaSrTiO_3$ thin film and bulk ceramic samples. Detailed discussion of a theoretical base of the electrocaloric effect is included. Demonstrated experimental and computational results exemplify rational approach to a problem of solid-state cooler construction.

ACKNOWLEDGEMENTS

This master's thesis was carried out in the laboratory of Physics, Lappeenranta University of Technology in cooperation with laboratory of Physical Electronics, Saint-Petersburg State Electrotechnical University "LETI".

I wish to express my gratitude to Professor E. Lähderanta and Professor S. Karmanenko for their guidance and support.

I thank Julia Vauterin kindly for her instructions during my studies at LUT.

My warm thanks to A. Eskow for his inestimable help during Master's Thesis preparation.

I also wish to express my deepest gratitude and respect to whole professor's stuff of Microelectronics Department of the Saint-Petersburg State Electrotechnical University "LETI" for providing high standard of knowledge, encouraging and supporting me during my studies.

Especially I wish to thank my mum.

Lappeenranta, May 2007

Elizaveta Vereshchagina.

TABLE OF CONTENTS

SYMBOLS

Roman letters

A	dielectric susceptibility
d	piezoelectric coefficient
f	frequency
F	free energy
E	electric field
I	current
K	elastic constant
m	mass
n	tunability
p	dipole moment
P	polarization
q	charge
Q	heat
r	radius-vector
s	strain
S	entropy
T	temperature
U	potential energy

Greek letters

α, β, γ	angles
π	Peltier coefficient
ρ	specific resistance
Ω	Ohm
ε	permittivity
σ	stress
ρ	density
λ	thermal conductivity

1 INTRODUCTION

1.1 Electrocaloric effect

From its early beginnings in the sixteenth century, the developements of low temperature technique has influenced the life of civilization more and more. Cryogenics and refrigerating techniques have achieved a great advance for human benefit. Without modern intellectual outcomes in this area would be impossible to have, for example, air-conditioning and products freezers. Nowdays, a further developement is possible through the investigation of the heat effects in the solid state. One of the exciting phenomenons, along with the magnetocaloric effect[1] in solid state, is electrocaloric cooling. An attempt to undestand its nature is one of the most challenging and unsolved mystery in ferroelectrics[2].

Recently there has been growing interest in study of the electrocaloric effect. It is represented as a reversible temperature change in a dielectric under adiabatic conditions when the applied electric field is removed from it [1]. It is belived that solid-state heat pump on its basis can provide up to 60% efficiency in Carno equivalent [2]. This makes electrocaloric cooling method competing with usual refrigerating tehniques such megnetocaloric system or pulse tube discussed later. Many scientists are excited about the electrocaloric effect because of its simplicity and curious application possibilities. Electrocaloric effect can be observed in ferroelectric materials that have high values of permittivity and show strong temperature dependence of permittivity derivative [3]. Therefore, production of materials that meet these requirements is one of the most challenging directions in this study. Present research provides theoretical description of the electrocaloric cooling, simulation and experimental results for thin film and bulk ceramic capacitors. Experimental data analysis allows us to suggest that solid-state refrigerating system based on electrocaloric transformation would be advantagable in many ways.

---

[1] Magnetocaloric effect is one of the methods in low temperature technique based on processes of magnetization and demagnetization in material.

[2] Ferroelectric is a material that changes its intrinsic polarization by applied electric field greater than coercitive field. Phase-transition temperature is a particular property of this material [4].

Thermodynanically effective system can achieve higher cooling efficiency. This is not the only requirement; cooling system should be also compatible with other electronic equipment.

1.2 Motivation for study

This research area was made a centre of attention due to opening and promising opportunity to construct electrocaloric based solid-state refrigerators. Long-standing energy and ecology issues have recently forced many investigators to search for an overall and effective application of cryogenics and refrigerating techniques achievements. This relatively new type of "refregeration units" based on the electrocaloric effect has several irrefutable advantages in comparison with the nowdays widely distributed domestic and industrial refrigerators where ozone layer depleting gases are still in use. Moreover, of the great theoretical and practical importance is developement of the refrigerator efficiency in combination with clean working materials causing no damage to environment. During last decades several American companies, working in the area of domestic electric and refrigerating systems, have announced about projects financing in refrigeration and cryogenic area. As a result was expected increase in efficiency by 30 - 50% and practically eliminating use of freones[3]. [5], [6] Freones have been replacing all other substacies used in cryogenics as refrigerating medium during many years. Nevertheless this situation has changed and nowdays people pay more attantion to natural working substancies, for instance to ammonia, water, air or carbon dioxide. Ammonia doesn't contribute to global warming and provides high cold production efficiency as a refrigerant. However, the alternative of the electrocaloric cooling affects not only the problem of the greenhouse gases. The second key point is a significant decrease in energy consumption by the new type of freezers representing a well promising commercial benefit. A careful analysis of possible profits by the Electric Power Research Institute has shown that "reducing the electrical consumption of the Nation's refrigerators and freezers by just 4.2% would save an estimated 479 million kWh that is equivalent of average

[3] Clorofluorocarbons group is primarily responsible for ozone layer depletion due to their general application as refrigerants. Common organic compounds are dichlorodifluoromethane (CFC-12) and tetrafluoroethan (HFC-134a). Rate of these harmful chemicals in atmosphere has grown dramatically because of human activity. [7]

base-level power plant". It is generally believed that the reachable increase in efficiency by 50% would equal in impact to 12 new plants. [8]

One of the exciting applications of the electrocaloric solid-state freezers that expected to get widely adopted is a computer chips cooling since the higher current density requirements for the integrated circuits and hence higher working load on cooling unit have to be met. Using currently applied "fan-based cooling solutions" it is not possible. [2] There are many other possibilities to cool down hardware, e.g. air-cooling, water cooling, nitrogen systems and new method as liquid metal cooling loops [9]. Furthermore, should be mentioned that electric fields are much easier and cheeper to obtain compared with the magnetic fields, serving as a basis for the magnetocaloric effect applications [6]. During last few centuries number of people living on Earth has grown many times over. The steady population growth imposes great demands on energy [10]. Products for people must be either refrigerated or transportated to long distancies. This leads to more intensive application of cost-effective low temperature technique in our life. All inefficient methods of energy production will be eliminated because of diminishing of our resources and miltiplication of our wastes. Application of new heat transformation systems that use natural sources of cold as well as secondary sources is very important. All mentioned reasons for investigation in this direction are interdependent and are all global in nature. Electrocaloric effect in this situation will have its own advantage-ground.

1.3 History overview

Challenging opportunities have appeared with the discovery of new ceramic materials and their combinations for cheep multilayer capacitors production. Following use of them for cooling systems construction is very attractive [5]. Thus, investigation of electrocaloric materials, ferroelectrics, has become a one of the central issues in the last decades after a long period indicating lack of interest to this topic. In 1930 P. P. Kobeko and I. V. Kurchatov carried out the first experimentally based examination of the electrocaloric effect in Rochelle salt. However, the results obtained by scientists didn't show the large effect, as a matter of fact, first scientific dicsussions of potential cooling solutions were possible only at the latest 1950-s. The second part of the twetieth century

has brought a number of technical breakthroughs in material science. 1956 was marked with the discovery of strontium titanate electrocaloric properties in the temparature range of 5 – 15 K by H. Granicher. Five years later the electrocaloric effect was studied at the 17.5 K in this material (E. Hegenbarth) [5]. Since that time the relationship between the applied electric field and tamperature changing within material has been investigated by many researchers. G. G. Wiseman and J. K. Kuebler continued the investigation of the electrocaloric model based on the measurement in the Rochelle salt crystals (1963) [11], which symmetry and structure features were well examined by that time [12]. At the middle of 1960-s the group of scientists of the University of California (I. Shepherd, G. Feher) obtained the temperature decrease from 1.3 K to 0.36 K for the KCl with OH^- centers [13]. In 1965 an electrocaloric effect was observed in KCl dopped with LiCl by G.Lombardo and R.O. Pohl. In 1968 R.O.Pohl with V.L.Taylor and their colleagues demonstrated the temperature change above 0.3 K for the KCl: Li and above 0.07 K for the RbCl: CN [14]. W. N. Lawless investigated the specific heat and electrocaloric properties of $KTaO_3$ (1976) [15]. That's not even the full list of research projects. The electrocaloric effect has become a relatively frequent topic for analysis of ferroelectric behaviour in 1950 - 1980s because more and more scientists have commonly held view that this study would give completely new and profitable industrial applications. Some individuals seem to believe in the electric energy conversion possibilities [16]. But their hopes didn't justify owing to the insignificance of the obtained results and unfortunatly all the scientific achievements have found few realization on practice.

The theoretical description of the phenomenon has been extensively studied; however, no clear and fully reliable results were shown at that time; partly because of the presented difficulties in mathematical provement ab initio, but also because of lack of quantum mechanical conception of the effect [2].

1.4 Current research activity

After 2000 interest in electrocaloric materials has quickened again. A. Mischenko working in close collaboration with other scientists of the Cambridge University (United Kingdom) declared about the "giant electrocaloric effect" (0.48 $K \cdot V^{-1}$) obtained in 300 nm sol-gel $PbZr_{0.95}Ti_{0.05}O_3$ films [2]. L. Shaobo and L.Yanqiu worked with 100 μm

PMN/PT85[4] ceramic material for the ferroelectrics MEMS[5] microcoolers application. The obtained electrocaloric effect (1.71 K) was maximal at 18 ˚C and under 16 kV/cm depolarizing mode [17]. The research group of French scientists have provided a description of the electrocaloric measurements in $0.75(PbMg_{1/3}Nb_{2/3}O_3) - 0.25(PbTiO_3)$ ceramics. They have observed heat in material up to 0.15 J g^{-1} with an external field of 1.35 kVmm^{-1} [19]. During last ten years appeared new proposals in electrocaloric theory made by researchers from Czech Republic (Marvan), Latvia (Shebanovs), United Kingdom (Mischenko) and China (Shaobo). Also in the State Electrotechnical University "LETI" in Saint-Petersburg (Russia) one of the scientific groups works successfully on the developement of the electrocaloric model description and the solid-state refrigerators conception. Thus, the detailed analysis of already existing results in the area of the electrocaloric materials study indicates a gap in logical proceeding of theoretical grounds of the electrocaloric effect as well as problems with its experimental realization. Typical investigations are directed to the study of polarization vs. temperature measurements upon variable applied fields, that it is not easy to arrange; moreover, it finds difficulties because of the lack of the accurate electrocaloric effect concepts.

The purpose of this experimental and analytical study is the investigation of the solid-state heat transforming lines based on the electrocaloric effect. The final objective is to complete the picture of the electrocaloric parameters in ferroelectrics and to prove their interconnections with the material properties and external conditions by carrying out the detailed analysis of the theoretical foundations, computer simulation and experimental results. Consequently, we prove an agreement between experimental data and theoretical model. Recent developments of solid-state refrigerators have attracted public attention throughout the world. There are many grants sponsoring nanocoolers construction projects, each year indicates increased number of publications about new cooling technologies in scientific journals.

---

[4] PMN/PT is synthesized ceramic material with general chemical formula (1-x)PMN-xPT composed of $Pb(Mn_{1/3}Nb_{2/3})O_3$ and TiO_3 metal oxide.

[5] MEMS refers to Micro-Electro-Mechanical Systems. Advance in microfabrication tehnology provides opportunity to place mechanical elements, sensors, actuators and other electronics components on one silicon substrate [18].

The only questions remaining concern the ferroelectric materials with appropriate properties and thermal switches to which production we must pay a lot of attention. The international cooperation in low-temperature technique must be sufficiently effective to overcome existing problems on the way to new cooling technology.

2 GENERAL INFORMATION ABOUT REFRIGERATOR

2.1 Thermodynamics of refrigeration

Before starting to analyze basic operational principles of refrigerator it is needed to mention laws that are in its scientific basis. The laws of thermodynamics decsribe transfer nature of heat and work. In our considerations it is preferable to make an overview for first and second laws of thermodynamics. Irreversibility is a distinct property of all thermodynamic processes in nature. It means that thermodynamic processes proceed only in one certain direction. For instance, heat flow from a hot body to cold one is irreversible. To identify direction of thermodynamic transformation we use the second law of thermodynamics. [20] In 1824 S.Carno postulated the second law of thermodynamics as "the entropy of an isolated system not in equilibrium will tend to increase over time, approaching a maximum value at equilibrium" [6], [21]:

$$dS/dt \geq 0\,, \tag{2.1}$$

where S is entropy and t is time. The first law of thermodynamics sounds as "The increase in the internal energy of a thermodynamic system is equal to the amount of heat energy added to the system minus the work done by the system on the surroundings" [6], [21]:

$$dU = \delta Q - \delta W\,. \tag{2.2}$$

Here dU is the infinitesimal increase in the internal energy of the system, δQ is the infinitesimal amount of heat added to the system and δW is the infinitesimal amount of work done by the system. [21] Two laws of thermodynamics help us to identify and better understand process of heat conversation in working medium of a refrigerating unit. There is preferred thermodynamic direction for every system. However, there are possible some idealized processes in system considered to be reversible. System at that is

always in thermodynamic equilibrium. If conditions are slightly changed than occured these reversible changes. Thus, reversible processes happen if the system is in equilibrum. This equilibrium state is not fully true because at that no change in state is possible. We consider an idealized case that can never take place in reality. If temperature gradients and pressure differencies are kept very small, than system is indeed very close to equilibrium and processes can be assumed as reversible. Therefore, it is scietfically preferred to call it a quasi-equilibrium process. Direction of process and disorder of resulting state are connected as well. There are two main classes of divices using the second law of thermodynamics as basis, heat engines and refrigerators. Heat engine converts heat into work. [20] The diagram below (fig. 2.1) shows heat engine device that allows getting useful work from two work bodies under different temperatures.

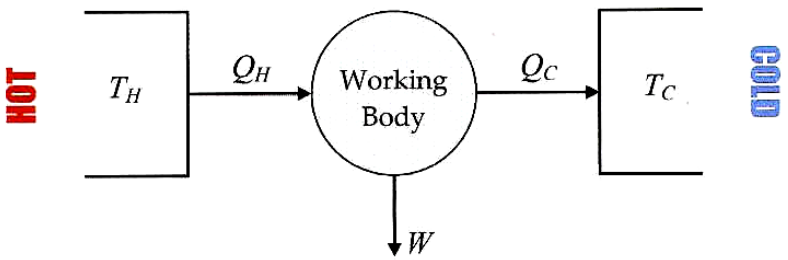

Figure 2.1 Heat engine diagram, where Q_H and Q_C are heat transferred from hot object to cold, T_H and T_C are temperatures of hot and cold objects, W is work obtained from system [22].

The heat transfers from a cooled body to a cooled environment that is usually water or air. Refrigerator transports heat from colder to hotter bodies. [20] We can consider engine and refrigerator operation very similar in its natur. Refrigeration is a thermodynamic process of heat transfer from a closed space or from a certain material elsewhere to reduce the temperature of this closed space or material and then to maintain that lower temperature.[23] There is alternative formulation of the second law. We know that heat can flow spontaneously from hotter to colder bodies and never reverse. In fact refrigerator does the reverse; it takes heat from colder body and transfers it to hotter one. Thus, there is so called “refrigerator” statement: “It is impossible for any pr (2.3) ave as its sole result the transfer of heat from a cooler to a hotter body”. Let us now examine energy flow in refrigerator. Refrigeration machines are used for obtaining temperatures from 10˚ to -150˚ C. The area of lower temperatures refers to cryogenic technology. Generally, refrigeration machine works as a heat pump. It is necessary to satisfy the

second law of thermodynamics (fundamental law of entropy increase) and therefore the certain amount of energy has to be carried by a force. [6], [23] Cooled environment has higher temperature than the cooled body. Considering first law of thermodynamics for cyclic process we can write:

$$Q_H + Q_C - W = 0 \text{, or } -Q_H = Q_C - W$$

Q_H and W are negative, therefore

$$|Q_H| = Q_C + |W| . \tag{2.4}$$

It is important to note that

$$|Q_H| \succ Q_C . \tag{2.5}$$

Or in other formulation, heat that leaves working medium is always greater than heat taken from cooling object. An absolute value relation looks finally as:

$$|Q_H| = |Q_C| + W . \tag{2.6}$$

Now we can define what refrigeration cycle is assumed to be better. The greater $|Q_C|$ heat rejected from refrigeration and the least expenditure of mechanical work $|W|$ the better refrigerator we have. If ratio $|Q_C| / |W|$ is high then refrigerator is good. Coefficient of performance of a refrigerator:

$$K = \frac{|Q_C|}{|W|} = \frac{|Q_C|}{|Q_H| - |Q_C|} . \tag{2.7}$$

According to the second law, heat transformer can not have 100% efficiency. To analyse how great the efficiency of our heat transformer we can use Carno cycle on fig.2.2. Sadi Carno (1796 - 1832), French engineer in 1824 developed an idealized cycle with maximum possible efficiency, Carno cycle. [20]

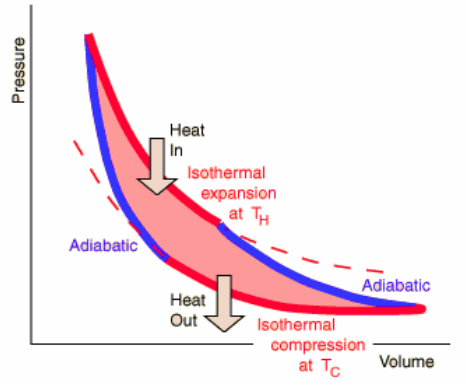

Figure 2.2 The Carno cycle [24].

The Carno cycle consists of two reversible isotherms and two reversible adiabats. Later we will analyse different type of refrigerating systems and compare their efficiencies in terms of Carno cycle. There is Carnot theorem telling that Carnot efficiency coefficient does not depend on nature of working substance. It is the only function of absolute temperatures of heater and cooler. A proof of this theorem can be derived from second law of thermodynamics. [25]

2.2 Refrigerating machines

Refrigerating equipment is a system of interrelated technical facilities, refrigerating units, assemblies, pipe lines and special construction sets meant for creation, distribution and use of a cold. It is difficult to overestimate the importance of the cooling techniques in our everyday life. For instance it affects production and storying processes of food, helps in such vitally important fields as pharmacy, medicine and biology, and makes a lot of use in electronics and nuclear industry. And of course no one can imagine a normal life without strorying of perishable goods in refrigerator. According to the sheme on fig. 2.3 the refrigerating equipment can be subdivided into industrial, commercial and domestic. Industrial refrigerating equipment usually involves refrigerating systems or (and) cooling plants with a cooling effect more than 15 kW. A need of the supermarkets and storehouses in freezing, storying and transportating of products caused the use of the refrigeration equipment for commercial purposes. The third area of application is of our every day use is domestic refrigerators. Refrigeration machine is a category of heat engine that absorbs the heat from low temperature bodies and further transmits it to higher temperature bodies. [26] From the position of thermodynamics machine realizes the heat transportation from low temperature area to higher one in an effort to cool down [23].

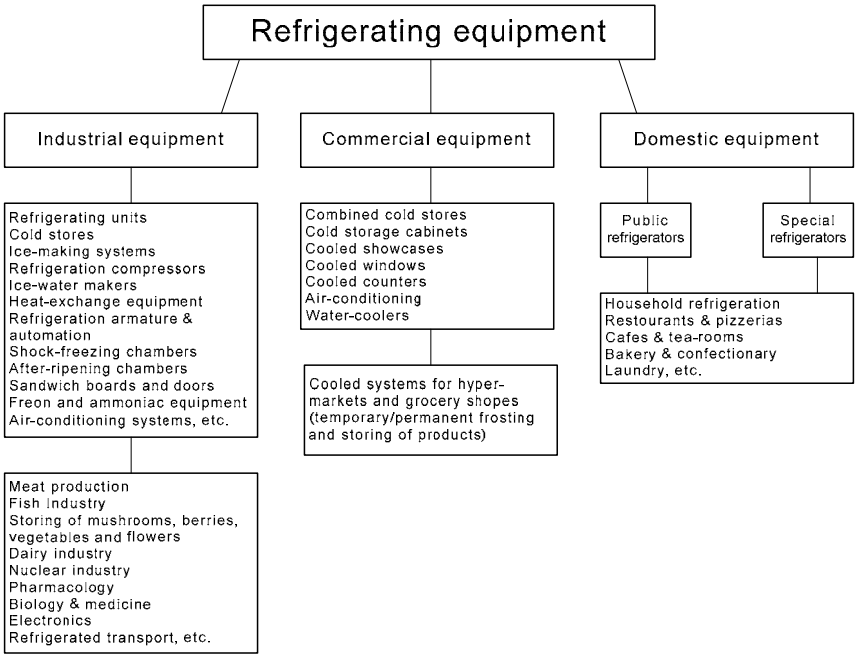

Figure 2.3 Refrigerating equipment classification [26].

According to the operation principle of the heat transformation systems they can be divided into two general categories: thermomechanical systems (based on increase or decrease in pressure of working medium) and electromagnetic systems (based on using constant and alternating magnetic/electric field). Nowdays there are following mashines used in refrigeration engineering: vapor compression system, absorbtion system, ejector system, air-expanded system. Due to external energy consumption the working media (refrigerant coolant) makes a reverse cyclic thermodynamic process, so called refrigeration cycle. In order to obtain the cooling effect in vapor compression, absorbtion and ejector refrigerating mashines a low-boiling liquid is usually used. For the same purpose we use the compressed air expansion in air-extended systems.

2.2.1 Mechanical compressive systems

Machanical mashines are the most common and multi-purpose compared with other refrigeration mashines. Thermomechanical systems according to the method of pressure increase of working medium are divided into: compressive machines, sorptive machines, jet refrigeration machines. The working principle of comressive systems is based on pressure increase by mechanical or thermal effect on refrigerating medium. For its turn, there are also several types of comressive mashines: vapor-liquid machines, gas-liquid

machines, gas machines. In the vapor-liquid and gas-liquid machines the aggregative state (gas, liquid or vapor) of the refrigerating medium changes during the working process - the process of condensation of compressed working medium and vaporization of expanded medim. In first case, the compression process is carried under the temperatures below critical (vapor area) or near critical temperature. In second case, we use the temperatures that are essentially higher than critical. In gas plants aggregative state of the refrigerating medium doesn't change because the working medium temperature is higher than critical within the whole range. Fig. 2.4 represents the T-S diagram of the working medium where we can see possible aggregative states.

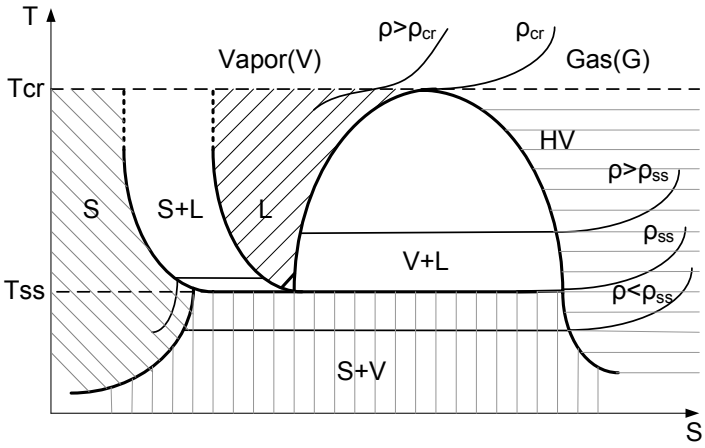

Figure 2.4 Phase plot for refrigerant and its possible aggregative states, where *S* is solid, *L* is liqiud, *V* is vapor, *HV* is superheated vapor, T_{cr}, ρ_{cr} are critical temperature and pressure, T_{ss}, ρ_{ss} are temperature and pressure of solid state.

Using the diagram above we can easily show the area of the aggregative state change for all types of the heat transformer, to be exact vapor-liquid, gas-liquid or gas. The sorptive machines are based on the pressure increase of working gas by consistent accomplishment of thermochemical reactions of sorption and desorption. The term sorption generally describes either process of absopbtion or adsorbtion. It means that liqiud or gaz has an ability being integrated with a material of different aggregative state and can adhere into another molecule surface [27]. In our case there is a sorption process of the working refrigerant with use of an appropriate sorbent accompanied by heat rejection. After that there is a desorption process of the working refrigerant from sorbent accompanied by heat application. In this kind of machines we use the property of many materials, i.e. they are able to change their temperature under adiabatic conditions or to

emit/to absorb heat under isothermal conditions. The soption and desorption processes here are analogous to processes of suction or delivery by machanical or thermomechanical compressors. This compression method is called thermochemical. There are several constituent elements of the vapour compression refrigeration system (fig.2.5 (a)): evaporator, refrigerating compressor, condenser and thermostatic expansion (throttling) valve.

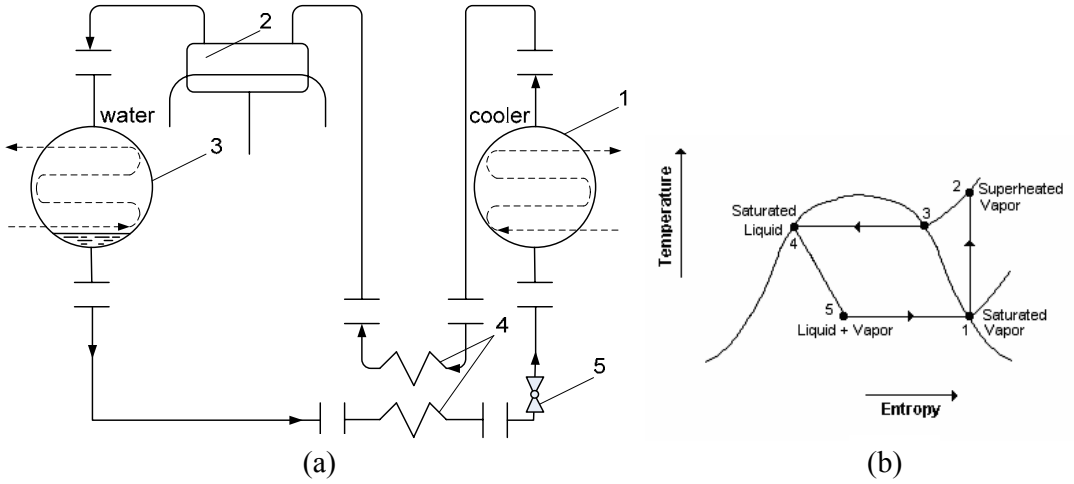

Figure 2.5 (a) Vapour compression refrigerating machine, where 1 is evaporator, 2 is compressor, 3 is capacitor, 4 is heat exchanger, and 5 is throttling valve [6]; (b) Temperature-entropy diagram of vapor refrigeration, where 1 to 2 is compression of vapor; 2 to 3 is vapor superheat removed in condenser; 3 to 4 is vapor converted to liqied in condenser; 4 to 5 is liqied flashes into liquid and vapor across expansion valve; 5 to 1 is liquid and vapor converted to all vapor in evaporator [21].

They are connected by tubing fit out with locking, adjusting and safety armature. To all elements of the refrigeration mashine made a demand of high containment. [6] Conversion cycle in this machine can be clearly understood by considering of temperature – entropy diagram below (see fig. 2.5 (b)). Depending on type of the refrigerating compressor all vapour compression mashines are subdivide into: reciprocating refrigerating machine, turboblower refrigerating machine, rotation refrigerating machine, screw refrigerating machine. Inside the vapour compression refrigeration machine realizes closed loop of the refrigerant circulation. The refrigerant boils in evaporator (or evaporates, in another words) under decreased pressure and low temperature conditions. The heat that is essential for the boiling process is rejected from the cooled object; hence, its temperature decreases down to boiling temperature of the refrigerating medium. Generating vapor is drawn off by the compressor and compressed

inside it up to condensing pressure level, than drawn to the capacitor where water or air cool it. The heat is taken out from the vapor and therefore it condenses. Obtained liquid refrigerant flows back to the evaporator (through the throttling valve where its temperature and pressure are decreased) to repeat the evaporation process and thus to close the machine's working cycle. For improving of cost-effectiveness (decrease in energy consumption per unit of heat rejected from cooled object) sometimes used the methods of vapor superheating before drawing vapor into compressor as well as liqiud supercooling before throttling process. For the same economical reason given above multi-step and cascade refrigerating machines are used if it is needed to obtain temperatures below 30˚C. As it follows from its name, in the multi-step refrigerating machine the process of compression goes step by step with the cooling on each stage. For instance, in two-step machine is possible to obtain already 80˚C for the refrigerating medium temperature. The cascade system is represented as series of machines and allows obtaining even -150˚C. Each machine has its own specific operating mode according to the thermodynamic requirements of the refrigerating medium.

Now we move to next type of refrigerating machine, namely absorption machine. Absorption refrigerating machine (see fig.2.6 (a)) consists of: boiling-tank, condenser, evaporator, absorber, pump, throttling valve. As a working substance in the absorption machines we take binary solutions with different boiling temperatures under equal pressure conditions. Component that starts to boil at the lower temperature used as a refrigerant, the second one's function is to absorb.

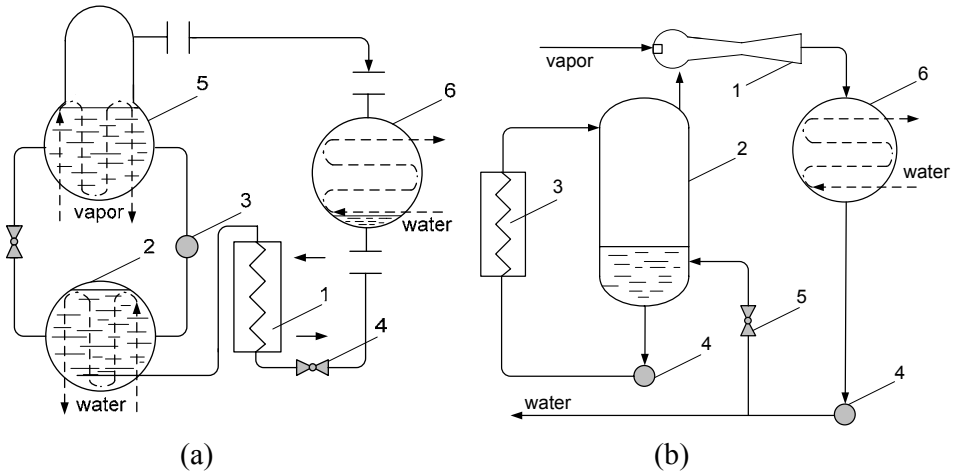

Figure 2.6 (a) Absorption refrigerating machine; (b) Ejection refrigerating machine [6].

A water solution of ammonia (refrigerant is ammonia) is usually used in machines for obtaining the temperatures in the range from 0˚C to 45˚C. For the cooling temperatures above zero typically used the absorption machines working on water solution of lithium bromide (refrigerant is water). The refrigerant evaporation inside is carried by means of heat rejected from the cooled medium. The vapors generating at that time are absorbed. Obtained concentrated solution is pumped to the boiling-tank where by energy application from some external source can be evaporated the refrigerant. Residuary solution goes again to the absorber. The gas refrigerant is transferred from boiling-tank to capacitor to condense and then it goes through throttling valve to evaporator and this cycle is repeated again. Application of absorption refrigerating machines has many advantages especially for a waste energy production (waste steam, hot water, gases of industrial oven, etc.). Additionally, important to mention that absorption machines are produced as one- or two-step machines.Above is also presented the ejection refrigerating machine including (see fig. 2.6 (b)): ejector, evaporator, condenser, pump, throttling valve. Water is used as a refrigerant. As an energy source we have the vapor with pressure of 3 - 10 kg/cm^2 . This vapor comes to the ejector's nozzle in order to be expanded. Following the expansion of vapor in the ejector and as a consequence in evaporator is generated decreased pressure. The water for "cold consumer" cooled in evaporator owing to partial evaporation there. The vapor pumped from the evaporator as well as working vapor of the ejector come to the capacitor to be transformed to the liquid state by emitting the heat into environment. Some water from the capacitor could be transferred to the evaporator for compensation. Air-expanded refrigerating machine belongs to the class of gas refrigerating units. Here we use air as a refrigerant. Unfortunatly, in the temperature range down to -80˚C the cost-effectiveness of these machines is lower compared to the vapor compression refrigerating units. Regenerative air systems, where air before expanding is cooled either in countercurrent heat exchanger or regenerator heat exchanger, are the most economical. Depending on the pressure value, machines are subdivided into low pressure and high pressure machines. Also there is another type of classification according to that machines can work in closed or opened cycle mode. [6], [23]

2.2.2 Thermosonic compressive systems

The Stirling cycle is an idealized thermodynamic cycle that theoretically is the most efficient among systems that have practical realization. Due to its effectiveness, the Stirling cycle is applied even in such extreme conditions found on submarines or space stations, however some technical requirements limit its wide universal application [28], [6]. In 19th century has been already shown that the Carno cycle is the most effective for engine or refrigerators constructions allowed by physics of nature. This effecicient cycle consists of two isothermal and two adiabatic processes as it has been already mentioned. The Stirling cycle, consisting from two isotherm and two isochores, is thermodynamically equal to the Carno cycle described above. Perfection and optimization of the Stirling cycle in engine or heat transformer mode is developing nowdays also. Let us consider machine that has in its operation principles the Stirling cycle (see fig.2.7).

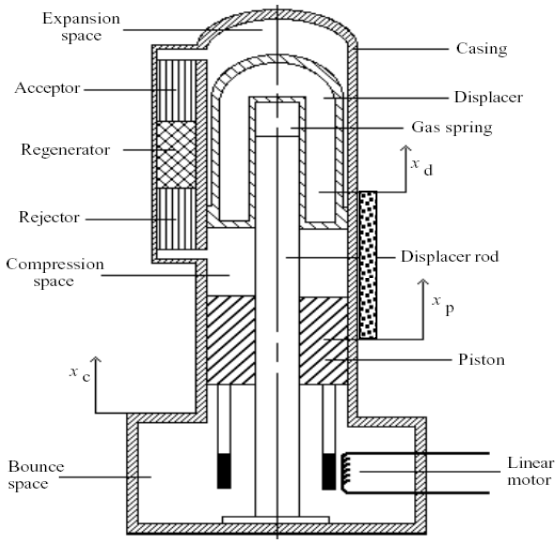

Figure 2.7 Refrigerating machine based on the Stirling cycle [6].

The gas, practically helium, is cyclically compressed in Stirling's mechanism on one level and the same gas is expanded on another level, so that by closed cycle either the heat is taken off or the thermodynamic work is accomplished. Additionally, the above shown machine construction has a free piston. One of the main parts of constraction is the regenerator that provides a phase shift between the heat transmission and mass transfer processes in communicating volumes. The regenerator must transfer the heat between the

volumes as fast as possible, but the mass transfer, i.e. gas transmission should be done very acceleratively, with the significant delay relative to heat exchange. On basis of Stirling effect was produced great amount of promissing and useful devices such as automotive radar, using superconducting circuits and detailes and operating at the temperature of 70 K[23]. Pulse tube on fig. 2.8 is one of the main competitors among refrigerating machines. Refrigerating machines, having as its basis the pulse tube construction, offer several advantages as compared with Stirling cycle based machines, e.g. they don't include any moving parts in low temperature range. This type of refrigerators represents as a closed system, using at one end of the tube an oscillating pressure that is produced by the compressor. Helium is the most common refrigerant for these machines. By proper conditions settings the refrigerant must take off the heat from cold end of the tube. There are some pulse-tube refrigerants providing the possibility for temperature gradient from room temperature and till 70 – 80 K, that is interesting for cryoelectronic superconducting devices.

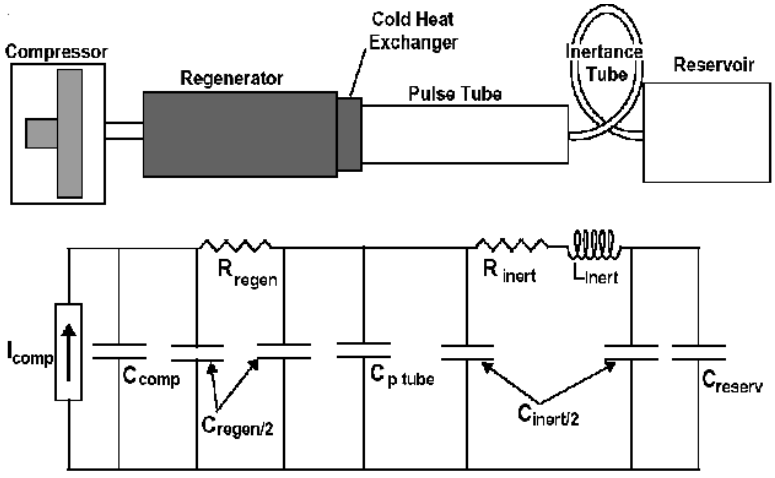

Figure 2.8 The pulse-tube based refrigerator sheme and analog electric circuit, where I_{comp} is current source, representing the piston's effort; C_{comp} is capacitor, representing the compressor's volume; R_{regen} is impedance of regenerator flow; $C_{regen/2}$ is distributed regenerator volume; $C_{p\ tube}$ is capacitor, representing the volume of pulse-tube; R_{inert} is changing resistance of the accelerative tube; $C_{inert/2}$ is distributed volume of the accelerative tube; $C_{reserve}$ is reservoir volume (it is assumed that reservoir's volume is big enough and thus parallel capacitors could be ignored); L_{inert} - induction [6], [23].

2.2.3 Solid state heat transformers

To this class of the refrigerating machines belong thermoelectric and thermomagnetic (thermomagneto-electric) systems. The key point of these systems is energy transfer inside the working medium with invariable in time parameters by means of elecric field or both electric and magnetic fields. The developement of thermoelectric refrigerators began in the middle of 20^{th} century. Thermomagnetic method is based on the Ettingshausen effect (galvanomagnetic effect). It appears in semiconductor material placed in magnetic field by constant cutoff current flow through it. It leads to temperature gradient inside the material with direction perpendicular to both magnetic and electric fields. As a result we have heat transfer from lower to higher temperature level exactly the same as in Peltier effect. In thermoelectric and thermomagneto-electric methods is difficult to manage with an inevitable influence of "parasitic" heat flow that is in opposite direction to useful heat transfer. This problem exists in any material types due to its thermal conduction, since the thermal-conductivity coefficient always differs from zero. Moreover, always exists so called Thomson effect, leading to the heat transfer from a hot to a cold section. Therefore, processes inside thermoelectric and thermomagneto-electric systems are always irreversible and coefficient of efficiency, limited by intrinsic loss depending on materials properties, is relatively little. [23]

Peltier effect or Peltier–Seebeck effect is thermoelectric effect consisting in conversion of temperature change into electric voltage and vice versa [29]. It becomes apparent by current flow through the contact (junction) of two different conductors or semiconductors (see fig.2.9). At that takes place additional heat evolution along with the Joule heat thar called Peltier heat; Q_p is originated from one current flow direction, and its absorption by the reverse flow direction. The value of Q_p depends on junction nature, current magnitude and current transit time:

$$\partial Q_P = \pi_{12} I \partial t \,, \tag{2.8}$$

where $\pi_{12} = \pi_1 - \pi_2$ is a Peltier coefficient for given junction concerned with absolute Peltier coefficients for each of contacting materials. It is assumed that current flows from the first sample to the second. By evolution of Peltier heat it is obvious that $Q_p>0$, $\pi_{12}>0$. By the absorbtion heat value is negative correspondingly. It is clear that $\pi_{12}=\pi_{21}$. The unit of Peltier coefficient in SI system is Joule/ Coulomb=V. Instead of Peltier heat is possible

to use power of heat generation determined as: $q_P = \pi_{12} j$, where $j = I/S$ is current density through the square section. Peltier coefficient is important technical characteristic that usually is not measured but determined by means of thermal electromotive force value (thermal e.m.f.).

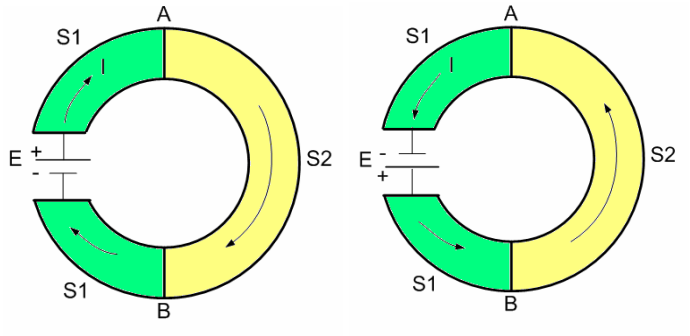

Figure 2.9 Peltier heat evolution and absorption, where *S1* and *S2* are different semiconductor materials, *A* and *B* are junctions and *E* is thermal e.m.f. [23].

Firstly, on the contact *A* takes place the heat evolution $Q_p(A) > 0$ and on the contact *B* its absorption $Q_p(B) < 0$. As a result occured the temperature change of these junctons, namely $T_a > T_b$. Than current direction is changed to opposite and correlation changes also: $Q_p(A) < 0$, $Q_p(B) > 0$, $T_A < T_B$. The reason for Peltier effect appearence on the contact of two semiconductors with one current carrier type (n- or p- type) is the same as on the metals contact (see fig.2.10). Current carriers (electrons or holes) from both sides of the soldered junction have an avarage energy that depends on several factors: energy spectrum, concentration, scattering mechanism of carriers. If carriers, passing through the soldered junction, fall into the area of lower energy, they can transmit excess of energy to a lattice. As a result a calorification process occurs near the contact, so that $Q_p > 0$ is Peltier heat evolution, and contact temperature increases. On the other junction carriers, passing to the higher energy area, take missing amount of energy from lattice, thus there is heat absorption, $Q_p < 0$ and temperature goes down respectively. However, the Peltier effect, as all thermo-electric effects, is stronger in systems where two types of semiconductors, namely, n – and p-type are included. Let us examine the case when current in junction goes from hole semiconductor to electron one (p $\rightarrow$ n). Holes and electrons move towards each other and recombine. Thus released energy appears in a form of heat.

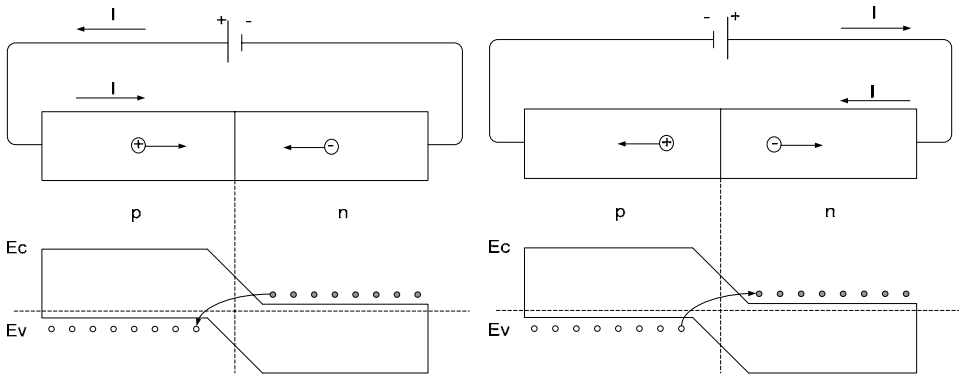

Figure 2.10 Illustration of Peltier heat evolution and absorbtion for *n*- and *p*-type semiconductors, where *Ec* and *Ev* are energy levels of conducting and valence band in semiconductor respectively [6].

The basic assembly of thermo-electric refrigerant devices is a battery made up of several tandem thermoelements (see fig. 2.11). One of the thermoelement branches has to be from hole semiconductor and other from electron semiconductor type. If current direction will be chosen in order to absorb heat on internal contacts and to emit heat to environment on external contacts than the temperature inside refrigerator is decreased and space around is heated up. The most important characteristic of refrigerating equipment is a cooling efficiency:

$$Z = a^2 / (\rho\lambda) \qquad (2.9)$$

where a is thermoelectric coefficient, ρ is specific resistance, λ is thermal conductivity of conductor. Parameter Z is a function of temperature and current carrier concentration. In addition for each of given temperature values exists optimal concentration value so that Z obtaines maximal value.

$$\Delta T_{max} = 0.5ZT^2, \qquad (2.10)$$

where T is temperature of the cold junction. The higher value possesses Z parameter the greater is an overall efficiency of thermoelement.

Generally it is better to use semiconductors with higher mobility and lower thermal conductivity.

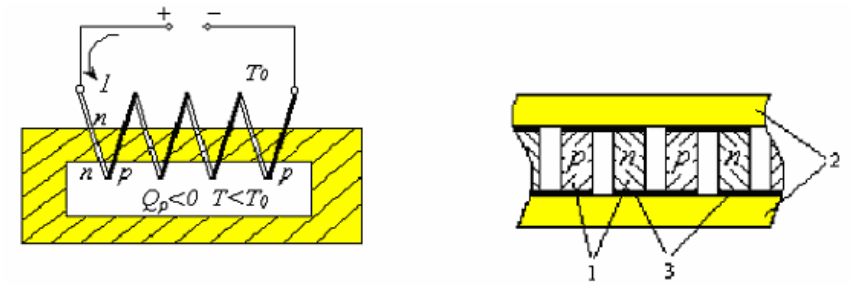

Figure 2.11 Electrical refrigerator sheme where with 1 is n- and p-type of semiconductor materials; 2 is heatconducting plate made from insulating material; 3 is metalic connectors, Q_p is Peltier heat; T_0 is reference tempertaure[6].

Ettinshausen effect is one more phenomenon on which basis can operate refrigerator. Ettinshausen effect is stronger for materials with equal concentration of holes and electrones. i.e. in mixed conduction semiconductors. One of the best materials for these purposes is bismuth-stibium alloy with stibium concentration of approximetely 3%. This material possesses mixed conduction and low thermal conductivity. On the fig.2.12 is shown system based on the Ettingshausen effect to obtain temperature gradient $\Delta T = T - T_0$ perpendicular to both electric and magnetic field direction.

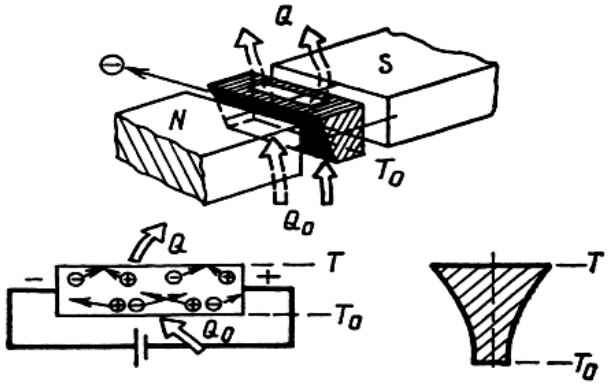

Figure 2.12 Ettingshausen effect illustration where T and T_0 are temperatures of upper and bottom side, N and S are magnetic poles, Q and Q_0 are rejected and injected heat respectively [23].

By the magnetic poles applying and selected current direction the upper side of sample is heated and bottom side is cooled. The steady-state conditions result in thermal current into heated area. In fact besides the charge motion along sample exists also the motion in the transverse direction, from down up to the heated area. Thermomagnetic systems have some advantages in comparison with thermo-electric devices: they made up from one material type as well as cascading sheme, they operate well by the temperatures lower

than 200 K that is impossible for thermo-electric devices). To sum up it is important to mention that combination of thermomagnetic and thermo-electric arrangements gives the best result. Summing up the electric and magnetic heat transformers classification is shown on fig. 2.13.

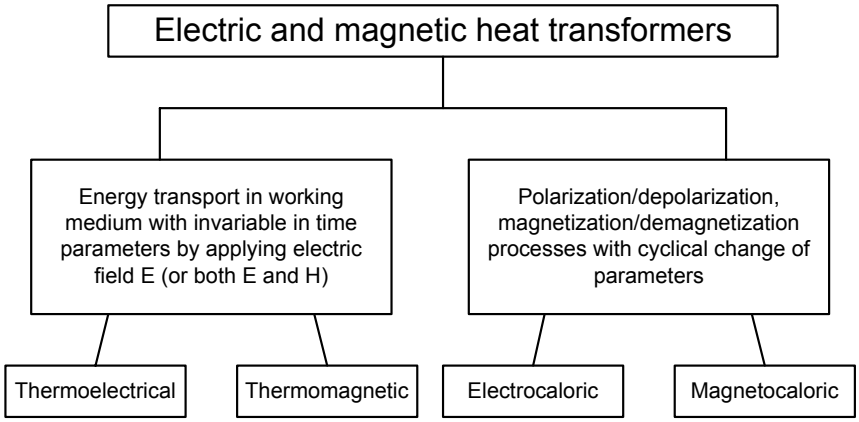

Figure 2.13 Classification of electric and magnetic heat transformers.

For the first type (thermoelectrical and thermomagnetic transformers) is significant relatively low efficiency due to permanent existing of "parasitic" flow in material, always possessing finite thermal conductivity. The second group is determined by electrocaloric and magnetocaloric effects. Polarization or magnetization (in case of electrocaloric or magnetocaloric effect respectively) is accompanied by temperature increase under adiabatic conditions. On the contrary, depolarization/demagnetization causes decrease in temperature, internal cooling. These phenomenons allow to conduct state changing cycles that in a similar manner as in thermomechanical system. Consequently, it is possible to arrange electrocaloric and magnetocaloric refrigerating devices. These systems don't have own losses and efficiency in this case is determined only by the technical losses. Ability of any magnetic material to change its temperaure and entropy by applied magnetic field underlies technology of magnetic cooling (as it is in traditional refrigerators by gas compression or expansion, see comparison on fig.2.14 (a) and fig.2.14 (b)) called magnetocaloric effect. When magnetic field is applied magnetic properties inside the material suffer some change that causes change in intrinsic magnetic energy and further reversible process of heat absorption or evolution.

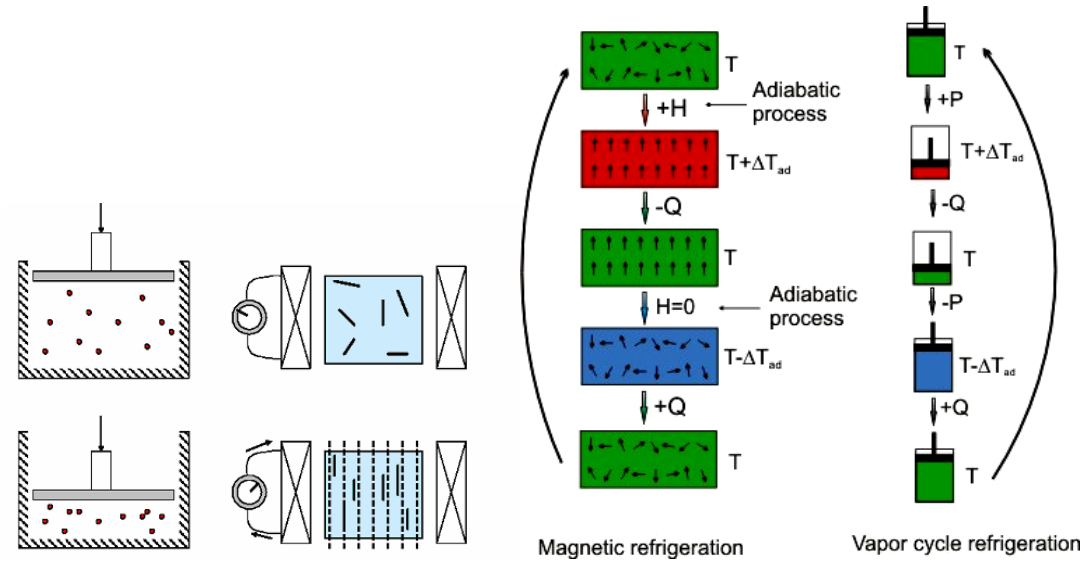

Figure 2.14 (a) Analogy between refrigerant compression/expansion and magneization/demagnetization of solid magnetic material [6]; (b) Analogy between magnetocaloric refrigerating cycle and cycle with gas using as refrigerating medium, where T is temperature of system, ΔT_{ad} is temperature difference, Q is heat, H is externally applied magnetic field and P is pressure [23], [30].

Under adiabatic conditions (e.g. by fast switching on/off of magnetic field) absorption or evolution appears as increase or desrease in temperature. This phenomenon is called magnetocaloric effect, see operaton principles on fig. 2.15. It is determined by entropy change in magnetic subsystem. Change in temperature of magnetic materials occures because of internal energy redistribution between magnetic moment system of single atom and lattice. Magnetocaloric effect is maximal in magnetically ordered materials, i.e. ferromagnetics, antiferromagnetics under magnetic phase transition temperatures. The magnetic ordering temperatures are Curie and Néel temperatures. Besides some reversible effects, in magnetically ordered materials also appear magnetothermal effects that are accompanied by irreversible processes of domain boundary displacement, essential rotation of magnetization vector and magnetic relaxation effects (magnetic viscosity). These effects have its origin in the fact of power waste by magnetization process. By one cycle of magnetic field changing in a majority of materials is possible to get small ΔT effect. It is significant that in rare-earth metals and alloys irreversable hysteresis effects occure mainly in junction area of antiferromagnetism – ferromagnetism, where hystereses loop is widened. By low field the hysteresis loop is narrow. Thus magnetocaloric effect measured by field change from 0 to H is practically constant under repeated on/off cycles. The maximum appeared at Curie point could be explained by the

fact that near T_c temperature derivative of magnetization also reaches its maximum. Among the materials used for magnetocaloric effect are: Fe, Co, Ni, Gd, Dy, ErAl2, GdNi2, GdAl2, (Fe,Rh), (La,Ca)MnO3, Gd5(Si,Ge)4, MnFe(P,As), etc. [6]. More suitable material for these purposes is gadolinium (Gd) with T_c of approximetely 20˚C. Giant magnetocaloric effect was observed in $Gd_5(Si_2Ge_2)$. At room temperature thermal capacity and entropy dependencies of this material have stick-slip nature that is advantageous and perspective for magnetocaloric coolers purposes. Relative temperature change at the phase transition area is about 15 K. Further investigations have shown that there are other materials with equal properties (sugnificant magnetocaloric effect) near the room temperature, e.g. $MnFeP_{0.45}As_{0.55}$, $Fe_{49}Rh_{51}$. The last one is difficult to use in action due to its high cost and essential hysteresis effects. [6], [23] It is not enough to obtain high caloric effect, additionally is needed to organize effective thermodynamic cycle to take off the heat from cooled object. Effective heat rejection is carried out in regenerative magnetic refrigerating cycle. According to theoretical estimations the effectiveness of magnetic regenerative refrigerating cycle is from 38 to 60 % of Carno cycle for the range from 4.5 to 300 K (about 52 % for 20 - 150 K, and 85% in the range 150 - 300 K). Magnetic refrigrators include few amount of moving parts and operate under low frequencies. Therefore, it is possible to reduce to zero the deterioration of equipment and to prolong life time of refrigerator.

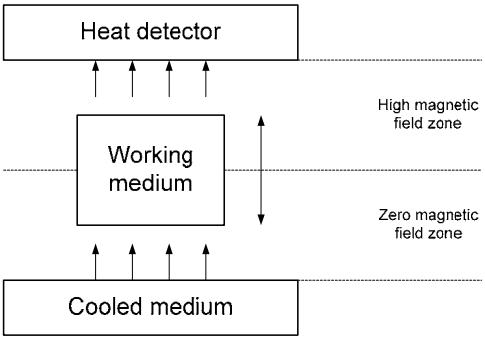

Figure 2.15 Mechanism of magnetocaloric machine operation.

Magnetic moves cyclically between receiver and source (cooled object) of heat. In high magnetic field zone the magnetic is isothermally magnetized and the heat from calorification process taken by thermal receptor. In zero field working medium become demagnetized (temperature is decreased) and heat from cooled body is transferred to it. After established equilibrium the cycle is repeated. All magnetic refrigerators could be

devided into two classes according to a magnet type in use: systems with superconducting magnet and systems with constant magnet. First type possesses wide temperature range and relatively high output power. Thus it is possible to use them to construct conditioning systems in big apartments or foodstuffs storehouses. Cooling systems with constant magnet possess relatively limited temperature range (not more than 30˚C during one cycle) and can be applied in middle power systems (up to 100 W), such as automobile refrigerator and portable picnic refrigerator. But both of the above discussed refrigerating machines have several advantages compared with combined-cycle refrigerating plants:

1) Low ecological danger;

The working medium is solid and can be easily isolated from environment. Using as the working medium metals, lanthanides, are not toxic and it is possible to use them secondly after device utilization. Heat-removing medium must possess low viscosity and sufficient heat conductivity that matches ideally to properties of water, helium or air. The last two are good compatible with environment.

2) High efficiency;

Magnetocaloric heating and cooling are practically reversible thermodynamic processes in contrast to vapor compression in working cycle of combined-cycle refrigerating machines. Theoretical calculations and experements have shown that magnetocaloric plants are characterized by high efficiency and economy. Particularly, for room temperature conditions they are potentially more effective on 20 - 30 % in comparison with combined-cycle machines.

3) Long operation life;

Technology assumes the use of few moving detailes and low operating frequency in cooling devices, thus it prolongs its operation time.

4) Flexibility of technological process;

There is posibility to use different magnetocaloric refrigerators depending on application.

5) Useful properties of cooling;

Magnetic technology allows proceeding a cooling of different substances (water, air, chemicals) with few operation changes in each case.

6) An advanced stage of superconductivity development and films magnetic properties improvement;

For instance there are several companies working on *NdFeB* constant magnetic systems. Along with supercondivity developement we can hope on further advance in magnetocaloric cooling systems. Disadvantages of magnetic cooling systems:

1) Necessity of magnetic source screening
2) Relatively high price for magnetic sources
3) Limited temperature range in one cooling cycle. [6], [23]

One of the most exiting cooling methods is optical cooling. The principle of optical cooling underlies pumping of an appropriate material by laser beam that absorbed or emitted as fluorescence (see fig.2.16 (a) and fig. 2.16 (b)). If the energy of fluorescent photons at instant is higher than energy of pumping photons occured waste of energy that is compensated by thermal energy absorption from the material. It makes this material cooled.

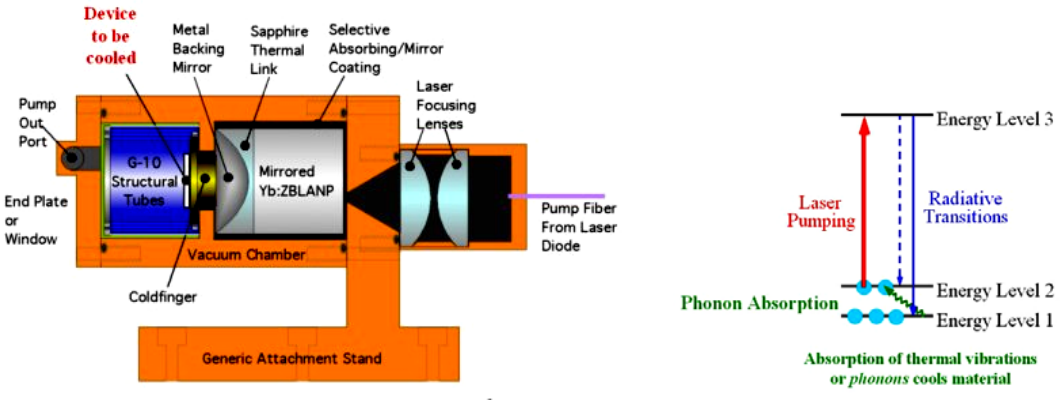

(a) (b)

Figure 2.16 (a) Optical cooling setup; (b) Phonon cooling of materials[6].

It is needed to select material with a certain energy levels arrangement. Until this time better a better characteristic has shown *ZBLAN*, glass based on zirconium fluoride. By powerful laser pumping 11W and by using *Yb: YAG* LED[6] of 1.02 mm wave lenght glass became colder after two hours. Temperature reached 208 K value. Lower temperature is possible with use of pure glass materials. The topic of present work is electrocaloric cooling. Let us briefly gains incite about electrocaloric refrigerating.

[6] Light Emitting Diode

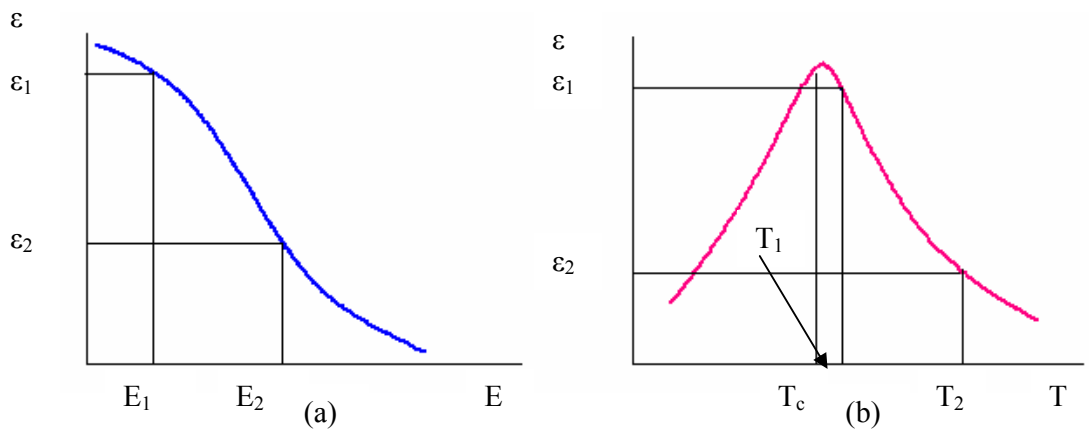

Figure 2.17 (a) Field dependence of permittivity ε (E), (b) temperature dependence of permittivity ε (T) for usual ferroelectric material.

Electrocaloric effect has a lot of common with described earlier magnetocaloric effect. Analogy is found in that we can substitute cycle "magnetization - demagnetization" on "polarization - depolarization" processes. Electrocaloric capacitor should have nonlinear field and temperature dependence of permittivity as it is shown on fig. 2.17. Choice of material for capacitor is rather difficult question. Material must have high values of permittivity and depend strongly and not linearly on applied electric field. Electrocaloric effect is a reverse of pyroelectric effect[7]. Applied electric field changes permittivity of material. This results in temperature gradient in material. Detailed mechanism of electrocaloric temperature change will be discussed later.

[7] Pyroelectric effect refers to a property of dielectric materials to change its intrinsic spontaneous polarization with temperature. All pyroelectrics show a reverse effect as well, namely electrocaloric cooling. [27], [31]

3 MAIN PROPERTIES OF FERROELECTRICS

A ferroelectric is a material exhibiting characteristics such as a reversal of intrinsic lattice polarization by applying an external electric field that greater than coercitive field E_c and phase transition from paraelectric to ferroelectric state [4]. Let us discuss the following properties of ferroelectrics: presence of spontaneous polarization, ferroelectric domains, hysteresis loop, Curie point, phase transitions.

3.1 Dipole moment and spontaneous polarization

A spontaneous dipole moment is essential attribute of ferroelectric material. By applying an electric field we can switch it. This process refers to spontaneous switchable polarzation. This happens if two charges of opposite signs are placed at a certain distance (see fig. 3.1) [32].

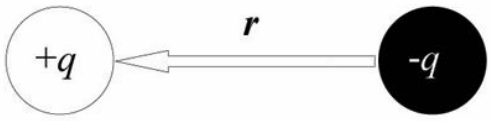

Figure 3.1 Dipole moment [32].

The dipole moment $\vec{p}$ is defined as:

$$\vec{p} = q \cdot \vec{r} \tag{3.1}$$

Vector sum of dipole moments at every unit cell $\sum \vec{p}$ is called net dipole moment of ferroelectric. Therefore, structure that possesses center of symmetry can not produce spontaneous polarization. Symmetry would force any dipole moment to be zero. As a consequence, all feroelectrics are non-centrosymmetric. There is one additional requirement. The central atom in structure should be in non-equilibrium position, i.e. there is spontaneous local dipole moment (see fig.3.2). In case (a) structure is non-polar, because there is no local dipole moment and central atom is in equilibrium position. Situation (b) illustrates displacement of central atom and polar state of structure. [32] The spontaneous polarization is expressed as dipole moment value per unit volume or in units of the charge per unit area on the surface that is placed at right angle to the axis of spontaneous polarization. The direction of spontaneous polarization usually coincides with one of the crystal axis. Only crystals possessing the unique crystal axis can develop

the spontaneous polarization. A phenomenon where spontaneous polarization depends on temperature is called pyroelectric effect. It will be determined precisely later. If a certain material introduces ferroelectric behavior, it means that spontaneous polarization and magnitude can be reversed by application of electric field [33]. All ferroelectric materials show pyroelectricity, and in one's part pyroelectrics possess piezoelectric properties. It is important to note that a reverse statement is not right. For instance, ZnO is pyroelectric but not ferroelectric [4]. Symmetric molecules such as methan CH_4 produce no local dipole (therefore no spontaneous polarization), but there are simple non-symmetric examples, for instance H_2O. Formally, we can describe a dipole moment as:

$$\vec{p} = \int dV \rho(\vec{r})\vec{r} \tag{3.2}$$

p(r) is the charge density of molecules, icluding both negative and positive nuclear charge densities.

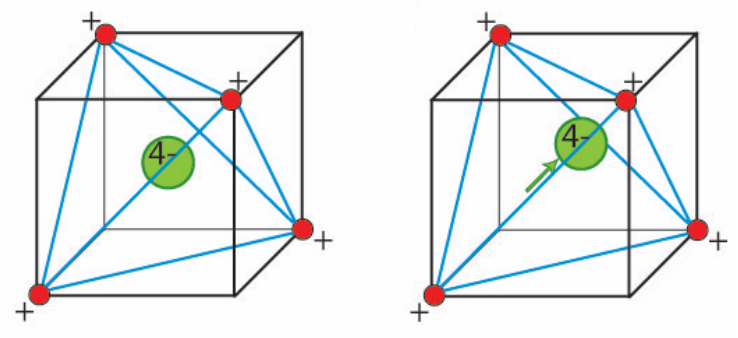

(a) (b)

Figure 3.2 Spontaneous local dipole moment in tetrahedral structure [32].

As above already mentioned, the definition in case of point charges is

$$\vec{p} = \sum_i Q_i \vec{R_i} \tag{3.3}$$

Where Q_i is point charge and R_i defines their position.

In our considerations we also operate with term net dipole moment or total dipole moment:

$$\vec{p} = \sum_{molecules} \vec{p}_{molecule} \tag{3.4}$$

Let us now define polarization:

$$\vec{P} = \frac{\vec{p}}{T_{totalvolume}} = \frac{\vec{p}_{molecule}}{Volume\_per\_molecule} = \frac{Dipole\_moment\_per\_unit\_cell}{Volume\_of\_unit\_cell} \tag{3.5}$$

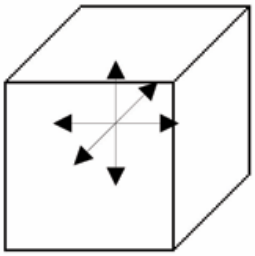

Figure 3.3 Axes directions in tetragonal $BaTiO_3$ [34].

There is a unique crystollagraphic axis (or axes in some structures) along which material can be polarized and dipole moment is produced (see fig.3.3). For instance in $BaTiO_3$ cooling from high temperature cubic phase to tetragonal phase (T_c = 120˚C) results in structure with six possible directions that correspond to initial cubic state.

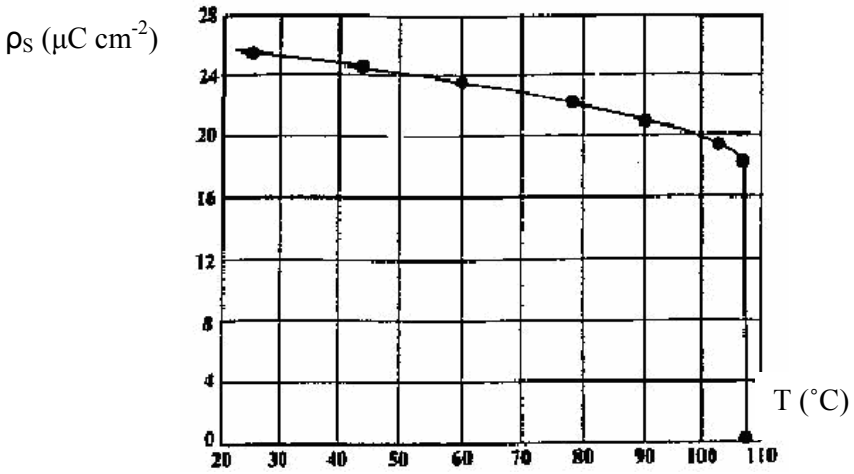

Figure 3.4 Temperature dependence of spontaneous polarization P_s for $BaTiO_3$ ferroelectric crystal [33].

Fig.3.4 represents temperature dependence of polarization for $BaTiO_3$. By increasing the temperature it is possible to obtain decrease in polarization. Above the Curie point polarization is zero.

3.2 Hysteresis loop and dielectric permittivity

Before considering phenomenon of hysteresis loop let us briefly define what domain structure is. Ferroelectric domain is an area characterized by uniform polarization. Electric dipoles inside the domain are aligned in the same polar direction. Interface called

domain wall separates different domains. By application of electric field, there is process of domain walls motion leading to formation of single domains. By increase of applied field domains can switch, or in other words, can change their polarization to reversal [31] - [33]. Ferroelectric hysteresis loop shown on fig.3.5 describes the phenomena of polarization reversal. Increase of electric field strength leads to increase in polarization. By maximal value of electric field there is a saturation value of polarization. However, removal of electric field doesn't turn to zero the polarization value.

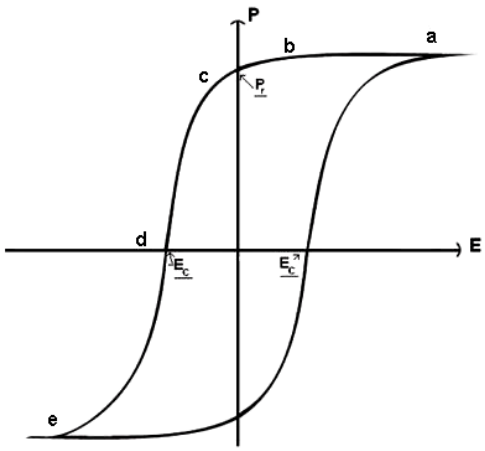

Figure 3.5 Polarization vs electric Field (*P*-*E*) hysteresis loop for a typical ferroelectric crystal [35].

On fig. 3.5 *abcde* is hysteresis loop, E_c is coercitive field and P_r is remnant polarization. If we would remove electric field polarization doesn't react instantaneously, i.e. it doesn't disappear resulting dielectric state (*a*, *b*, *c*). P_r is remnant polarization that characterizes polarization value of material that was fully polarized and from which we removed electric field. Polarization reduces significantly only after application of electric field in opposite direction (*d*). E_c is a specific field called coercitive. It leads to zero net polarization. Finally, if we increase applied field in this direction polarization became saturated (*e*) [33], [34]. At zero fields some domains still remain in previous polarization direction, and some do not. To complete the depolarization process negative field E_c is applied, namely coercive field (see E_c on fig. 3.6) that is needed for reducing polarization to zero. The hysteresis loop can be observed by applying more negative electric field. Full spontaneous polarization is found by extrapolation to the polarization axis [31], [32]. All steps of domain growth are shown on fig. 3.6.

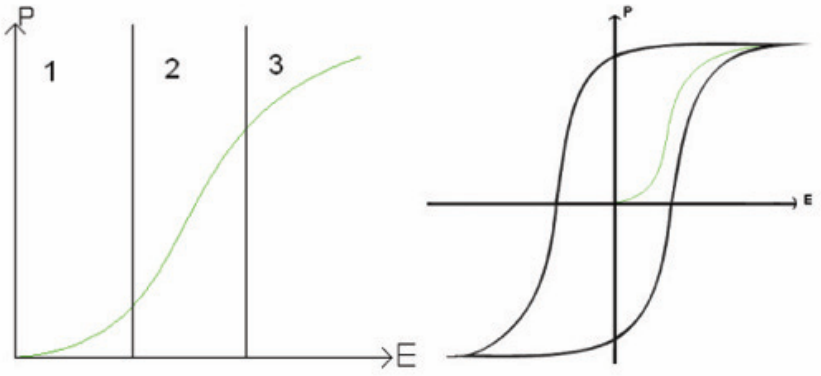

Figure 3.6 Minor and major hysteresis loop and the part of curves: 1 is reversible domain wall motion, 2 is linear growth of new domains and 3 characterizes new domains reaching the limit of their growth [36].

The Curie point T_c is a transition temperature from a non-ferroelectric state to ferroelectric state. Above T_c material doesn't possess ferroelectric properties and below T_c it becomes ferroelectric [31], [33], [36].

3.3 Ferroelectric phase transition

In electric field material has energy $-\vec{P}\cdot\vec{E}$, thus it is lowered by application of field. There are dipole moments that can be parallel, perpendicular or antiparallel to electric field direction ($+\vec{P}\cdot\vec{E}$) [34].

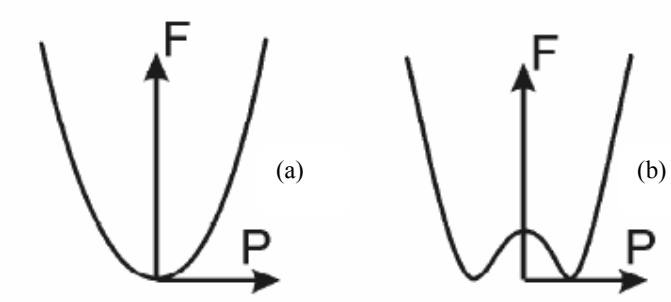

Figure 3.7 Free energy as a function of polarization for (a) paraelectric state, and for (b) ferroelectric state [34].

The (b) of fig. 3.7 helps us to define properties of ferroelectric. It is 1D crystal consisted of two atoms that charged oppositely (see fig. 3.8). It is possible to orient all dipoles either to the right or to the left. Above shown structures have the same energy and at that

point they are equal, but at that we keep in mind that they have opposite sign to dipole moment direction.

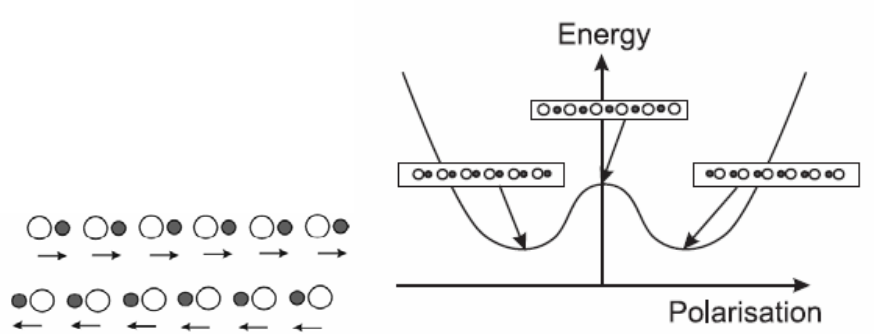

(a) (b)

Figure 3.8 (a) Fictitious model of crystal; (b) Shematic potential well [34].

By means of dragging one atom type toward other one we can transform the structure to opposite one. This results in switching of bulk polarization to opposite. Then we can consider that crystall has only two stable states and, thus energy barrier between them (b), see energy function of polarization. This energy barrier is needed to overcome. Below is demonstrated this process step by step on diagram of free energy vs polarization (fig. 3.9). If all domains switch at once moment (idealised ferroelectric) by aplication of electric field then appeared hysteresis loop shown on fig. 3.5 In practice not all domains have the same reaction on external field, therefore they do not overturn uniformly as we consider in simplest considerations. As it has been already mentioned the potential energy well between two polarized states can be desribed in terms of free energy diagram. These two states are rather stable. The potential barrier is clearly seen on diagram free energy vs polarization.

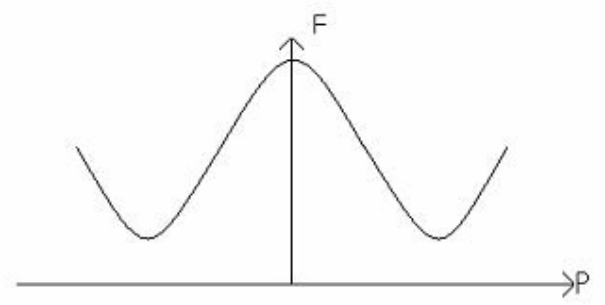

(a)

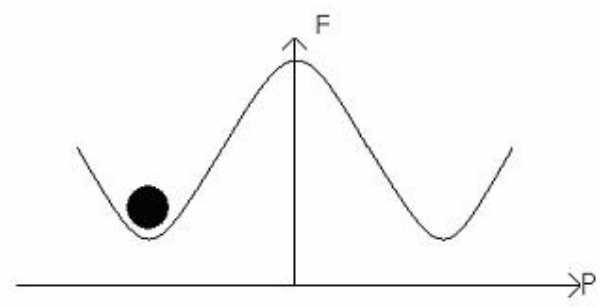

(b)

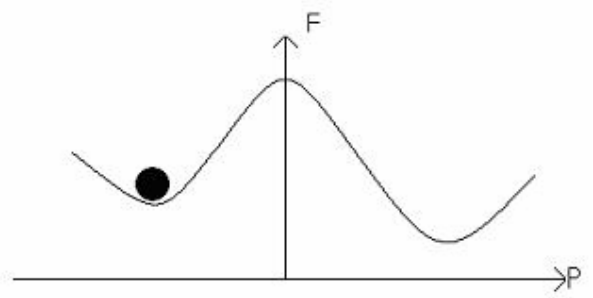

(c)

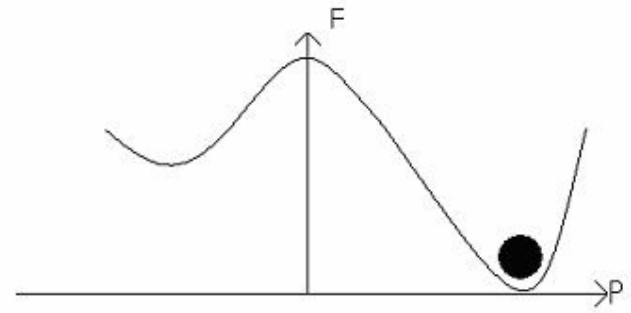

(d)

Figure 3.9 Free energy vs polarization diagram: (a) Potential barrier, (b) E.g. polarization point is left, (c) "Tilting" of the potential well, (d) Greater tilt and dipole moment switching [37].

Summing up we have fig. 3.10. There are more features of hysteresis loop that should be considered. Change in temperature results in change of hysteresis loop form, namely it becomes sharper and thinner by increase of temperature and finally disapears (see fig.3.11) [34], [38]. Here should be noted following aspects:

1) Disorder

When temperature is increased this results in randomly directed dipole moments within each unit cell. Thus there is not ordered material with net polarization anymore.

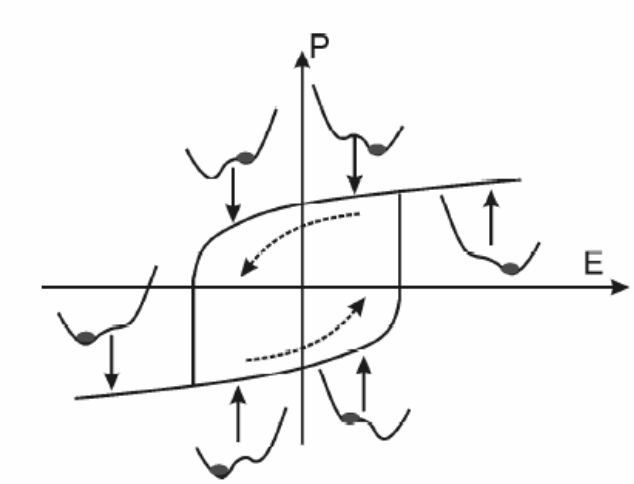

Figure 3.10 Shematic picture of hysteresis in idealised ferroelectric [34].

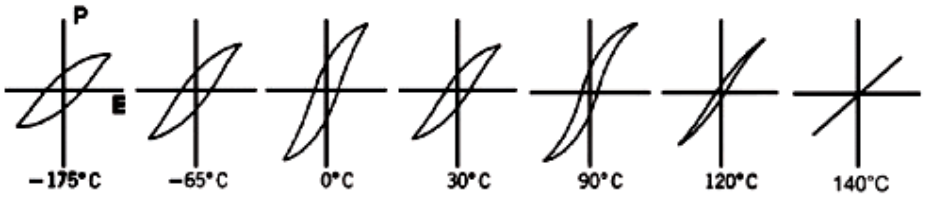

Figure 3.11 Temperature dependence of hysteresis loop form [38].

2) Phase transitions

Transition processes lead to particular chages in materials. For instance, there are jumps at 0˚C and 90˚C accompaying with specific change in loop form.

We know also that at increasing temperature bulk polarization reduces and vanishes completely at Curie temperature. This means phase transition defined further. There are two types of ferroelectric phase transition: first order and second order transitions. It is described by changes of order parameter during the transition. Order parameter is spontaneous polarization. [39] In case of first order phase transition (shown on fig.3.12) order parameter, i.e. polarization varies continiously until Curie temperature, where discontinuity is occured. Second order transition (fig. 3.13) requires order parameter itself to chage continiously, but its first derivative has a discontinuity at Curie temperature [39]. It is possible to find several ferroelectric phases with phase transitions each characterized by its own temperature.

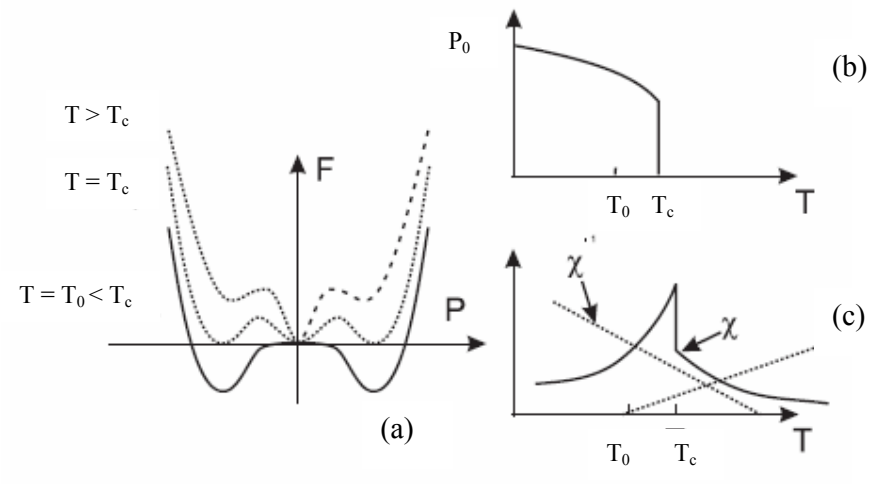

Figure 3.12 First order transition, where (a) Free energy as a function of polarization at $T > T_c$, $T = T_c$, and $T = T_o < T_c$, (b) Spontaneous polarization $P_0(T)$ as a function of temperature, (c) Susceptibility χ as a function of temperature [34].

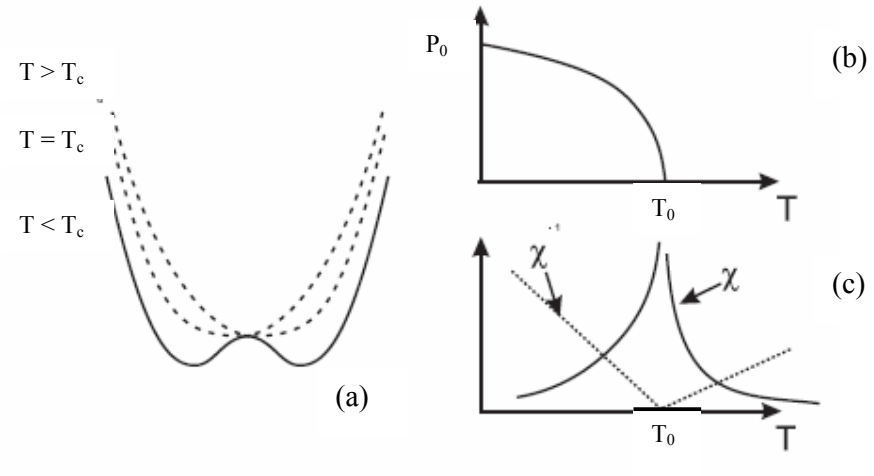

Figure 3.13 Second order transition, where (a) Free energy as a function of polarization at $T > Tc$, $T = Tc$, and $T = T_o < T_c$; (b) Spontaneous polarization $P_0(T)$ as a function of temperature; (c) Inverse of susceptibility χ , where $\chi = \frac{\partial P}{\partial E}(P_0 = const)$ [34].

As an example, let us consider fig. 3.14 where the temperature dependence of dielectric constants is presented.

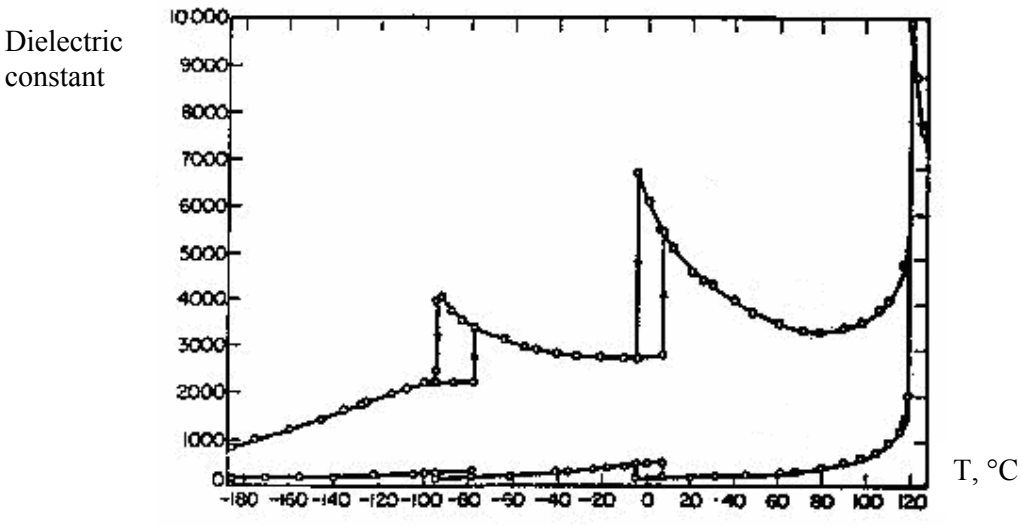

Figure 3.14 The variation of dielectric constants with temperature for $BaTiO_3$ [33].

The barium titanate is cooled, thus changed from its paraelectric cubic phase to the ferroelectric tetragonal, orthorhombic, and finally to rhombohedral phase. There is an anomalous behavior of properties near transition temperatures due to changing in phase character and expanded distortion. The Curie-Weiss law helps us to identify temperature dependence of permittivity above the transition temperature:

$$\varepsilon = \varepsilon_0 + C/(T-T_o), \tag{3.6}$$

where ε is permittivity, ε_0 is permittivity of vacuum, C is Curie constant and T_o is Curie temperature. It should be noted that the Curie temperature T_o and Curie point T_c are not the same. T_o is obtained by extrapolating and T_c is a real phase transition temperature [33]. There is a high dielectric permittivity in ferroelectric material under the paraelectric state conditions. The reason for that is a presence of microscopic forces keeping a non-poled state inside the material if microscopic electric field is absent. Due to this compensation, so called restoring force of material is not strong. That is opposed to poling process after electric field application. It leads to higher values of permittivity in paraelectric phase as well as in ferroelectric phase (spontaneous polarization is not really stable phenomena). Moreover, the permittivity can be increased by action of ferroelectric domains. It is needed to be mentioned that the dielectric permittivity does depend on bias electric field. Parameters used for characterization of tunability $n = \varepsilon(0)/\varepsilon(E_0)$ and relative tunability is $n_r = (\varepsilon(0)- \varepsilon(E_0))/ \varepsilon(0) = (n-1)/n$. The relative tunability is strong function of permittivity under zero bias field, namely n_r is proportional to ε^3. Under applied electric field this dependence will slow down [40].

3.4 Landau theory of phase transition

It is enough to specify following variables as thermodynamic equilibrium in crystal: temperature T, entropy S, electric field E, polarization P, stress σ and strain s. Normally electric field and stress are applied to structure, so that polarization and strain are considered to be dependable or, in other words, "internal". We keep in mind two fundamental thermodynamic postulates:

1) Free energy can be regarded as function of the ten variables (three components of polarization, six components representing stress tensor and temperature);
2) Values of "internal" (dependent) variables in conditions of thermal equilibrium are deduced at minimum of free energy.

$$F_p = \frac{1}{2}aP^2 + \frac{1}{4}bP^4 + \frac{1}{6}cP^6 + \ldots - EP \tag{3.7}$$

a, b, c are undefined coefficients depending on temperature; they may have any sign, but if they are positive free energy has an original minimum as on fig. 3.7 (b) for free energy for paraelectric state. The minimum of free energy results in:

$$\frac{\partial F}{\partial P} = 0\,. \tag{3.8}$$

We can take into account only terms up to quadratic to deduce equation for polarization after applied electric field:

$$\frac{\partial F}{\partial P} = aP - E = 0 \tag{3.9}$$

On pictures of phase transitions above also found susceptibility:

$$\chi = \frac{P}{E} = \frac{1}{a}. \tag{3.10}$$

It should be noted that susceptibility of dielectric is proportional to capacitance measured in electric circuit. If coefficients are partly positive partly negative, $a < 0$, while b and $c > 0$, situation refers to fig. 3.7 (b) ferroelectric state. There is an energy minimum at a finite polarization. Presented phenomenological theory leads to definition of phase transitions shown on fig.3.12 and fig.3.13 [34].

3.5 Piezoelectric and pyroelectric properties

It should be mentioned one more interesting feature of ferroelectric materials. It is their sensitive reaction on elastic stress (see fig. 3.15). Some materials can develope voltage as a response on mechanical force application, so called piezoelectric effect. Going deeply to understand these phenomena we should have a look at Landau theory again.

$$F_S = \frac{1}{2}Ks^2 + dsP^2 + \ldots - s\sigma \tag{3.11}$$

This is defined for uniaxial ferroelectric.

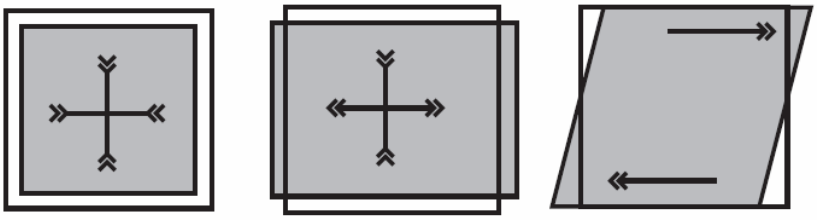

Figure 3.15 Sketch of a volume strain and two types of share strain that are volume preserving [34].

In the above equation *s* is a component of strain field. First term in equation has its origin in Hook's law, ''the elastic energy stored in a solid is quadratically dependent on the distortion''. *K* represents elastic constant. Second term defines coupling between the elastic strain and the polarization. There is usual definition of strain in solid followed from how displacement $\vec{U}$ of a point depends on its position $\vec{r}$:

$$s_{ij} = \frac{1}{2}\left(\frac{\partial U_i}{\partial r_j} + \frac{\partial U_j}{\partial r_i}\right) \tag{3.12}$$

Here *i* and *j* mean *x, y, z* components of the vector. Thus, s is described as 3×3 matrix with six independent components. There are three independent components in cubic structure, so called volume strain (see fig. 3.16).

$$\frac{\partial F(P,s)}{\partial P} = \frac{\partial F(P,s)}{\partial s} = 0 \tag{3.13}$$

Thus, we minimize the free energy with respect to both *P* and *s*. Let us consider the second part of equation:

$$\frac{\partial F(P,s)}{\partial s} = Ks + dP^2 - \sigma \tag{3.14}$$

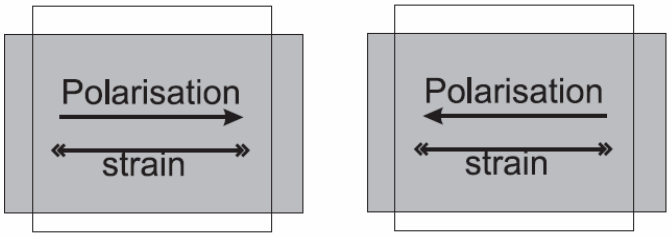

Figure 3.16 Strain in a polarized crystal: the spontaneous polarization chooses an axis, and distorts the crystal from cubic to tetragonal. By symmetry, if the polarization is reversed, the strain stays the same, so the allowed coupling term must be quadratic in the polarization [34].

If now polarization is reduced to zero we get Hook's law: $s = \sigma / K$. There is possible another situation when strain is applied to force the strain to be zero at any point. In third case, there is no external stress applied (σ = 0) and thus:

$$s=-dP^2/K \tag{3.15}$$

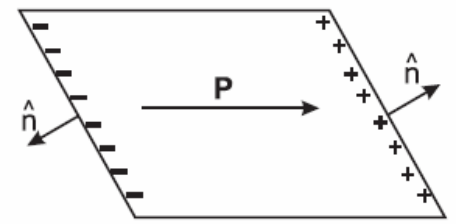

Figure 3.17 Surface charge density generated by a bulk polarization at an interface[34].

Now free energy is defined as follows:

$$F(P,s(P)) = \frac{1}{2}aP^2 + \frac{1}{4}(b-2d^2/K)P^4 + \frac{1}{6}cP^6 + ... - EP \tag{3.16}$$

The only change can be done by reducing quadratic coefficient (sign of *d* doesn't influence anything). Thus, if $b < 0$ the transition is strongly forced to be first order, at that T_c is rised. If $2d^2/K > b > 0$ then there is second order transition transforms to first order when strain is reduced. Pyroelectrics take a separate position connecting ferroelectrics and piezoelectrics. Pyroelectricity in material also assumes presence of spontaneous polarization under certain conditions, but it is not necesseraly switched by applied eletric field. If pyroelectric shows ferroelectric properties it is usually used as a ferroelectric only. And vice versa pyroelectric properties are more useful if material doesn't possess strong ferroelectricity. Ionic arrangement in material results in spontaneous dipole moment and, thus, polarization existence. Then, if some stress is applied to pyroelectric material would indicate increase in polarization, but this is only in case if pyroelectric has

piezoelectric features as well. However, reversal effect is not possible by aplying electric field.

$$\Delta P = p \Delta T \tag{3.17}$$

where p is pyroelectric coefficient. Temperature sensitivity of a burglar alarm is one of the most useful applications of pyroelectricity.

3.6 Origin of domains

There is a microscopic region in material called domain that containes dipole moments that are oriented in one direction. Complexities of domain motion, switching, pinning lie at the center of device understanding. Domains formation can be referred to following reasons:

1) Non-uniformly strained structure;
2) Microscopic defects in material;
3) Thermal and electrical history (technological conditions of production);
4) Energetic advantage; etc [31], [33], [34].

Let us have a look at fig.3.17 where the net charge density on opposite sides of surface is presented. The microscopic displacement of positive and negative charges produces bulk polarizaton. If we would consider a small geometry, then charge density on syrface can be expressed as

$$\sigma = \vec{P} \cdot \hat{n}\,, \tag{3.18}$$

where n is vector normal to the boundary. Charge produced on surface results in appearence of internal and external fields that can themselves generate process of energy storing. Energy can be stored exactly in the same way as in capacitor. According to natural law of energy minimum, system will try to minimize produced energy by abolishing as far as possible. Therefore, for instance in thin films polarization will be oriented “lying down” on the film plate rather than perpendicular to it. Let us consider the situation of thin film that is thick in all dimensiones. Here it is advantagable to have domains with polarization parallel to the crystal surface. It can be arrange by appropriate orientation of domain walls.

$$\sigma = (\vec{P_1} - \vec{P_2}) \cdot \hat{n} \tag{3.19}$$

$\overrightarrow{P_1}, \overrightarrow{P_2}$ are polarizations of two domains. This formula describes interface charge density between two closely placed domains. There are two cases when charge density is equal to zero:

1) Polarizations are in antiparallel direction to each other;
2) Polarizations are parallel to the domain wall (this phenomena is called 180˚ domain wall).

There is 90˚ domain wall in nearly cubic lattice (that we usually have). It is shown on fig.3.18. Pictures presented below have something analogous with ideal configuration of magnet. The phenomenon of domain walls requires energy wasting due to following facts:

1) Microscopic difference between domain walls and bulk (there is no energy gain of polarized state formation);
2) Coupling of polarization to elasticity (strain fields sgould be compatible).

Complex subject of strain field affects more strongly in case of 90˚ domain walls (although for 180˚ domain wall there is no problem). Fig.19 (a) doesn't consider all homogenities that produced due to strain effects and therefore it is idealized in that way. In real ferroelectric we should remember that polarization charges on the surface can be screened by actual electric charges (generated from impurities, defects, migrating ions, etc.). This leads to one more fascinating effects as "imprinting" and "fatigue".

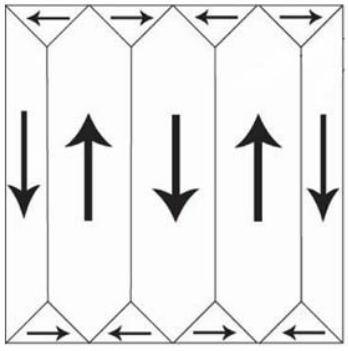

Figure 3.18 Individual domains illustration [41].

The polarization process is arranged in such way that +ve heads of pointers are placed near –ve heads, therefore strain field can be reduced as on fig.3.19 (b). The domains organization depends on grain size as well. If there is grain size less than 1 micron then the structure is likely one domain per one grain.

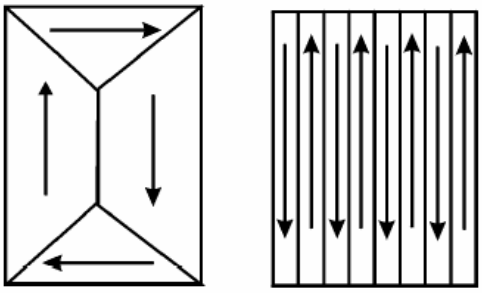

(a) (b)

Figure 3.19 Ideal domain configuration in a single crystal of cubic ferroelectric material where the coupling to strain is negligible (a), and configuration adopted when strain effects are important [34].

Of course, it is possible to find more than one domain in larger grains. The picture of domains within one grain is shown on fig. 3.20 [31], [33], [34].

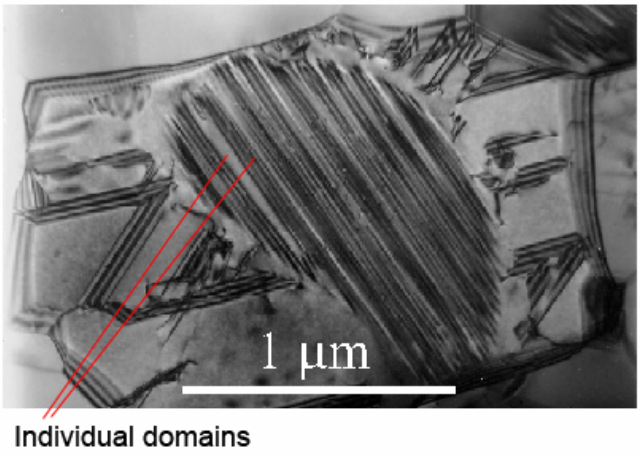

Figure 3.20 Individual domains in a single grain [41].

3.7 Microscopic features of ferroelectrics

Let us consider following model (see fig. 3.21) in order to understand lattice vibrations in simplest case. Top row represents atoms in their equilibrium conditions. Below that there is shown applied periodic distortion. Displacement U_n is plotted on the bottom figure, and sine wave shows periodical process with period $6a$. Oscillations in atom are occured near equilibrium position. Atoms are uniformly placed at a certain disctance a. Our crystal is regarded to be harmonic. There is restoring force depending linearly on extension. Then motion of n^{th} atom is

$$m\frac{\partial^2 U_n}{\partial t^2} = K(U_{n+1} - U_n) + K(U_{n-1} - U_n). \tag{3.20}$$

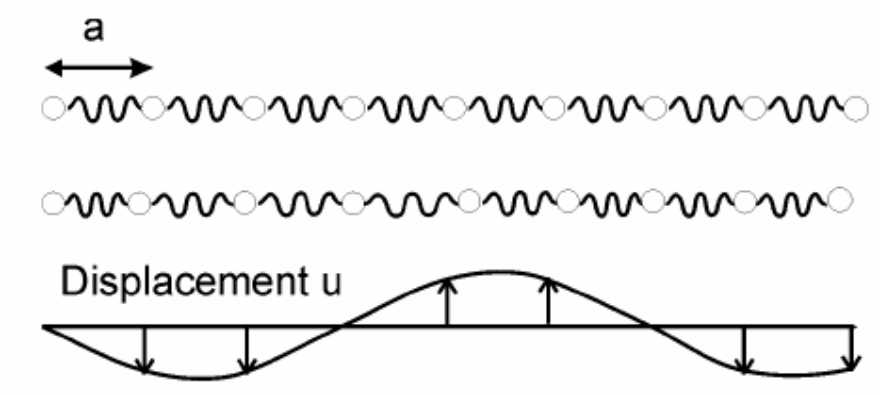

Figure 3.21 One dimensional linear chain [34].

Solution of equation is in a wave form:

$$U_n(t) = U_0 \cos(qr_n - \omega(q)t). \tag{3.21}$$

Wavelength and period are defined as follows:

$$\lambda = 2\pi/q \cdot T = 2\pi/\omega(q). \tag{3.22}$$

We can check the solution by substituting in equation that describes motion:

$$m\omega^2(q) = 2K(1 - \cos(qa)) = 4K\sin^2(\frac{qa}{2}), \tag{3.23}$$

at that

$$\omega(q) = 2(K/m)^{1/2}\sin(\frac{qa}{2}). \tag{3.24}$$

Now we derived a dispersion relation, i.e. relation between frequency and wavevector or wavelenght and period. In case of long wavelenght modes ($q \rightarrow 0$) equation reduced to linear form:

$$\omega(q) = (K/m)^{1/2}(qa). \tag{3.25}$$

There is a compressive sound wave at long wavelenght limit with velocity $v = a(K/m)^{1/2}$. It is defined as an acoustic mode due to similarity with sound.

However for larger q dispersion becomes periodic as it is shown on fig.3.22. We suppose that $q = 2\pi/a$. Then we can write that $qr_n = \frac{2\pi}{a} \times na = 2\pi n$. If $q = 0$, all atoms will be

uniformly displaced. Our considerations will be siplified to q vector in the range $-\frac{\pi}{a} \le q \le \frac{\pi}{a}$. This is actually the first Brillouin zone.

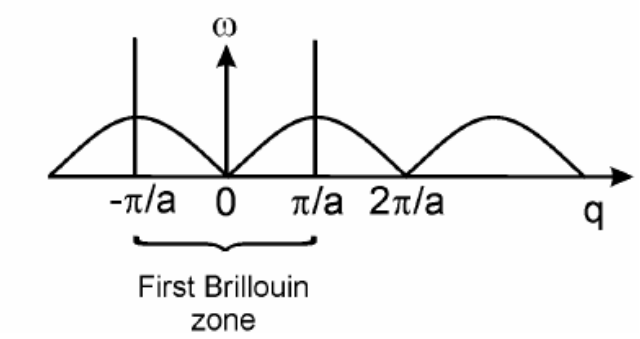

Figure 3.22 Dispersion relations between frequency and wavevector for a one-dimensional monoatomic chain [34].

However, monoatomic chain can not fully describe phenomena of ferroelectricity, in fact it is just the simplest case useful in superficial undestanding. Hence, futher we suggest two atoms in unit cell, i.e. the diatomic chain (fig. 3.23). Atoms (balls for simplicity) have different masses and different spring constants.

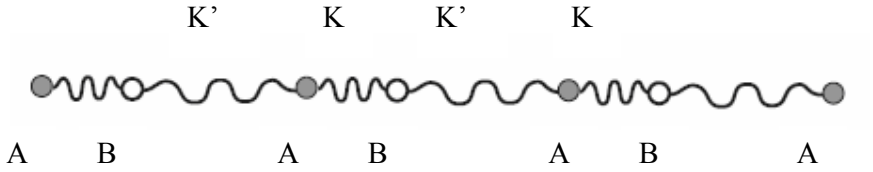

Figure 3.23 Diatomic chain [34].

Motion equation for each atom is:

$$m_A \frac{\partial^2 U_{nA}}{\partial t^2} = K(U_{nB} - U_{nA}) + K'(U_{n-1,B} - U_{nA}), \tag{3.26}$$

$$m_B \frac{\partial^2 U_{nB}}{\partial t^2} = K'(U_{n+1A} - U_{nB}) + K(U_{n,A} - U_{nB}). \tag{3.27}$$

To find out solution of these equaions we make several assumptions:

1) Two atoms are strongly connected together in pairs (as it is shown on fig.3.23);
2) Therefore, in first approximation, the pairs are regarded to be independent molecule ($K >> K'$);
3) $m_A = m_B = m$.

There is a vibrational mode originating from oscillation of two atoms out of phase with frequency:

$$w_0^2 = 2K/m. \tag{3.28}$$

Coordinate corresponded with it:

$$U_{opt}(q=0) = U_A - U_B \tag{3.29}$$

At $q = 0$, molecule undergoes oscillation in phase with next one. There is a frequency that vanishes linearly with wavevector along one part of dispersion curve (at that there is a finite frequency in the other mode, $q \rightarrow 0$). By means of absorbtion of scattering the optical phonons interact with light at long wavelenghts. Thus, they possess adequate properties of solids in the infrared spectrum (in the absorbtion and Raman spectra).

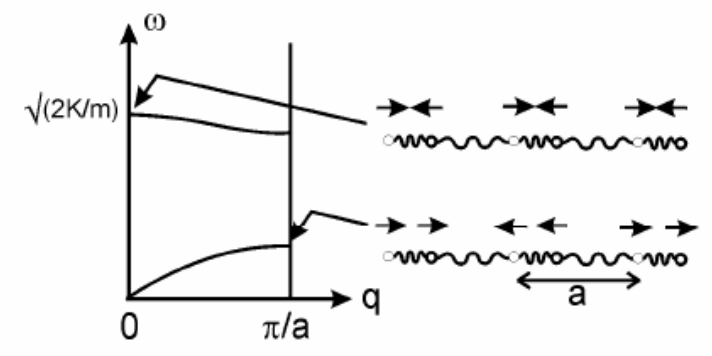

Figure 3.24 Optical and acoustic phonon branches have a dispersion in a diatomic chain. Displacement of atoms in optical mode ($q = 0$) [34].

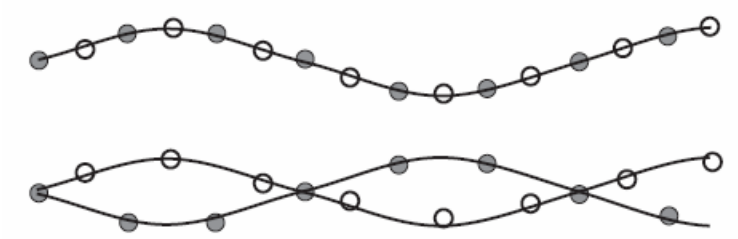

Figure 3.25 Displacement of acoustic and optic phonon of the same wavevector [34].

Presented above 1D and 2D cases can be generalised to 3D chain. It is, however, mathematically not easy, bacause we must consider propagation in different direction regard to a three-dimensional dispersion. There are found three branches of phonons in each unit cell: two transverse and one longitudinal. If there are N atoms in solid, thus it is expected *3(N-1)* optical modes in unit cell. Each optical mode consists from two transverse and one longitudinal (see fig. 3.24 and fig. 3.25). [34]

3.8 Softening mode

Let us now examine a question of phase transition in ferroelectric from the point of view of lattice vibrations theory. There is transition at Curie temperature to which we cool ferroelectric. At that we have double minimum on free energy vs polarization diagram. In order to understand what happens with phonons we follow certain steps in our considerations. It is assumed that vibration amplitudes are small (possible to spread out the potential regard to minimum of the energy). We again follow Hook's law, because there is elastic energy in spring:

$$U(x) = \frac{1}{2} K x^2 , \tag{3.30}$$

where K is spring constant.

It is supposed that the internal energy in above presented formula can be substituted by the free energy from the Landau theory. Polarization is connected directly with the amplitude of a certain lattice displacement U.

$$U_{opt} = U_A - U_B \tag{3.31}$$

Thus, the optical phonon amplitude and the polarization depend on each other as

$$P = \frac{1}{V_{cell}} (e_T^* U_{opt} + O(U_{opt}^3)) \tag{3.32}$$

e_T^* is "transverse effective charge". The frequency of $q=0$ in equation must be eliminated due to transition. It can be explained by following equations

$$m \frac{\partial^2 U_{opt}}{\partial t^2} = -\frac{\partial F}{\partial U_{opt}} \propto -a(T) U_{opt} \tag{3.33}$$

$$\text{and } w(q=0)^2 \propto \frac{1}{\chi} . \tag{3.34}$$

The last equation suits well to many material types. The softening mode can be clearly seen on the fig.3.27 where presented phonon dispersion relation for $SrTO_3$. There is lowest optical phonon branch near originl one that rapidly gets stronger by increase of q. As soft we can consider long wave components of the optical phonon mode. Temperature influences modes only within small region. Softening mode exists not only at the center of zone but also at the zone edge in acoustic mode. The last one is assumed to be not fully ferroelectric even at high values of permittivity, so called latter mode.

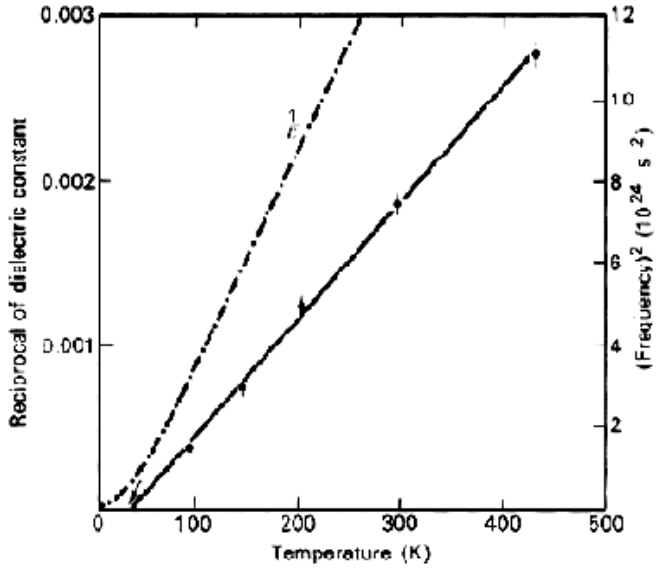

Figure 3.26 Comparison of the temperature-dependence of the square of an optic phonon frequency with the inverse of the dielectric susceptbility in $SrTiO_3$ [42].

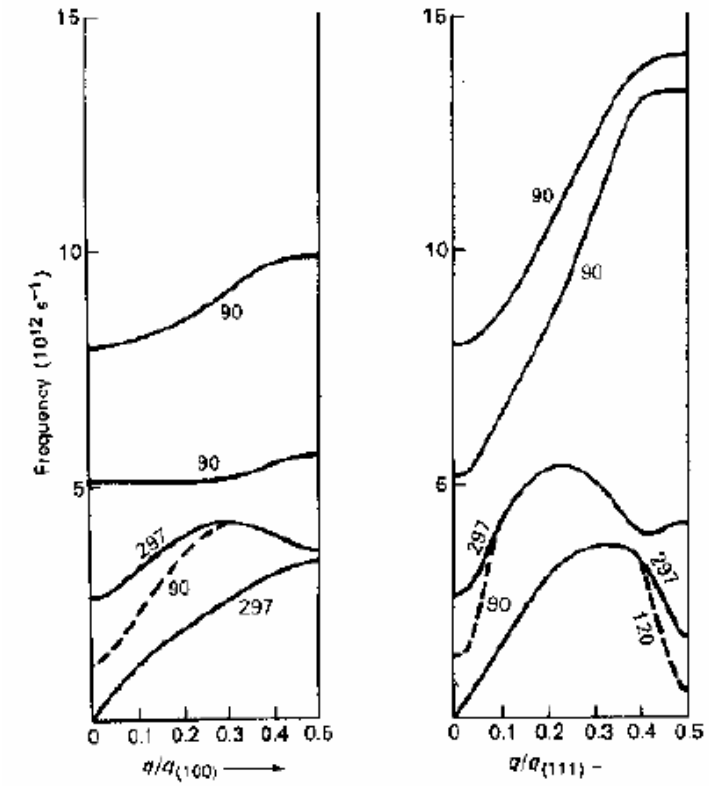

Figure 3.27 Phonon dispersion relations for $SrTiO_3$ measured at different temperatures for those modes where a considerable change with temperature is seen. There is both softening of the optical phonon near $q = 0$ as well as a zone boundary phonon ($q = (\pi/a)$ (111)) [43].

3.9 Crystalline structure of the most important ferroelectrics

The Bravais unit cell describes the lattice structure and determines the crystal symmetry of a certain material. According to the symmetry elements all variety of crystal types can be divided into 230 space groups and there are just 32 point groups. There are seven crystal systems assigned into 32 point group in the table 3.1 [33].

Table 3.1 Crystal systems classification [33].

Crystal Structure	Point Groups	Centro-symmetric	Non-centrosymmetric	
			Piezoelectric	Pyroelectric
Triclinic	1, 1	1	1	1
Monoclinic	2, m, 2/m	2/m	2, m	2, m
Orthorhombic	222, mm2, mmm	mmm	222, mm2	mm2
Tetragonal	4, 4, 4/m, 422, 4mm, 42m, (4/m)mm	4/m, (4/m)mm	4, 4, 422, 4mm, 42m	4, 4mm
Trigonal	3, 3, 32, 3m, 3m	3, 3m	3, 32, 3m	3, 3m
Hexagonal	6, 6, 6/m, 622, 6mm, 6m2, (6/m)mm	6/m, (6/m)mm	6, 6, 622, 6mm, 6m2	6, 6mm
Cubic	23, m3, 432, 43m, m3m	m3, m3m	23, 43m	-

Further classification gives us possibility to identify crystals with and without a center of symmetry. In the above mentioned table there are eleven point groups labeled as a centrosymmetric. These groups don't possess polarity. Other twenty one groups are not characterized by the center of symmetry (non-centrosymmetric). With the exception of 432 group, all other groups show piezoelectric effect along certain axes. This is property of material to obtain an electrical charge proportionally to a mechanical stress. Below the equations for direct and converse piezoelectric effect are presented.

$$P_i = d_{ijk}\, s_{jk}$$
$$\varepsilon_{ij} = d_{kij}\, E_k\ , \tag{3.35}$$

where P_i is polarization, s_{jk} is applied stress, d_{kij} is piezoelectric coefficient, ε_{ij} is strain generated after application of an electric field E. From twenty point groups possessing piezoelectric properties ten point group (1, 2, m, mm2, 4, 4mm, 3, 3m, 6, and 6mm) can obtain spontaneous polarization because they have only one unique direction axis. These crystals are called polar.

The pyroelectric effect is a property of material to change its spontaneous polarization due to change in temperature.

$$\Delta P_s = \pi \Delta T \tag{3.36}$$

ΔP_s is spontaneous polarization vector, π is pyroelectric coefficient and ΔT is change in temperature. [33] Let us now move on to lattice structure properties of the most investigated ferroelectric materials.

3.9.1 Barium titanate

Discovery of $BaTiO_3$ stimulated growing interest to ferroelectrics. Simple structure and set of unique properties of $BaTiO_3$ encouraged many scientists to investigate it after the war time, 20th century [4].

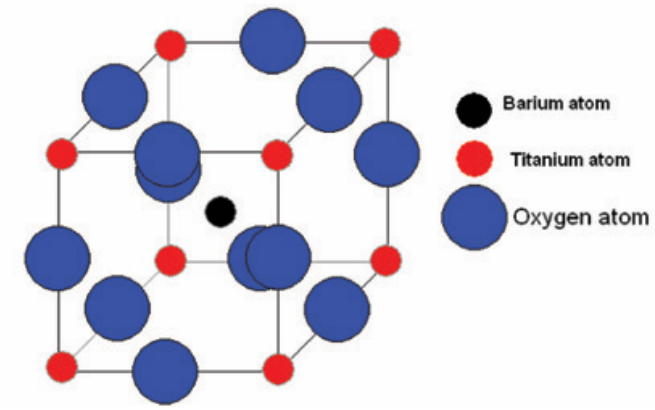

Figure 3.28 Barium titanate [44].

Perovskite structure type is characteristic of many ferroelectric materials. In addition to $BaTiO_3$ itself, in this type are crystallized, for instance, lead titanate ($PbTiO_3$), lead zirconate titanate (PZT), lead lanthanum zirconate titanate (PLZT), lead magnesium niobate (PMN), potassium niobate ($KNbO_3$), potassium sodium niobate ($K_xNa_{1-x}NbO_3$), and potassium tantalate niobate ($K(Ta_xNb_{1-x})O_3$) [33]. Perovskite type is usual for materials with chemical formula ABX_3, where A and B are cations, and X is anion. The structure consists from BX_6 octahedrons (see fig.3.29 and fig.3.31) connecting with each other in crystal tips. Octahedrons are arranged in such a way, that along all three orthogonally related axes one can distinguish octahedrons series parallel with each other (see fig.3.29). The cations A are situated in space between octahedrons.

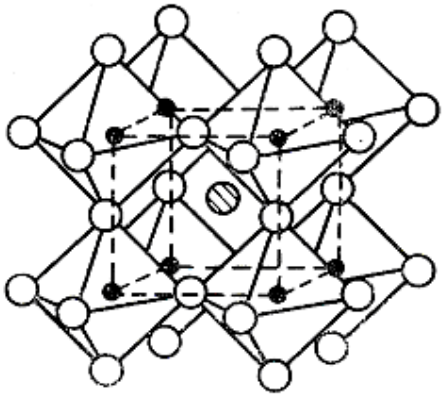

Figure 3.29 Perovskite structure [45].

Thus, cations B are surrounded by six anions X, and cations A, placed at the center of cubooctahedron, are surrounded by twelve anions X. The anions X are surrounded by six cations:

1) Four cations A at a distance of $a/\sqrt{2}$ (a represents cubic lattice parameter) and they are placed in square's tips. The center of this square is anion.
2) Two cations B at a distance *a/2* placed in a direction perpendicular to the square consisting of ions A.
3) Classic lattice structure of nonferroelectric perovskite phase has a cubic symmetry and belongs to space group O^1_h-Pm3m. [45]

For compound ABX_3 there is requirement concerning size of ions:

$$R_B \geq 0.41R_X,\ t_1 \prec t = \frac{R_A + R_X}{\sqrt{2}(R_B + R_X)} \prec t_2 \tag{3.37}$$

Here R_B and R_X are ionic radiuses for coordination number 6, and R_A is ionic radius for coordination number 12 (R_{12} is equal to $1.12R_6$). As a rule coefficients t_1=0.76 and t_2=1.03.

In case of difficult perovskite compound there is general chemical formula:

$$(A'_{X_1} A''_{X_2} ... A^{(i)}_{X_i} ... A^{(k)}_{X_k})(B'_{Y_1} B''_{Y_2} ... B^{(j)}_{Y_j} ... B^{(l)}_{Y_l})X_3, \text{ where } \sum_{i=1}^{k} X_i = 1 \text{ and} \sum_{j=1}^{l} Y_j = 1. \tag{3.38}$$

At the same time the rule of electrical neutrality for the crystal must be observed:

$$\sum_{i=1}^{k} X_i n_i + \sum_{j=1}^{l} Y_j n_j + 3n_X = 0, \tag{3.39}$$

where n_i, n_j and n_X are valences of A, B and X ions respectively.

However, not at all combinations of ions that meet above mentioned requirements, the desirable compound with perovskite structure will be formed. [45] Reason for that is bias of ions towards formation of different types of hybrid bonds. It leads to different anionic surroundings and consequently can lead to some discrepancies between perovskite and resulting structures [45]. By substituting various A and B in different concentration it is possible to affect ferroelectric properties of material [33]. Barium titanate is one of the most investigated ferroelectric materials with the perovskite structure. Above Curie temperature (120˚ - 130˚C) this compound has cubic structure with lattice parameter of approximately 4 Å.

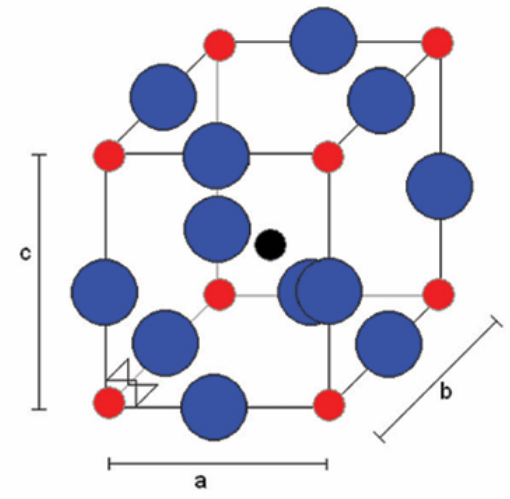

Figure 3.30 Change of cubic phase to tetragonal of barium titanate with lengthening of the c lattice parameter. This is generally associated with a movement of Ti atom iside O ochtahedron. O and Ba atoms moved also, $a = b \neq c$, $\alpha = \beta = \gamma = 90^\circ$ [46].

Below 120˚C it becomes ferroelectric and tetragonal (see fig. 3.30) with space group C^1_{4v}-P4mm. Spontaneous polarization is directed along axis *z*. Along the same direction the ions are shifted. Around 0˚C there is phase transition from tetragonal to ferroelectric orthorhombic phase (fig.3.32) with spontaneous polarization along diagonal of cubic cell's side. Along the same diagonal occurred lengthening of the cell. Therefore, the cell shows monoclinic distortion.

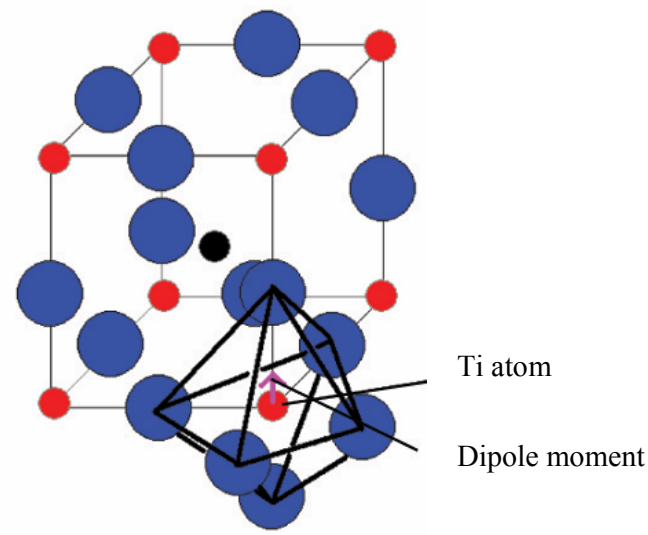

Figure 3.31 Ti atom is surrounded by O6 ochtahedron [46].

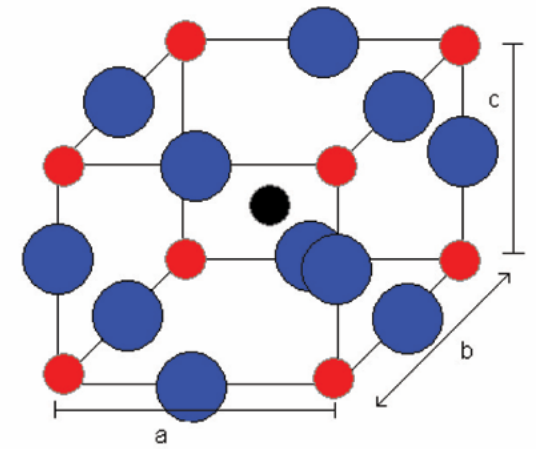

Figure 3.32 Ortorhombic phase, $a \neq b \neq c$, $\alpha = \beta = \gamma = 90^{\circ}$ [46].

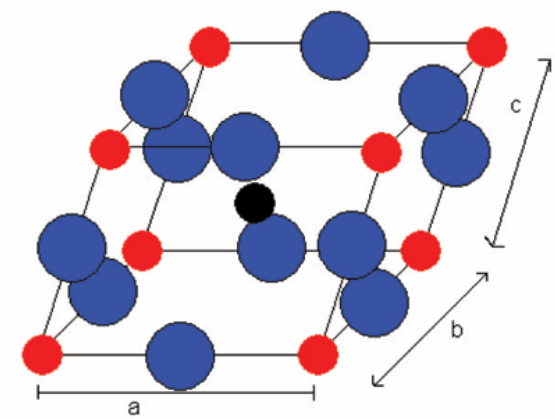

Figure 3.33 Rhombohedral phase, $a \neq b \neq c$, $\alpha = \beta \neq \gamma$ [46].

.

At temperatures from -70˚C up to -90˚C there is phase transition to ferroelectric rhombohedral phase with space group – C^5_{3v}-R3m (fig.3.33). In this case the spontaneous polarization and cell lengthening are directed along main diagonal of cubic cell. It has been shown that dielectric properties of BaTiO3 are affected by the grain size [45], [47] – [49].

3.9.2 Lead Titanate ($PbTiO_3$, PT)

This ferroelectric has the same structural properties as barium titanate. The Curie point is approximately 490° C. The transition from paraelectric cubic phase to ferroelectric tetragonal phase takes place at the Curie temperature. One serious disadvantage of lead titanate is difficulties in production of free-crack ceramic. There is large number of cracks appeared due to change of sample volume during cooling below the Curie temperature. However, this problem can be avoided by use of a special doppants such as Ca, Sr, Ba, Sn, and W. One example is a recently investigated compound $(Pb_{0.76}Ca_{0.24})((Co_{0.50}W_{0.50})_{0.04}Ti_{0.96})O_3$. This has shown better characteristics with proper use of dopants [50] – [53]. It has the Curie point at 255˚C.

3.9.3 Potassium dehydrogenate phosphate (KDP)

KH_2PO_4 has tetragonal lattice structure at 20˚C and belongs to noncentro-symmetrical space group $D^{12}_{2d} - I\bar{4}2d$ with *a*=7,453Å and *c*=6,959Å lattice parameters (*a, c* are parameters of monoclinic cell). Crystals described by this space group are piezoelectric. It is possible to choose another low-level cell in space group *F4d2*. Atomic arrangement in tetragonal low-level cell is shown on fig. 3.34. The lattice consists of almost regularly shaped tetrahedrons PO_4. In space between tetrahedrons are situated ions of potassium, each of them is surrounded by eight atoms of oxygen from PO_4; moreover, four from these oxygen atoms are more close to potassium than other four. Each group of PO_4 is connected with four neighboring groups of PO_4 with hydrogen bonds of about 2.4 Å. At -150˚C is ferroelectric phase transition; lattice obtains rhombohedral symmetry and belongs to space group $C^{19}_{2v} - Fdd$. The length of hydrogen bonds doesn't change a lot. The spontaneous polarization has direction along c axis and its origin depends on shifts of heavy atoms along *c* [33], [45].

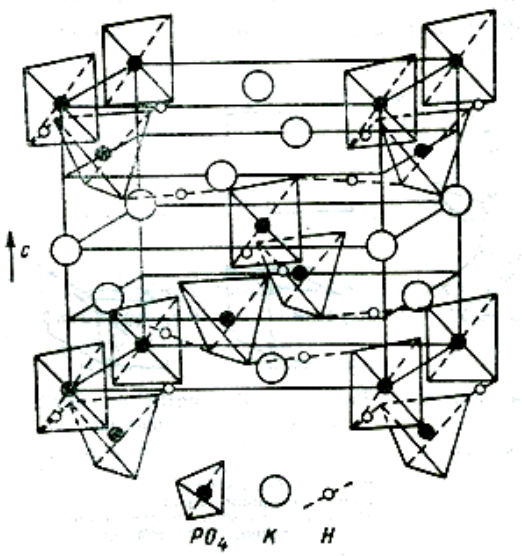

Figure 3.34 KDP low-level cell [45].

3.9.4 Rochelle salt (Seignette salt)

Seignette salt is double tartrate of natrium- potassium $NaKC_4H_4O_6 \cdot 4H_2O$. In non-ferroelectric state above 23 - 24˚C it has rhombic structure. Lattice structure parameters at 35˚C are a = 11.878; b = 14.246; c = 6.812Å. Lattice is decribed by space group $D_2^3 - P2_12_12$. Projection of structure on (100) is shown on fig. 3.35. Each ion of natrium is surrounded by six oxygen atoms at an average distance of 2.39 Å. Three of these oxygen atoms belong to tartrate group and three to water molecule. Atoms of potassium have coordination number four and eight. Ferroelectric phase that exists in the temperature range from -18˚C up to +24˚C is monoclinic. Low temperature phase of Seignette salt is stable below -18˚C.

According to neutron diffraction analysis for the existence of ferroelectric state it is important which orientation has hydroxyl group marked with number 5 on the fig.3.35. Change in orientation of this group can lead to change in electrical torque direction and thus influences the process of spontaneous polarization. [45]

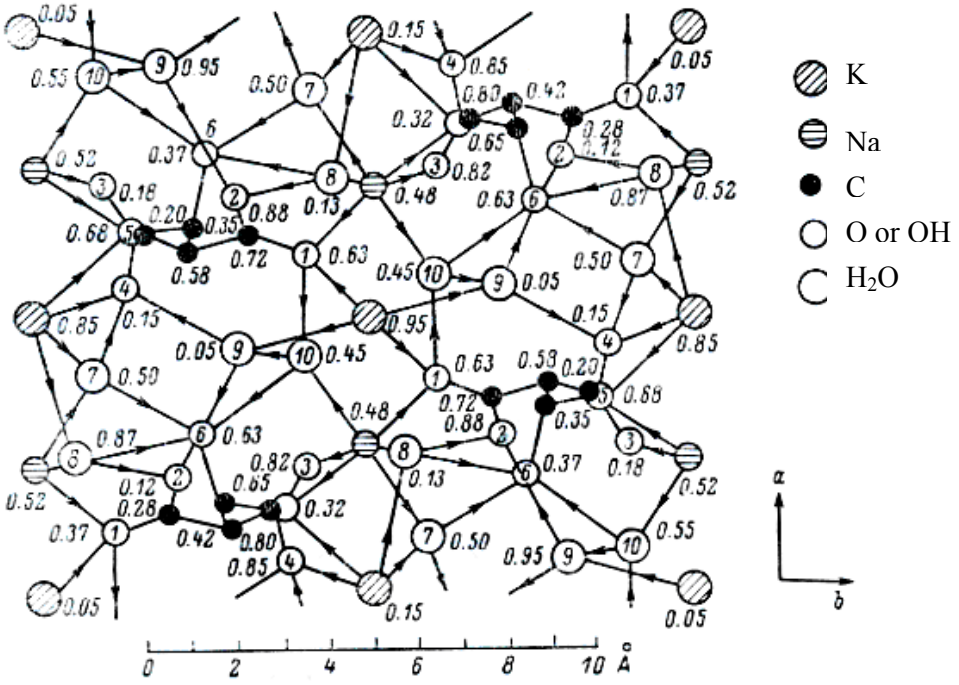

Figure 3.35 Projection of Rochelle Salt structure on (001) [45].

3.9.5 Stibium sulfoiodide

SbSI is ferroelectric with Curie temperature of about 22˚C. Lattice structure in both paraelectric and ferroelectric phases has rhombic symmetry. The investigations have shown that ferroelectric phase transition belongs to displacement transition type or very close to it. Fig.3.36 reflects the lattice structure of *SbSI*. [45]

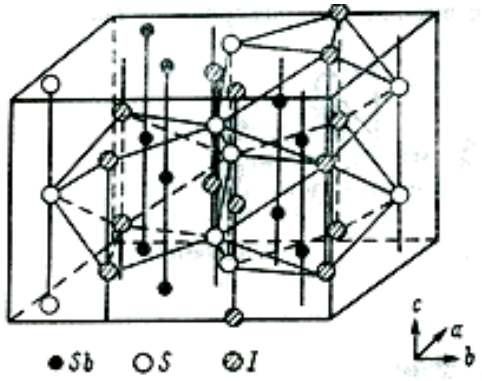

Figure 3.36 SbSI structure [45].

3.9.6 Sodium nitrite

$NaNO_2$ is ferroelectric below 163˚C. It has rhombic structure at room temperature with space group is $C_{2v}^{20} - \mathrm{Im}2m$ and lattice periods a = 3.560Å; b = 5.563Å; c = 5.384Å. $NaNO_2$ can be presented as NaCl lattice where Cl is substituted for NO_2^- with angle O-N-O equal to 115˚. Natrium atoms are surrounded by six NO_2^- ions, and NO_2^- ions are surrounded by six natrium ions. NO_2^- group has strong covalent bonds.

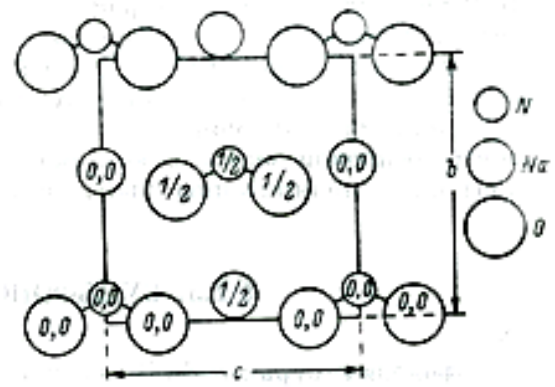

Figure 3.37 Projection of $NaNO_2$ structure on (001) [45].

Between paraelectric and ferroelectric phases there are some intermediate phases in narrow temperature range. At 163˚C occurs a phase transition from usual ferroelectric phase to sinusoidal modulated ferroelectric phase. Electrical torque of low-level cells changes in this phase from its minimal to maximal value. However this modulated phase exists only in narrow temperature range of about one degree or even less. Temperature range of modulated phases depends strongly on thermal history of crystal, meaning on temperature parameters of crystal growth and processing [45].

3.9.7 Gadolinium molybdate

$Gd_2(MoO_4)_3$ is an example of extrinsic ferroelectric. Above the Curie temperature (T = 159˚C) it has tetragonal symmetry with the space group $D_{2d}^3 - P\bar{4}2_1m$. The lattice structure of $Gd_2(MoO_4)_3$ contain three different alternate layers of isolated octahedrons

$(MoO_4)^{2-}$ connected with each other by gadolinium ions. Gd^{3+}gadolinium ions are surrounded by seven oxygen ions that belong to different tetrahedrons [45].

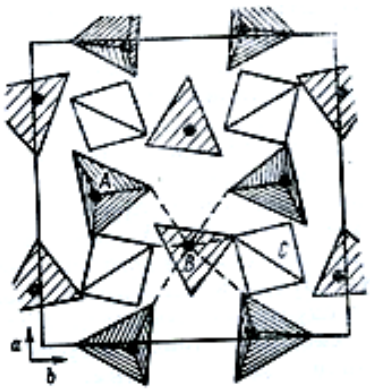

Figure 3.38 $Gd_2(MoO_4)_3$ projection on ab surface [45].

3.9.8 Lead Zirconate Titanate [$Pb(Zr_xTi_{1-x})O_3$, PZT]

Lead Zirconate Titanate (PZT) is synthesized from of $PbZrO_3$ (antiferroelectric, orthorhombic structure) and $PbTiO_3$ (ferroelectric, tetragonal perovskite structure), thus it is a binary solid solution. Fig.3.39 represents phase diagram of this material.

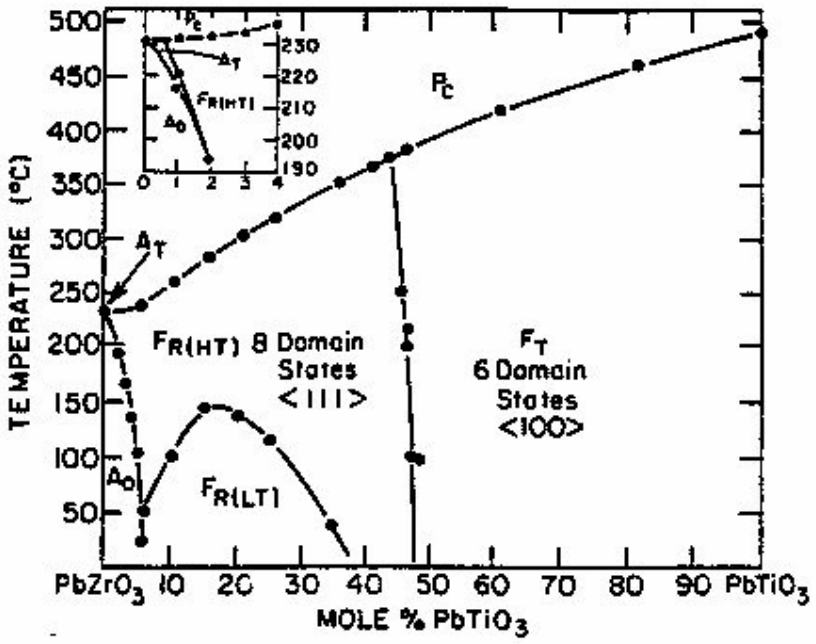

Figure 3.39 PZT phase diagram [33].

Below the Curie temperature PZT structure has ferroelectric tetragonal or rhombohedral phase. <100> is a polarization direction for the tetragonal phase, while <111> is a direction in rhombohedral phase. At high temperatures PZT possesses cubic perovskite structure (paraelectric phase) [33].

3.9.9 Lead Lanthanum Zirconate Titanate ($(Pb_{1-x}La_x)(Zr_{1-y}Ti_y)_{1-x/4}O_3V^B_{0.25x}O_3$, PLZT)

PLZT is a ferroelectric obtained by means of doping La^{3+} ions into lead zirconate titanate (PZT) structure. As well as barium titanate and PZT it has the perovskite structure. There are two possibilities to deduce general chemical formula for this compound:

1) $(Pb_{1-x}La_x)(Zr_{1-y}Ti_y)_{1-x/4}O_3V^B_{0.25x}O_3$

2) $(Pb_{1-x}La_x)_{1-0.5x}(Zr_{1-y}Ti_y)V^A_{0.5x}O_3$

The difference in these formulas consists in fact that La^{3+} ions can be placed on the A site, thus vacancies are situated on the B site V^B (1st formula) in order to keep charge balance. For the 2nd formula vacancies are obviously on the *A* site. Of course the real structure can contain combination of the A and B vacancies. The phase diagram at a room temperature is presented on fig.3.40.

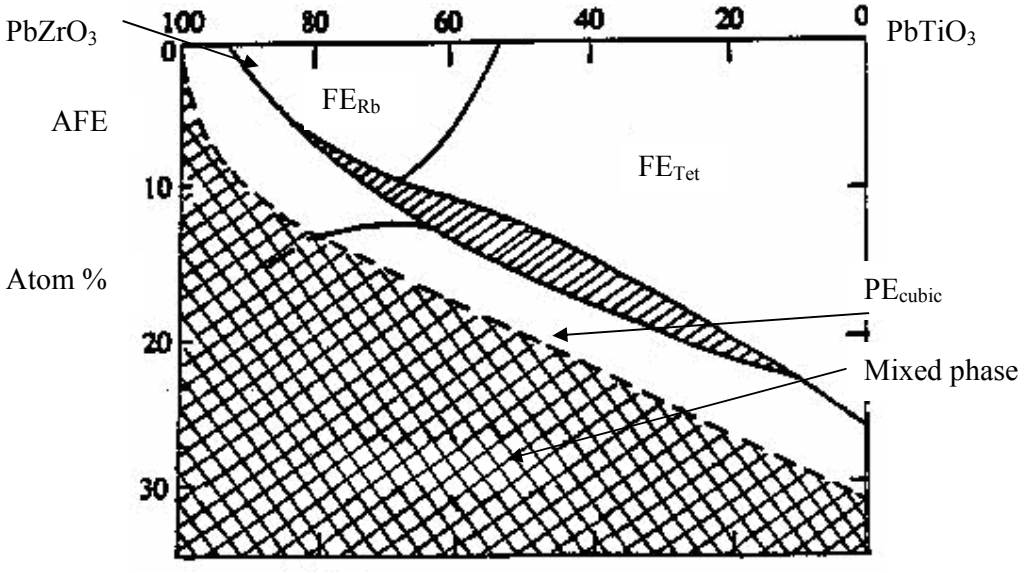

Figure 3.40 Room temperature phase diagram of the *PLZT* system, where FE_{Rb} is rhombohedral ferroelectric phase, FE_{Tet} is tetragonal ferroelectric phase, PE_{cubic} is cubic relaxor paraelectric phase, *AFE* is antiferroelectric phase [54].

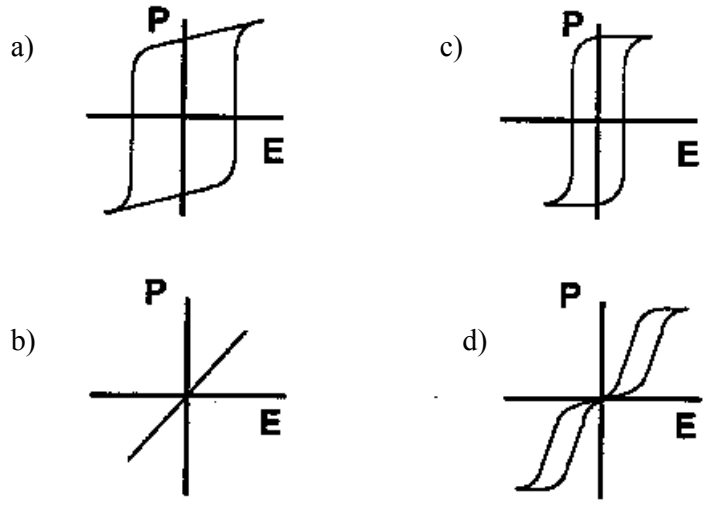

Figure 3.41 Representative hysteresis loops (a) FE_{Tet}, (b) FE_{Rb}, (c) FE_{cubic} and (d) AFE for different ferroelectric compositions [54].

Fig.3.41 shows the variety of hysteresis loops for this material in ferroelectric, tetragonal; ferroelectric rhombohedral; ferroelectric cubic and antiferroelectric states.

3.9.10 Lead Magnesium Niobate ($Pb(Mg_{1/3}Nb_{2/3})O_3$, PMN)

This group of relaxor ferroelectrics can be expressed generally with formula $Pb(B_1,B_2)O_3$. B_1 is a cation of lower valence (Mg^{2+}, Zn^{2+}, Ni^{2+}, Fe^{3+}). B_2 represents the cation with higher valence (Nb^{5+}, Ta^{5+}, W^{5+}). Clean PMN has Curie temperature -10˚C. For easier understanding of the difference between relaxor and normal ferroelectric their properties are analyzed in table 3.2. Temperature dependence of dielectric permittivity for PMN is on fig.3.42 which shows that this group of materials possesses strong frequency dependence of dielectric constant. In addition, it is relevant to mention that the most investigated relaxor ferroelectric is PMN - PT (see diagram fig.3.43). This solution shows shift in Curie temperature to higher regions. Material compositions 0.65 PMN + 0.35 PT show piezoelectric properties, 0.95 PMN + 0.10 PT have extremely large values of permittivity (ε > 20,000). These properties make PMN attractive for different application solutions.

Table 3.2 Difference between relaxor and normal ferroelectric [33].

Property	Normal ferroelectric	Relaxor ferroelectric
Dielectric temperature dependence	Sharp 1st or 2nd order transition at Curie point T_c	Broad diffused phase transition at Curie maxima
Dielectric frequency dependence	Weak Frequency dependence	Strong frequency dependence
Dielectric Behavior in paraelectric range ($T > T_c$)	Follows Curie - Weiss law	Follows Curie - Weiss law
Remnant polarization (P_R)	Strong P_R	Weak P_R
Scattering of light	Strong anisotropy	Very weak anisotropy to light
Diffraction of X-Rays	Line splitting due to deformation from paraelectric to ferroelectric phase	No X-Ray line splitting

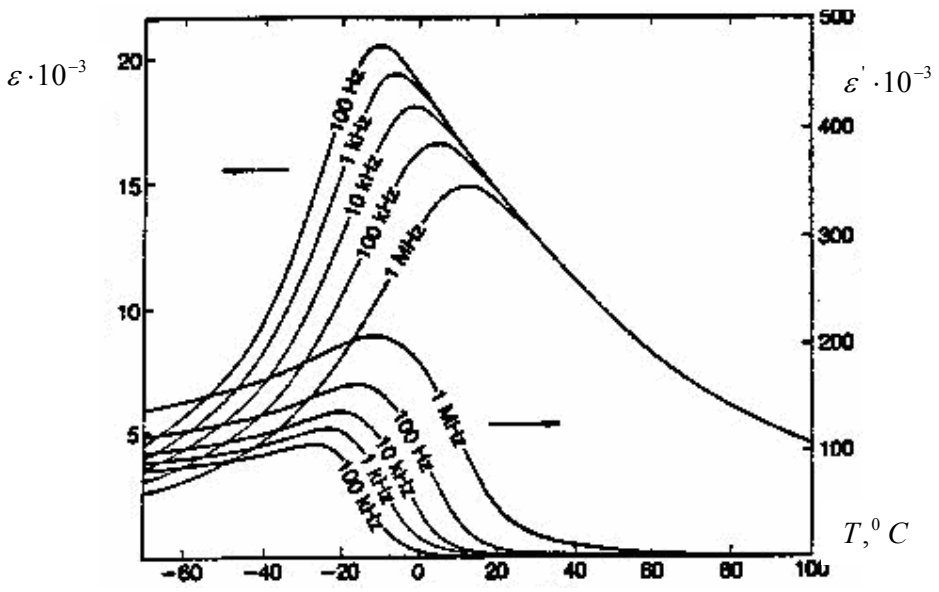

Figure 3.42 Temperature dependence of the dielectric permittivity of PMN [33].

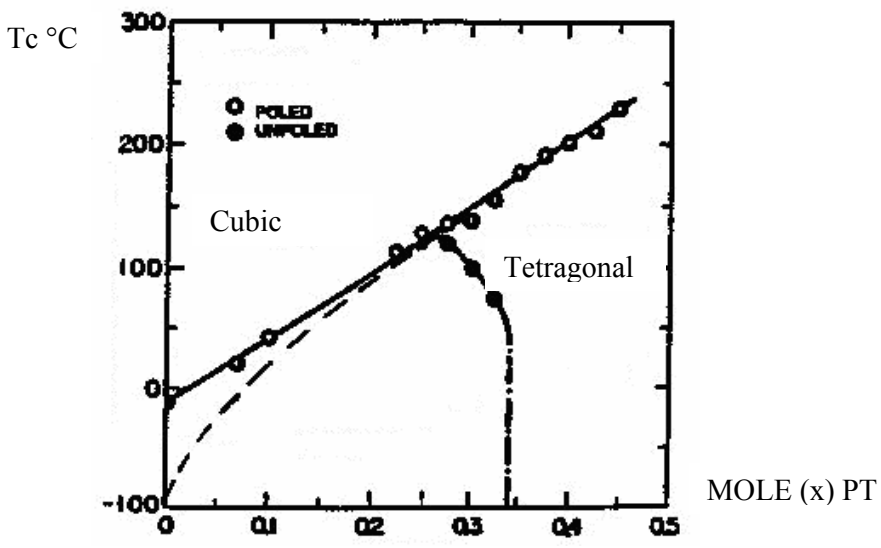

Figure 3.43 Phase diagram for PMN-PT solid solution [33].

3.9.11 Tungsten Bronze type Compounds

$PbNb_2O_6$ is the most famous representative of tungsten bronze group. The projection of this structure type on (001) plane is shown on fig.3.44. Production of this ceramic material assumes certain difficulties; therefore it represents a lack of use. [45]

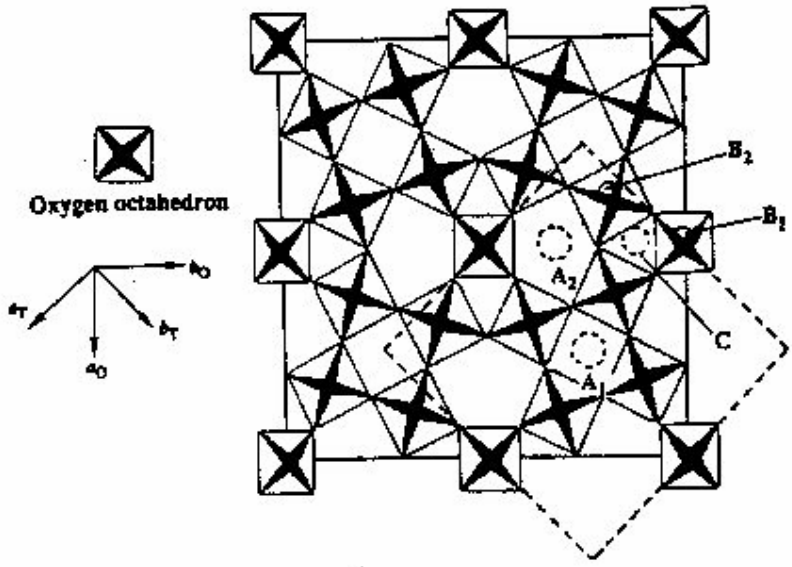

Figure 3.44 Tungsten-bronze structure projection on the (001) plane;
The orthorhombic and tetragonal cells are shown by solid and dotted lines respectively [45].

3.9.11 Lithium Niobate and Tantalate

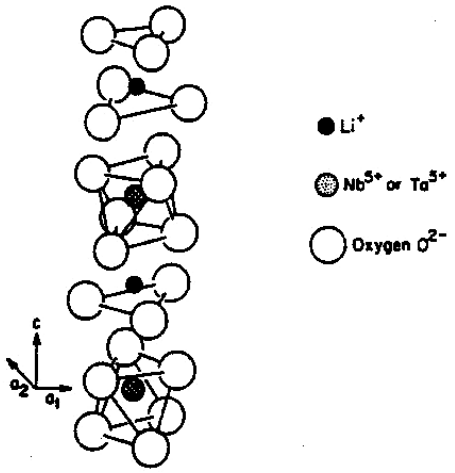

Figure 3.45 Structure of $LiNbO_3$ and $LiTaO_3$ [56].

$LiNbO_3$ and $LiTaO_3$ are discussed together due to similarity of their lattice structures and properties (see fig.3.45). $LiNbO_3$ has transition temperature at 1210 ˚C and $LiTaO_3$ at 620 ˚C [33], [45].

3.9.13 Organic Polymers

Organic materials such a polyvinylidene fluoride (PVDF, $(CH2\text{-}CF2)_n$) and copolymers of PVDF with trifluoroethylene {P(VDF-TrFE)} are adopted as piezoelectric and pyroelectric materials. The Curie temperature varies between 70 – 100 ˚C [33].

The list of ferroelectric materials could be preceded further. However, we took as objectives just to make a short overview.

4 SCIENTIFIC ACHIEVEMENTS IN THE ELECTROCALORIC EFFECT

In order to obtain low temperatures in macroscopic systems, physical effects such as thermodynamic change in pressure, volume, electric and magnetic field intensities are used. In case of a gas microscopic systems there are throttling and adiabatic expansion effects. These effects are in basis of refrigerating machines that provide cooling down to liquid helium temperature. Further application of these machines, for instance, in radio electronics, clearly indicated some discrepancies in electronic compatibility issues:

1) Disproportion between mass, HWD of refrigerating machine and cooled object;
2) Significant power consumption of refrigerating machine in comparison to power consumption of radio electronic device;
3) No-failure operation intervals are shorter for refrigerating systems compared to radio electronic device.

All discrepancies between refrigerators and electronic devices can be avoided only by adaptation of a new refrigerator type. At the present moment this possibility is given by two similar effects in solid state – magnetocaloric (magnetization/demagnetization processes induce temperature change) and electrocaloric cooling (polarization/depolarization processes induce temperature change). There are two relevant construction schemes for refrigerator. First one assumes addition of gaseous refrigerating medium. It must lead to effective heat exchange between refrigerator elements, between its element and cooled object, as well as between a certain element and thermal reservoir of big capacity. Electrocaloric effect is a property of all dielectrics. But it is more significant in materials with high polarization and strong dependence of dielectric properties on temperature. In a best way these requirements are met in ferroelectric materials. First steps in electrocaloric effect study were made by Kurchatov and Kobeko (1930). Till 1960 researchers paid only little attention to this phenomenon. In 1970 interest to electrocaloric effect had been growing again. Nowadays work under creation of solid state refrigerator is continuing.

Unfortunately, information about electrocaloric coefficient $\alpha = \left(\frac{\partial T}{\partial E}\right)_S$, temperature change under applied electric field $\Delta T = \int_0^E \alpha \cdot dE$ and value of cooling efficiency of

ferroelectric material is not presented in literature. In this situation neither theoretical nor design of solid state refrigerator are possible [6], [23].

4.1 Phenomenological theory of electrocaloric effect in ferroelectrics

Theory discussed in this section was developed in Saint-Petersburg State Electrotechnical University (LETI). At the heart of effect is temperature change of a dielectric under adiabatic conditions by applying or removing field. In practice the information about temperature ranges where effect is stronger and fields at which it can be achieved is of great importance. Below are given temperature and field dependences of ferroelectrics due to electrocaloric effect. As an initial point in our considerations we will use common expansion of free energy in thermodynamics - Ginsburg-Devonshire expansion:

$$F = F_0 + \frac{1}{2} a_{ij} P_i P_j + \frac{1}{4} b_{ijke} P_i P_j P_k P_e + G_{ijke} U_{ij} P_k P_e + c_{ijke} U_{ij} U_{ke} \qquad (4.1)$$

where F is free energy per unit volume, P_i is polarization vector projection on basis directions of low-level cell, a_{ij} is tensor components of low-level signal dielectric susceptibility, b_{ijke} are tensor components of dielectric nonlinearity, U_{ij} are components of crystal resilience, G_{ijke} are tensor components of electrostriction, c_{ijke} are tensor components of elastic modules, F_0 is component of free energy that doesn't depend on polarization. Free energy presentation in this form considers influence of thermal action, electric field and mechanical deformation on ferroelectric. Reasoning from a well-known entropy description $S = -\left(\frac{\partial F}{\partial T}\right)_p$ and adiabatic conditions, i.e. there is no heat transfer from environment to working medium and vice versa ($dS = 0$) for uniform electric field in sample with volume V that is free from mechanical stress we can write a balance equation for all increments in system (equation 4.2). Change of entropy dS is induced by change of polarization dP and temperature increase dT. F_0 is free energy of system. a is low-level dielectric susceptibility. $b' = b + 4 \cdot \frac{G^2}{c}$ is a constant of dielectric nonlinearity in stress-free sample. This hardly understandable equation leads, however, to clear mathematical form of the electrocaloric effect. Unfortunately, there is no possibility to argue about reliability of derived equation, because the electrocaloric effect is not

presented in literature in full measure. Derived futher equation describes effect from the position of thermodynanamics.

$$\begin{bmatrix} 2\frac{\partial V}{\partial T}\left(-\frac{\partial F_0}{\partial T}-\frac{1}{2}\frac{\partial a}{\partial T}p^2-\frac{1}{4}\frac{\partial b'}{\partial T}p^4\right)-V\left(\frac{\partial^2 F_0}{\partial T^2}+\frac{1}{2}\frac{\partial^2 a}{\partial T^2}p^2+\frac{1}{4}\frac{\partial^2 b'}{\partial T^2}p^4\right)- \\ -\frac{\partial^2 V}{\partial T^2}\left(F_0+\frac{1}{2}ap^2+\frac{1}{4}b'p^4\right) \end{bmatrix}\times dT + \\ + \begin{bmatrix} V\left(-\frac{\partial a}{\partial T}p-\frac{\partial b'}{\partial T}p^3\right)-\frac{\partial V}{\partial T}\left(ap+b'p^3\right)+\frac{\partial V}{\partial T}\left(-\frac{\partial F_0}{\partial T}-\frac{1}{2}\frac{\partial a}{\partial T}p^2-\frac{1}{4}\frac{\partial b'}{\partial T}p^4\right)- \\ -\frac{\partial^2 V}{\partial p\partial T}\left(F_0+\frac{1}{2}ap^2+\frac{1}{4}b'p^4\right) \end{bmatrix}\times dP=0 \quad (4.2)$$

Presented theoretical explanation is unique in its nature, therefore we can suggest that our research group is in the lead position in a problem of effect theoretical substantiation. For a majority of ferroelectric materials with second phase transition (there is no spasmodic[8] change of permittivity under transition temperature) following equation is also true:

$$\frac{1}{a}\frac{\partial a}{\partial T}\succ\frac{1}{\mathrm{V}}\frac{\partial V}{\partial T},\ \frac{1}{b}\frac{\partial b}{\partial T},\ \frac{1}{a}\frac{\partial^2 a}{\partial T^2},\ \frac{1}{b}\frac{\partial^2 b}{\partial T^2},\ \frac{1}{V}\frac{\partial^2 V}{\partial p\partial T}. \quad (4.3)$$

Almost all terms in equations 4.2 and 4.3 are negligible corrections, so it could be rewritten in a simple form:

$$\frac{\partial^2 F_0}{\partial T^2}dT+\frac{\partial a}{\partial T}PdP=0. \quad (4.4)$$

Here we assume that *S* is thermodynamically independent quantity. Let us rewrite it:

$$\frac{\partial^2 F_0}{\partial T^2}dT+\frac{P(E)}{a+3b'P^2(E)}\frac{\partial a}{\partial T}dE=0. \quad (4.5)$$

From thermodynamical relations follows:

$$\frac{\partial^2 F_0}{\partial T^2}=-\frac{C_{V_0}}{T}, \quad (4.6)$$

C_{V_0} is thermal capacity for a unit of volume, measured in zero bias electric field. Differential form of equation describing electrocaloric temperature change in ferroelectric that is in paraelectric phase:

[8] Irregular, convulsive.

$$dT = \frac{T}{C_{V_0}} \frac{P(E)}{a + 3b' P^2(E)} \frac{\partial a}{\partial T} dE \,. \tag{4.7}$$

It reflects, but not in obvious way, *dT* dependence on electric field and temperature. Field dependence is dictated by *P(E)*. Temperature dependence has in its origin polarization *P(E,T)*, thermal capacity $C_{V_0}(T)$, low-level signal dielectric susceptibility *a(T)*. To obtain total temperature change ΔT of ferroelectric, that induced by transition from state with zero bias field to non-zero field state, is needed to integrate (4.7). In general case, equation (4.7) has no solution because there is no possibility to separate variables *E* and *T*. However, in assumption of $\frac{\Delta T}{T} << 1$ solution can be found:

$$\Delta T = \frac{1}{2} \frac{T}{C_{V_0}} \frac{\partial a}{\partial T} p^2(E) \,. \tag{4.8}$$

From this one can get by means of elementary transformations the amount of heat needed to be rejected in order to keep material at initial temperature:

$$Q = \frac{1}{2} T \frac{\partial a}{\partial T} P^2(E) \,. \tag{4.9}$$

The temperature value in both (4.8) and (4.9) is an initial temperature. Electric field intensity describes the polarization process. In paraelectric phase *P* vs. *E* dependence has the only meaning and can be developed further. In accordance with well-known thermodynamic relation $E = (\frac{\partial F}{\partial P})_T$ let us construct the following equation:

$$E = aP + bP^3 \tag{4.10}$$

Its solution is presented below:

$$p = (2b)^{-\frac{1}{3}} \left\{ \left[\left(E^2 + \frac{4a^3}{27b} \right)^{\frac{1}{2}} + E \right]^{\frac{1}{3}} - \left[\left(E^2 + \frac{4a^3}{27b} \right)^{\frac{1}{2}} - E \right]^{\frac{1}{3}} \right\} . \tag{4.11}$$

Now it is already possible to collect values for electrocaloric change in paraelectric phase. For this purpose we need to know just three parameters of substance:

1) Dielectric nonlinearity constant;
2) Thermal capacity;
3) Low-level signal dielectric susceptibility.

It is necessary to say that above shown equations are in good correlations with experimental results [6], [23], [56].

4.2 Temperature dependencies of main ferroelectrics parameters

4.2.1 Low-level signal dielectric susceptibility (a)

From the mathematical point of view it is an aspect ratio in equation $E = aP$, where E is electric field, P is polarization (if E and P are small). In literature more often could be found low-level signal permittivity $\varepsilon(0) = (\varepsilon_0 a)^{-1}$. For virtual ferroelectrics (typical for $SrTiO_3$) the transition from paraelectric to ferroelectric state is not found down to helium temperatures. Therefore function above is in good agreement with experimental data obtained by scientific group of Prof. A.Prudan [23]:

$$\varepsilon(0,T) = \frac{A}{\frac{T_1}{2} cth\left(\frac{T_1}{2T}\right) - T_0}. \tag{4.12}$$

A, T_1, T_0 are function parameters and $\varepsilon(0,T)$ is low-level signal permittivity. For ferroelectrics with transition at $T = T_{ph.t.}$ the temperature dependence of low-level signal permittivity in paraelectric phase yields to the Curie-Weiss law:

$$\varepsilon(0,T) = \frac{C_k}{T - T_c} \quad . \tag{4.13}$$

In the equation 4.13 C_k is Curie constant, T_c is Curie temperature. Hence, $a(T)$ dependence at $T > T_{ph.t.}$ can be described by two function types:

$$a(T) = \frac{1}{\varepsilon_0 A}\left[\frac{T_1}{2} cth\left(\frac{T_1}{2T}\right) - T_0\right], \tag{4.14}$$

$$a(T) = \frac{1}{\varepsilon_0 C_k}(T - T_c). \tag{4.15}$$

Dielectric constant is $\varepsilon_0 = 8{,}85 \cdot 10^{-12} F/m$. In two-component ferroelectric solutions, for instance, $SrTiO_3$-$BaTiO_3$, $SrTiO_3$-$PbTiO_3$ negligible change in one of the components leads to significant Curie temperature shift. Below is presented a theoretical relation between Curie temperature and x (second component content) for solid solutions based on strontium titanate.

$$T_c(x) \propto (x - x_k)^{\frac{1}{2}}, \tag{4.16}$$

x_k is critical content of second component in solid solution. Exceed of x_k leads to appearance of ferroelectric phase transition. Theoretical justification for $T_c(x_k)$ is not presented in literature at all [6].

4.2.2 Constant of dielectric nonlinearity (b)

Information about b can be obtained from experimental data about field dependence of polarization in ferroelectric material:

$$\varepsilon(E) = \frac{1}{\varepsilon_0}\frac{dP(E)}{dE}. \tag{4.17}$$

For ferroelectric with second order phase transition constant *b* can be determined by following equation:

$$b = \frac{(\varepsilon(0) - \varepsilon(E))(\varepsilon(0) + 2\varepsilon(E))^2}{(3\varepsilon_0\varepsilon(0)\varepsilon(E))^3 E^2}, \tag{4.18}$$

E is electric field intensity and *ε* is permittivity. This method for determination of *b* is not the only one, there are also other possibilities:

1) Measurements of spontaneous polarization at $T < T_{ph.t.}$;
2) Second harmonic observation in amplifier scheme (based on ferroelectric), where *b* is assumed to be constantly dependent on temperature;
3) Thermal capacity measurements for low temperature ferroelectrics[9] in the temperature range < 100 K that has strong temperature dependence of permittivity. [6]

[9] Low temperature ferroelectrics is a group of ferroelectric materials distinguished by its special dielectric response on electric field and temperature in low temperature range. Common examples are strontium titanate ($SrTiO_3$) and potassium tantalate ($KTaO_3$).

4.3 Electrocaloric properties of some low temperature ferroelectrics

Among pure compounds the most intensive electrocaloric change was detected in $KTaO_3$, $SrTiO_3$. Further will be described main properties of these compounds:

1) Chemical formula of solid compound is $KTiO_3$;
2) Density is $\rho = 6.97 \cdot 10^3$ kg/m^3;
3) Temperature dependence of low-level signal permittivity:

$$\varepsilon(0,T) = \frac{A}{\frac{T_1}{2} cth\left(\frac{T_1}{2T}\right) - T_0}. \qquad (4.19)$$

Parameters of equation 2.3.18 are $A = 5.01 \cdot 10^4 K$, $T_1 = 52.8K$, $T_0 = 12.3K$.

4) Constant of dielectric nonlinearity

$b = 7.27 \cdot 10^9 m^5 / C^2 F$

5) Specific heat $C_{V_0} = 7.04 \cdot T^3$. [6], [57]

Experimental dependences of specific heat are shown below.

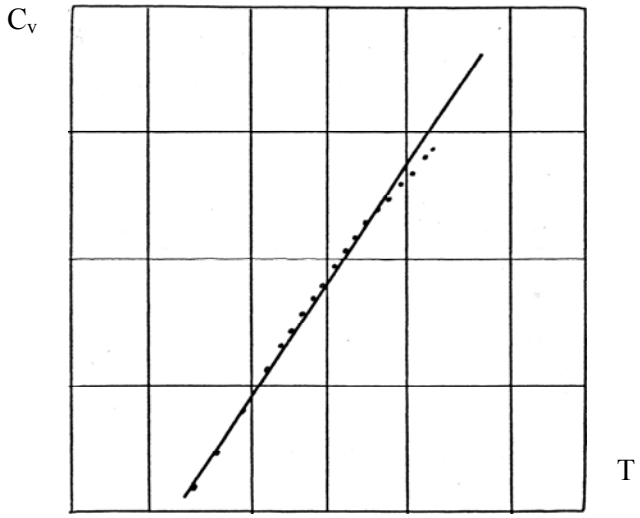

Figure 4.1 Specific heat vs. temperature in $KTaO_3$. Solid line is approximated straight line and points are experimental data [23].

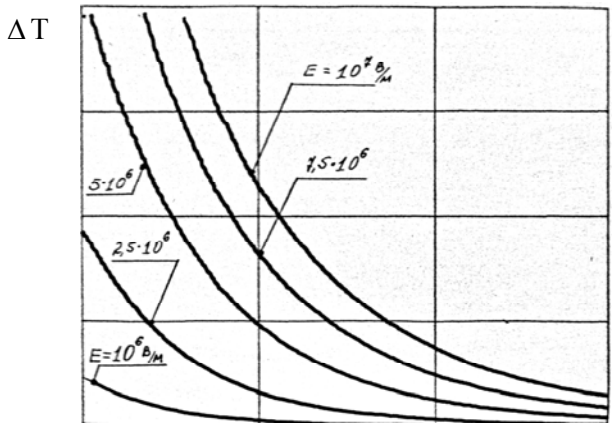

Figure 4.2 Temperature dependencies of electrocaloric change in the monocrystalline $KTaO_3$ by different values of applied electric field [23].

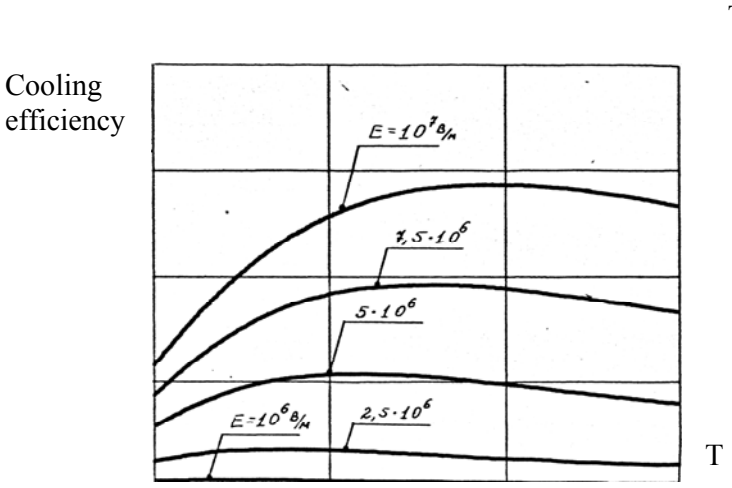

Figure 4.3 Temperature dependencies of cooling efficiency of unit volume in monocrystalline $KTaO_3$ by different values of applied electric fields [23].

4.4 Analysis of electrocaloric proprties in low temperature ferroelectrics

In our considerations low temperature ferroelectrics are more important in comparison from the whole majority of ferroelectric materials. Selection criterion here is paraelectric phase transition within the temperature range of 20 - 80K. Ferroelectrics show their anomalous properties only in narrow temperature range near $T=T_0$. Only in this temperature range is possible to obtain high values for polarization and its derivative. In the same temperature range material possesses significant electrocaloric effect. As main electrocaloric properties we take temperature change ΔT and heat Q that needed to transmit in order to return ferroelectric to its initial state. Both ΔT and Q are very sensitive functions of electric field intensity. In weak fields this dependence is quadratic,

i.e. $\Delta T \sim E^2$ and $Q \sim E^2$. In strong fields it is ΔT, $Q \sim E^{2./3}$. $\Delta T(T)$ and $Q(T)$ are based on temperature dependence of following parameters: $\frac{\partial a}{\partial T}$, P and C_v. There are characteristic features of $\Delta T(T)$ and $Q(T)$:

1) $\frac{\partial a}{\partial T}$, P and C_v are turned into zero;

2) Q decreases for $T > T_c$ range due to decrease in polarization;

3) ΔT can be increased for $T > T_c$ range because increase of specific heat leads to decrease in polarization.

$\frac{\partial a}{\partial T}$ increases from zero point up to a certain value. $\frac{\partial a}{\partial T} = 0$ is observed near helium temperatures for virtual ferroelectrics ($KTiO_3$, $SrTiO_3$) and near $T=T_{ph.t.}$ for ferroelectrics that possess phase transition ($CdTiO_3$, $(Ba,Sr)TiO_3$, $(Pb,Sr)TiO_3$, etc.). Above mentioned relationships bring us to understanding of following statements – firstly ΔT increases and after that it becomes monotonically decreasing. With all this going on a slope of a curve in the increasing area is higher than in decreasing area. *Q(T)* dependence is increasing from zero at $T < 4$ K for virtual ferroelectrics and at $T=T_{ph.t.}$ for ferroelectrics with phase transition. Further *Q(T)* slowly turns to weakly temperature dependence. Both dependencies have maximums with different locations on temperature axis. Maximum of *Q(T)* is always at higher temperature than *ΔT(T)*. For example for $SrTiO_3$ $Q_{max}(T)$ at T = 100 K, but $\Delta T_{max}(T)$ at T = 20 K. To compare the properties of low temperature ferroelectrics let us consider following parameters:

1) ΔT_{max} is maximal electrocaloric temperature change by certain electric field value;
2) Temperature range T_2 - T_1, where electrocaloric temperature $\Delta T(E)$ caused by certain value of electric field exceeds minimum efficiency ΔT_p ($\Delta T \geq \Delta T_p$) required for normal operation of refrigerator;
3) Average value of cooling efficiency Q in temperature range T_2 - T_1.

To the low temperature ferroelectrics group can be included clean materials $SrTiO_3$, $KTaO_3$, $CdTiO_3$, $LiTlC_4H_4O_6 \cdot H_2O$ and solid solutions based on strontium titanate or potassium tantalate. Among the clean materials large electrocaloric temperature change is observed in $KTiO_3$ and smallest temperature observed in $LiTlC_4H_4O_6 \cdot H_2O$. $(T_2\text{-}T_1)$ is an operating range of refrigerator made up from ferroelectric material of certain composition. This interval can be changed by adjusting the composition parameters. But the absolute

values of $(T_2\text{-}T_1)$ are determined by reqiured electric field intensity E and allowable temperature change ΔT_p. For instance, by $E = 10^7$ V/m and $\Delta T_p = 0.5$ K values of $(T_2\text{-}T_1)$ are within *20 - 40K* for different ferroelectrics. Going closer to ΔT_p temperature range becomes narrower. Comparison of Q values for different materials shows that higher values possess strontium titanate and solid solutions on its basis. Summing up, we can suggest that only use of $SrTiO_3$ and $KTaO_3$ (and solid solutions based on these materials) as a refrigerator material is rational. $SrTiO_3$ and $KTaO_3$ can provide temperature change $\Delta T = 1$ K by applied electric field $E \geq 10^7$ V/m. Average value of heat flow trough surface of unit mass after the field removal is $p = 100$ W/kg. This value must be maintained by 1Hz frequency. By field intensities about $E \geq 10^7$V/m it can be achieved only in high temperature range 20 – 80 K, because in low temperatures range it is 3 - 5 times less. However, one can adjust it by increase of electric field switching frequency. As we have already mentioned for $\Delta T = 1$K is required $E \geq 10^7$V/m, therefore it imposes limitation on used materials because10^7 V/m is about breakdown voltage of dielectric. Hence, all works under development of new refrigerator type have to go first trough physical and technological examination of material's reliability and should provide an uniform distribution of electric field on the surface for ferroelectric materials with different stoichiometric compositions. At the same time the electrocaloric effect in ferroelectrics has some side benefits:

1) Possibility of electric field commutation with high frequency;
2) Electrically controlled specific heat and coefficient of thermal conductivity.

Combination of significant electrocaloric temperature change in ferroelectrics and electrically controlled refrigeration system allows us to suggest it as very effective cooling effect. [23], [56]

4.5 Temperature conversation in real electrocaloric element

The general thermodynamic theory of the electrocaloric effect and above discussed calculation method give us following theoretical values for some of ferroelectric materials (see table 4.1). It is clear that highest temperatures changes ΔT=1K are obtained in solid solutions $SrTiO_3$-$BaTiO_3$ and solutions based on $KTiO_3$.

Table 4.1 Properties of some ferroelectric materials [6].

	Material	Composition	Maximal EC temperature change by $E=10^7$ V/m	Temperature range where it is achieved
1.	$SrTiO_3$	-	$\Delta T_{max} = 0.8$ K	$\Delta T = 25$ K
2.	$KTaO_3$	-	$\Delta T_{max} = 1$ K	$\Delta T = 35$ K
3.	$CdTiO_3$	-	$\Delta T_{max} = 0.75$ K	$\Delta T = 55$ K
4	LTT $(LiTlC_4H_4O_6 \cdot H_2O)$	-	$\Delta T_{max} = 0.25$ K	$\Delta T = 20$ K
5.	$Ba_xSr_{1-x}TiO_3$	x=0.15…0.075	$\Delta T_{max} = 1$ K	$\Delta T = 30…60$ K
6.	$Pb_xSr_{1-x}TiO_3$	x=0.01…0.03	$\Delta T_{max} = 1$ K	$\Delta T = 25…60$ K
7.	$K_{1-x}Li_xTaO_3$	x=0.001…0.01	$\Delta T_{max} = 1$ K	$\Delta T = 40…65$ K
8.	$KTa_{1-x}Nb_xO_3$	x=0.01…0.04	$\Delta T_{max} = 1$ K	$\Delta T = 30…65$ K

Application of such high electric fields with uniform distribution across the surface is practically insoluble problem. The reasons for inhomogeneous field distribution are:

1) Mechanically destroyed layers under electrodes (it is possible to avoid it for $SrTiO_3$ [110], [111]);
2) Bulk charge layers generated due to carrier trapping by deep traps.

Let us discuss as an example one electrocaloric element made up from strontium titanate. Object of our investigation is plane-parallel monocrystalline structure of $SrTiO_3$. By means of thermocouple, with one end fixed on thermally isolated sample and another one on isothermal screen, temperature change with regard to environment is determined. The temperature change occurred by applying external electric field (electrocaloric heating) and after disconnecting with proceeded shunt of electrodes (electrocaloric cooling). Temperature change during cooling and heating processes are not distinguished numerically, thus confirms its electrocaloric nature. Due to the fact that thermal contact between thermocouple and sample is not ideal, meaning thermal conductivity of current leads and thermocouple wires are finite; realization of measurements seemed to be rather difficult. Starting from the moment of switching signal of thermocouple increased and then slowly became zero value. After each voltage switching the time dependence of thermocouple signal was registered. Further approximation finally gave desired ΔT values.

In addition, experimentally was observed temperature change dependence on potential between electrodes. The result for structure $8.5 \times 8.5 \times (2 - 2.5)$ mm is shown on fig.4.4:

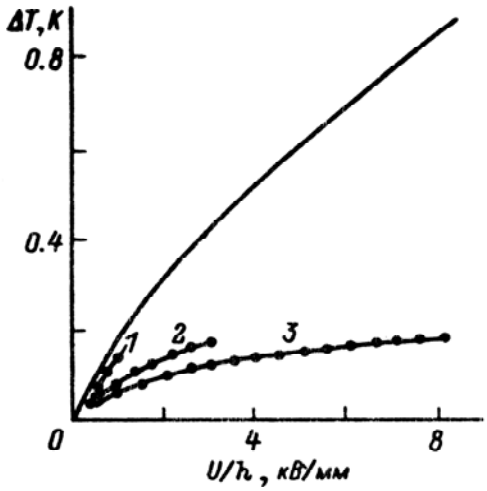

Figure 4.4 Dependence of electrocaloric temperature change on external field for plane-parallel sample of $SrTiO_3$, where h thickness of sample (1) 2mm, (2) 0.59mm and (3) 0.25mm [23].

Theoretically, maximal electrocaloric effect in $SrTiO_3$ is 0.8 K by applying 10^7 V/m. However experimentally pure monocrystalline samples of $SrTiO_3$ show just 0.2 K ($U = 2kV, E = 5 \cdot 10^6 V/m$). Decrease of ΔT, compared with theoretically expected values, is because of electric field intensity that can be applied mostly to near-electrode areas. It can be wasted up to 40 % of applied voltage to this area, depending on linear sizes of investigated samples. In that way, electric field is not uniformly distributed across the crystal structure. Another phenomenon, bulk charge, doesn't disappear during depolarization process. Therefore, avoiding residual polarization and requirement towards uniform electric field distribution are very important problems.

4.6 Dimensional effect

Electrocaloric effect, as experimentally observed depends on structure thickness. During experiment sample is disconnected from external source and its electrodes are shunted. After switching the voltage external circuit provides zero potential between electrodes. Residual polarization in strontium titanate was discovered experimentally. Polarization process is connected with presence of bulk charge. Local loss of neutrality in $SrTiO_3$ as a result of charging and its redistribution is some kind of special response on electric field application. Regulation of this response is not completely understood till this time. Many scientists had set up hypothesizes about uniform as well as non-uniform bulk charge distribution in $SrTiO_3$. Ambiguity of these conceptions makes a lot of barriers on a way to defy effect description. Additional data is needed to eliminate all contradictions.

Presented results in work [56] define more precisely the field distribution inside ferroelectric $SrTiO_3$. Monotonous decrease of ΔT due to decrease of thickness can be considered as dimensional effect of electrocaloric cooling. Possible reason for the dimensional effect is in fact that macroscopic field inside a plate doesn't disappear instantly after electrodes short. Electric charge that distributed across the thickness of structure is generated by external electric source. In 1D case induction field $D(x)$ has uniform and nonuniform terms:

$$D(x) = D(0) + \int_0^x \rho(x)dx \quad . \tag{4.20}$$

After turning voltage on, local changes in temperature occurred:

$$\Delta T(x) = \frac{T}{2C_V}\frac{\partial a}{\partial T}(D^2{}_H(x) - D_K{}^2(x)), \tag{4.21}$$

where T is initial sample temperature, C_v is specific heat, $D_H(x)$, $D_K(x)$ are local induction values before and after commutation respectively.

Sample comes to electrically and thermally nonequilibrium state. Heat exchange between different parts of plate is faster than heat exchange between sample and environment. Thermocouple can register average temperature change on the sample $\overline{\Delta T}$:

$$\overline{\Delta T} = h^{-1}\int_0^h \Delta T(x)dx\,. \tag{4.22}$$

By substituting (4.19) in (4.21) and reorganizing gives us:

$$\overline{\Delta T} = \frac{T}{2C_V}\frac{\partial a}{\partial T}(d_H{}^2 - d_K{}^2), \tag{4.23}$$

d_H, d_K are average values of inductions before and after commutation respectively. Conversion of the structure to new state is accompanied by bulk charge relaxation. Charges on electrodes provide zero fields in external circuit. Charge migration can lead to change in average induction d_k. Thus, measured values of ΔT are functions of smoothing process in system "sample - environment" Δt_1 and relaxation process Δt_2. If $\Delta t_1/\Delta t_2 >> 1$, then ΔT is maximal and close to ΔT_0, if measurements would not show understated values. Set up for experimental investigations provides Δt_1 of about 10 s, relaxation times in high-resistance $SrTiO_3$ samples is a long process. Hence, in this experiment the situation is $\Delta t_1/\Delta t_2 << 1$ and $\Delta T < \Delta T_0$ that is in agreement with experimental results.

Dimensional effect in electrocaloric cooling is induced by slow relaxation of macroscopic field in comparison to heat exchange of system "sample-environment". Average value of induction (residual field) increases when thickness of the sample is decreased. Foreign charge is located not only on the electrodes. Partly it penetrates to internal regions of plate, thus distributed nonuniformly [56], [57].

4.7 Recent development of systems based on electrocaloric effect

In 1990 group of Latvian scientists (Latvian State University) reported about electrocaloric cooling of 1˚C in Pb-Sc-Ta ceramics (PST).

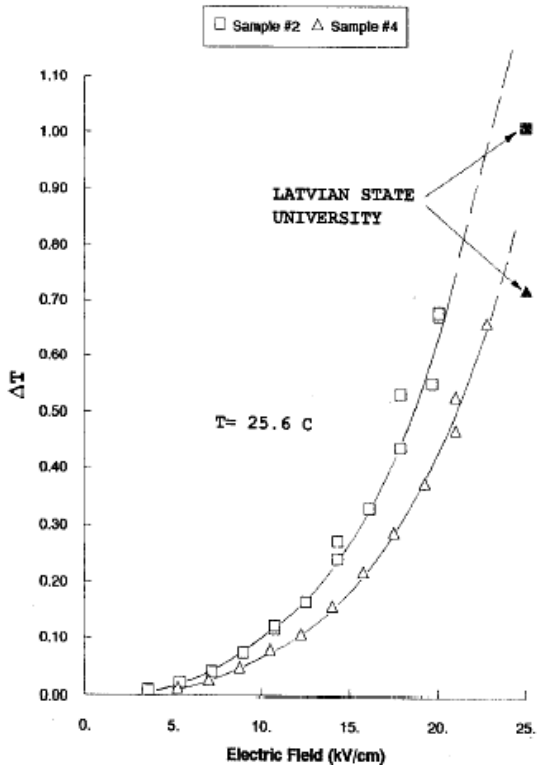

Figure 4.5 Experimentally observed electrocaloric cooling for two ceramic compositions PST (E = 25 kV/cm); by square marked sample B2 and by triangle B4. [6]

Scientific society didn't appreciate this result at its true value because philosophy of measurement was not properly presented. However, scientific company CeramPhysics expressed an intense interest and repeated measurements of PST samples that further proved the results obtained earlier. After confirmation of achieved results the CeramPhysics started to develop technology of electrocaloric cooling. To begin with PST

ceramics was carefully investigated and researchers came to a conclusion that this composition is unsuccessful and can't be further used for electrocaloric cooler construction. The central failures are:

1) High temperature of synthesis for this ceramic type, 1450˚C, that is incompatible with existing productive capacities;
2) Scandium oxide is extremely expensive material;
3) Finishing requires 350 hours at 1050ºC.

For subsequent research was needed several alternative compositions of *PST* that meet production and costs requirements. During further selection process two samples were chosen. Produced capacitors had quite big sizes $1.1 \times 1.0 \times 0.1$ cm and obtained values of breakdown voltages were optimistic (see fig. 4.6).

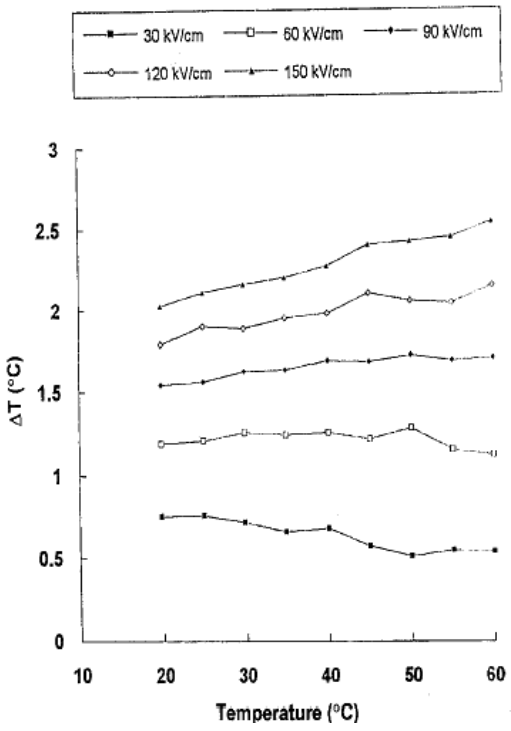

Figure 4.6 Electrocaloric temperature change by different values of applied fields [6].

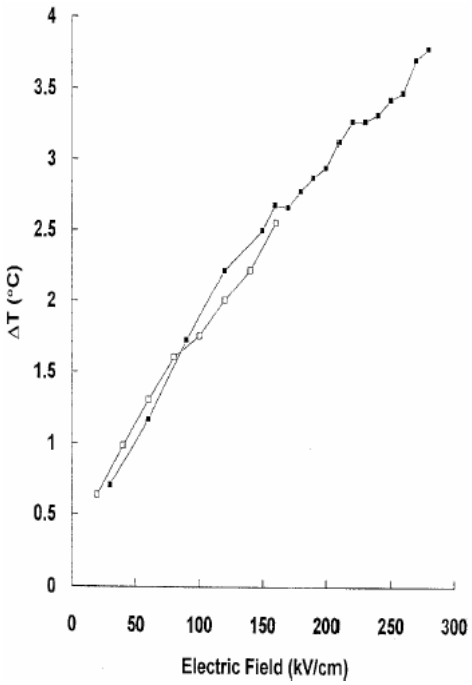

Figure 4.7 Electrocaloric temperature change as a function of applied field [6].

Experimentally was observed that ΔT of cooling and heating processes is equal (see fig. 4.7). This is very important result because it means low hysteresis losses in sample. After that scientists turned their attention to specific heat dependencies (see fig. 4.8 and fig. 4.9).

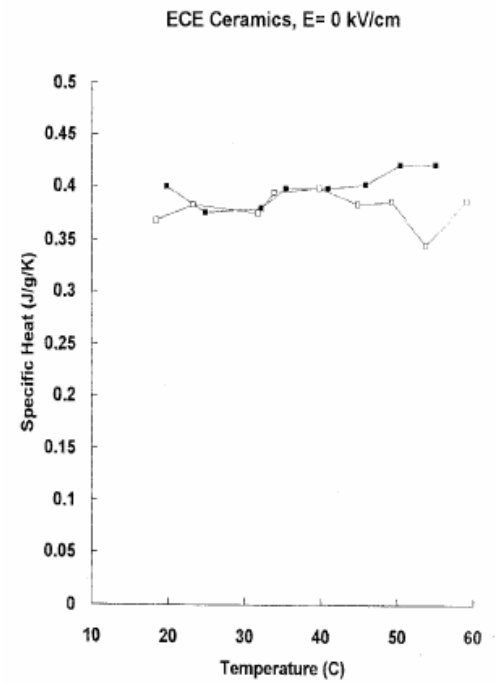

Figure 4.8 Specific heat data for two ceramic compositions B2 (filled) and B4 (empty) at zero electric field [6].

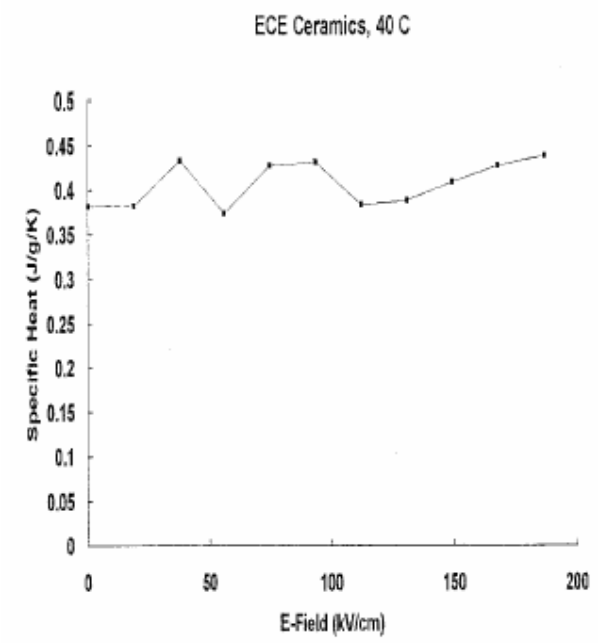

Figure 4.9 Electric field dependence of the specific heat on a capacitor of one of the ceramic compositions (40ºC) [6].

According to experimental results specific heat does not depend on electric field nor temperature. This result distinctly simplifies thermodynamic equation for dielectrics and T-S diagram can be obtained (see fig. 4.10).

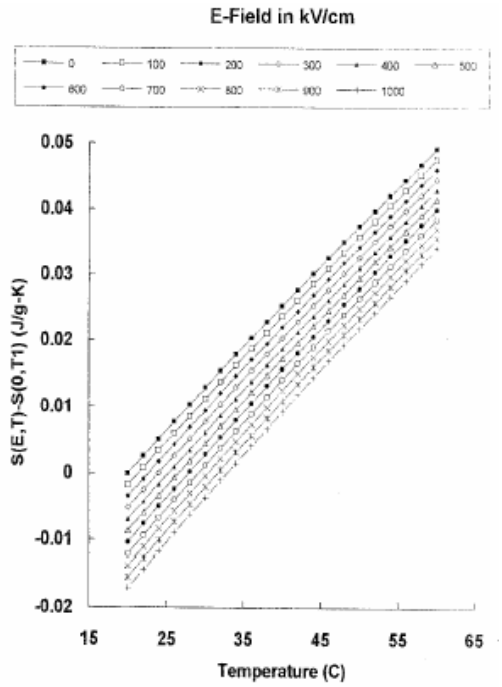

Figure 4.10 Entropy-temperature diagram derived using the electrocaloric data [6].

4.8 Technical realization

The idea of offered electrocaloric refrigerator consists of capacitors which are thermally connected through thermal switches with load and radiator. Practically, by adaptation of two capacitors group can be achieved high efficiency, because discharge of one group is used for charging another group of capacitors. The scheme such this was discussed earlier – patent USA № 3.638.440 – and requires effective thermal switches. Cascading electrocaloric cycle is based on tandem connection of Carno cycles each of that overlaps required temperature range. Electrocaloric elements change their states in accordance with two isotherms and two adiabats. But indispensable condition in this case is presence of effective thermal switches that control heat flow between electrocaloric elements.

4.9 Influence of synthesis conditions and crystal properties over electrocaloric effect in ceramics

Let us discuss as an example $Pb(Mg_{1/3}Nb_{2/3})O_3$ or simply PMN that is a typical representative of ferroelectric with carefully investigated relaxation properties (1993, 1996). PMN crystal is widely studied and applied to electroceramics purposes due to its perfect dielectric and electrostriction features. For instance, there is a wide maximum below room temperature. Dielectric properties can be improved by adding $PbTiO_3$ (PT). This leads to change in maximum temperature dependence of permittivity. Thus it is shifted from -15˚C (typical for PMN) to 40˚C for $0.9PMN\text{-}_{0.1}PT$ and 100Hz. Original chemical formula of compound is $(1-x)PMN_{-x}PT$. Important technological parameters (temperatures of burning and synthesis, saturation of MgO and PbO, and other thermal conditions for dielectric and ferroelectric properties) for PMN were investigated earlier.

Electric field in PMN crystal induces first order phase transition from crystalline phase to macroscopic ferroelectric phase with Curie temperature and threshold voltage at E = 1.75 kV/cm. Therefore strong electrocaloric effect was expected in (1-x) $PMN\text{-}_xPT$ near room temperature. Composition parameters can be varied in a range x = 0.08, 0.10, 0.25, giving the most suitable material synthesized. $(1-x)Pb(Mg_{1/3}Nb_{2/3})O_{3-x}PbTiO_3$ ceramic with x = 0.08, 0.10, 0.25 was made using MgO, Nb_2O_5, PbO and TiO_3 metal oxides with 99%

purity by bimodal synthesis of pure PMN-PT ceramic (with avoidance of pirochlorine phase). First step consisted in a crunching of MgO and Nb_2O_5 with different excess of magnesium oxide from 2 to 5% in deionized water, then drying and annealing at 800 ºC during 10 hours. After that this mixture was again threshed[10] and maintained under thermal treatment at 1050ºC during 1.5 hours to obtain powder $MgNb_2O_6$. Next step consisted in thermal treatment of mixture $MgNb_2O_6$, PbO and TiO_2 (with excess about 2% of PbO) at 800ºC during 10 hours.

Obtained powder was pressed in granules with diameter 10 mm and thickness 3 mm. These granules were conglomerated at 1050, 1120, 1180, 1250 and 1300ºC during the time from 1 to 2 hours with heating rate 10 - 15ºC per minute. After that granules were cooled in atmosphere. Sintered samples of (1-x)$PMN_{-x}PT$ were connected with silver electrodes to measure the electrocaloric effect. Crystal structure of obtained samples was investigated with X-ray diffractometry, and internal structure was observed by SEM (Scanning Electron Microscope). Different composition types and conditions of thermal treatment are in the table 4.2 [6].

Table 4.2 Summary of the compositions and processing conditions of (1-x)$PMN_{-x}PT$ ferroelectric ceramics [6].

Sample number	Composition		Calcination conditions (Temperature/Soak time)	Sintering conditions	
	x	Excess of MgO and PbO		Temperature/ Soak time	Heating rate
1	0.08	2 mol% MgO	800 °C/10 hrs	1120 °C/2 hrs	10 °C/min
2	0.10	0 mol% PbO			
3	0.25				
4	0.08	5 mol% MgO	850 °C/10 hrs	1200 °C/2 hrs	50 °C/min
5	0.10	0 mol% PbO			
6	0.25				
7	0.08	2 mol% MgO	850 °C/10 hrs	1180 °C/2 hrs	15 °C/min
8	0.10	2 mol% PbO			
9	0.25				
10	0.08	2 mol% MgO	850 °C/10 hrs	1250 °C/1 hr	15 °C/min
11	0.10	2 mol% PbO			
12	0.25				
13	0.08	5 mol% MgO	800 °C/10 hrs	1180 °C/2 hrs	15 °C/min
14	0.10	2 mol% PbO			
15	0.25				
16	0.08	5 mol% MgO	800 °C/10 hrs	1250 °C/1 hr	15 °C/min
17	0.10	2 mol% PbO			
18	0.25				

[10] Process of mechanical treshing needed for producing highly ordered chemical solution.

Abundance of perovskite and pyroclorine phases in obtained composition is calculated:

$$PerovskitePMN\% = 100 \times I_{perov.} / (I_{perov.} + I_{pyroc.}), \quad (4.24)$$

where $I_{perov.}, I_{pyroc.}$ are basic peaks on roentgenogram.

All ceramics without excess of PbO has daffodil surface in atmosphere. The surface of ceramics is represented mostly as pyroclorine phase (because of PbO evaporation). Ceramics (1-x)$PMN_{-x}PT$ (x = 0.08, 0.10, 0.25) with 2% excess possesses required properties of perovskite structure. Additionally, increase in temperature during thermal treatment process strongly influences crystal structure of ceramics. On the picture below (fig. 4.11) presented 0.9PMN-0.1PT ceramics sintered under 1180 ºC during two hours and at 1250 ºC during one hour with 2% excess of PbO. It is clear that ceramics is very strong with few amount of pores, all grains are clearly seen.

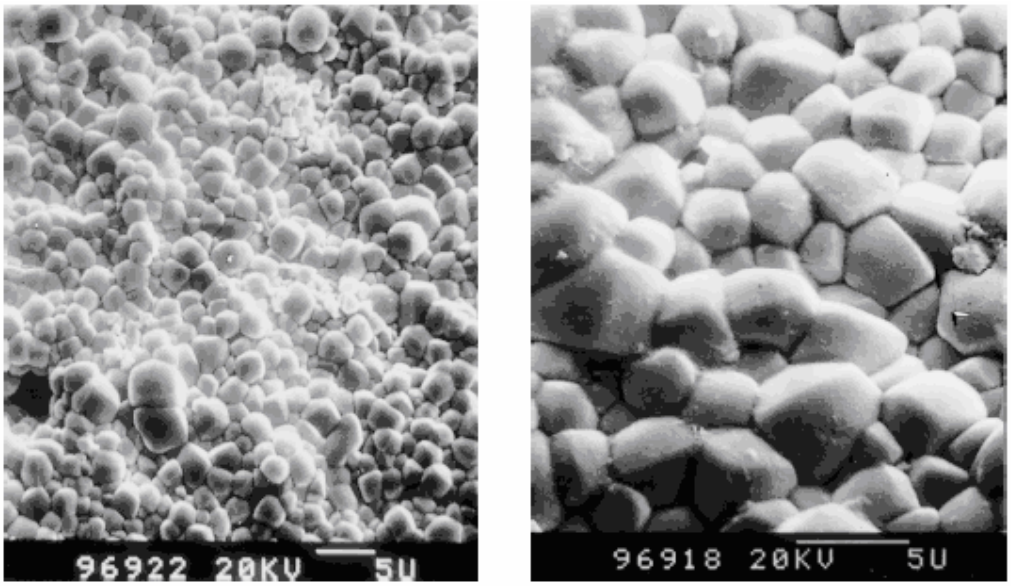

Figure 4.11 SEM photographs of the ac-fired surfaces of 0.9PMN-0.1PT (excess of 2% MgO and 2mol% PbO) ceramics sintered at 1180 ºC/2hrs (a) and 1250ºC/1hr (b) respectively. For comparison were used different sintering conditions: 800ºC/10hrs, 850ºC/10hrs, 850 ºC/12hrs. Change of these conditions does not influence in a critical way the crystal's properties) [17].

Electrocaloric properties of (1-x)$PMN_{-x}PT$ (x = 0.08, 0.10, 0.25) ceramics are presented on fig.4.12, where x axis is environmental temperature and y axis is electrocaloric

temperature change due to applied E = 1.5 kV/mm. It is seen from the picture that three different ceramics composition have strong electrocaloric effect near room temperature.

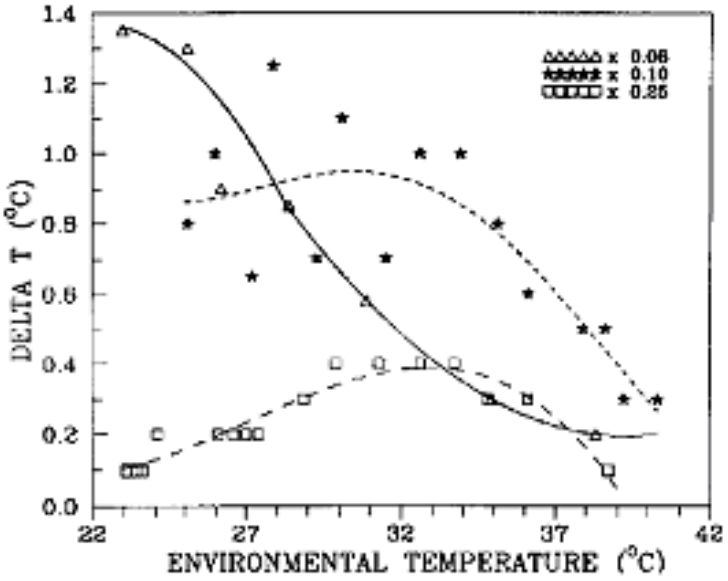

Figure 4.12 Electrocaloric temperature change ΔT versus temperature T for (1-x)PMN$_x$PT ceramics of samples (x = 0.08; 0.1; 0.25) with the excess of 2 mol% MgO and 2 mol% PbO, respectively) sintered at 1250 ˚C/1hr under a dc electric field of 1.5 kV/mm [23].

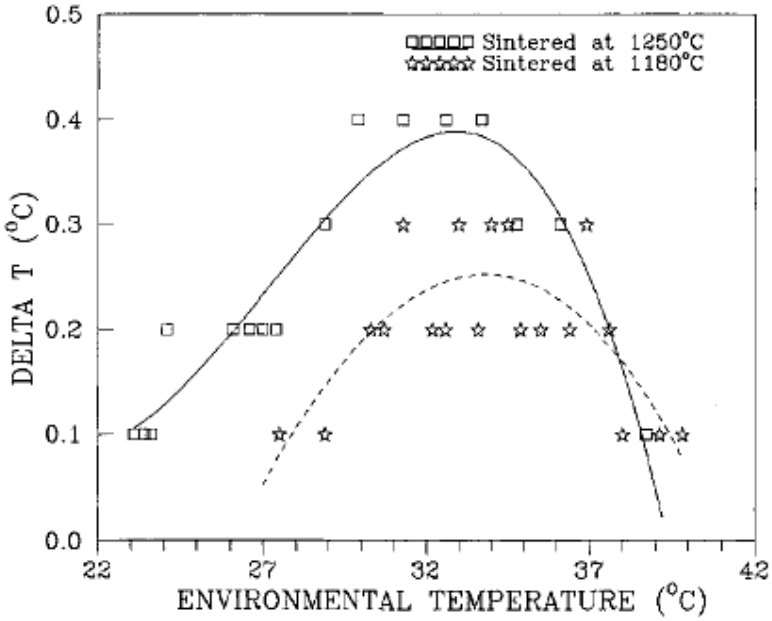

Figure 4.13 The electrocaloric temperature change ΔT versus temperature T for 0.75PMN-0.25PT ceramics sintered at (a)1180 ˚C/2hrs 9(b) 1250 ˚C/1hr respectively under a dc electric field of 1.5 kV/mm [23].

From analyzing of above presented dependencies, we see that temperature range with maximal electrocaloric effect is equal for compositions with different sintering temperatures, however effect value ΔT itself is different in these cases. It is explained by the fact that ceramics sintered by 1250 ˚C/1hr has more solid and good granular structure. Summing up, investigation of (1-x)$PMN_{-x}PT$ (x = 0.08, 0.10, 0.25) composition with different PbO/MgO excess had shown that crystal properties of ceramics are greatly influenced by excess of one of the components and annealing temperature. It was determined during the experiments that in ceramics (1-x)$PMN_{-x}PT$ with 2% excess of PbO by 1250 ˚C/1hr electrocaloric temperature change is about 1 K under 1.5 kV/mm. Relationship between synthesis conditions, crystal structure properties and electrocaloric effect was observed for several samples (1-x)$PMN_{-x}PT$. [6], [23], [59]

4.10 Electrocaloric effect in thin films

On 19th of November 2005 group of scientists from the Cambridge University reported about giant electrocaloric effect (12 K) in thin film (350 nm) of antiferroelectric $PbZr_{0.05}Ti_{0.05}O_3$. They proposed that their achievements resolve all the contradictions between existed macroscopic theories of the electrocaloric effect. Earlier published books contained contradictions in physical description of the effect. For instance, one research group said that electrocaloric effect is possible only above the Curie temperature (phase transition), where by applying an electric field the polarization gets a finite value. Other group suggested that effect is significant only below the phase transition temperature, thus in the area where the polarization depends on temperature. Also were presented opinions that effect is possible in both below and above Curie temperature, but is stronger above the phase transition. In other words, there is no agreement among specialists in theory describing electrocaloric effect ab initio. Even quantum-mechanical derivations are available only during last decade. Mischenko and his colleagues emphasize that investigation was carried out not on atomic level due to several contradictions in macroscopic theory of effect. Analyzed material is Zr-rich PZT. It shows pronounced electrocaloric effect detected by IR detectors. Materials such Zr-rich PZT and $PbZr_{0.48}Ti_{0.52}O_3$ composition can be used as a capacitors, high-strain actuators/transducers and as a prototype of microelectromechanical systems, etc. They possess required value

of dielectric constant and can be good controlled electrically, let alone their piezoelectric properties. However, cooling possibilities on thin films of this composition were not considered earlier. At room temperature $PbZr_{0.48}Ti_{0.52}O_3$ has orthorhombic low-level cell. By further thermal treatment at 120˚C it transforms into rhombohedral structure. By a transition from antiferroelectric to ferroelectric phase at approximately 80˚C is observed a steady thermal hysteresis. Structure is transformed to cubic paraelectric state at temperatures above 242˚C. This first order phase transition with Curie-Weiss temperature is linearly extrapolated with respect to dielectric susceptibility. Earlier there was no information about electrocaloric effect in Zr-rich PZT in literature. The preparation of components for further experiment was preceded. $Pb(OAc)_2 \cdot 3H_2O$ dissolving in methanol was refluxed under conditions 70 ˚C/2hrs. Apart from that, a mixture of acetic acid and methanol was combined with $Zr(O^nPr)_4$ and $Ti(O^nBu)_4$ and kept during two hours at room temperature. The solution based on Pb and Zr/Ti was mixed with a former (with 20% excess of former to compensate loss of Pb). Obtained yellow solution was passed trough a filter (0,2 μm) and ethylene glycol was added in order to stabilize the solution. Substrates of $Pt(111)/TiO_x/SiO_2/Si(100)$ were cleaned with acetone and propanol. Sols prepared before were deposited at 3000 rpm/30 s. a 70 nm layer is a result of pre-firing on a hot plane at 300 ˚C/60 s and 650 ˚C/10 min on another hotplate. This process was repeated five times in order to obtain 350 nm thin film. Method of X-diffraction was used to investigate the quality of surface. Pyroclorine was not found after careful scanning of surface with undefined orientation. Pt electrodes (diameter is 0.2 mm) used for measurements were mechanically connected with silver area on the edge of substrate. Permittivity and dielectric loss tangent were measured by HP 4192A Impedance Analyzer (100 kHz, 100 mV) with use of Radiant Technologies Precision Premier and high temperature (280 ˚C) detector. Temperature was controlled by thermocouple with accuracy of 0.3 ˚C.

Electric hysteresis measurements were done in 35 – 280 ˚C with interval T = 15 ˚C. Presented dependence of *P(E)* (see fig.4.10.1) reflects antiferroelectric propeties change in above mentioned temperature range. [2]

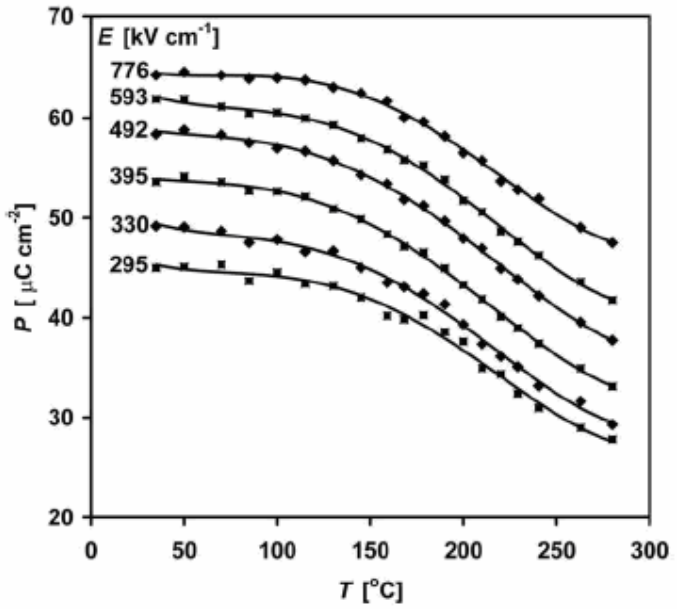

Figure 4.14 Temperature dependence of polarization at selected applied fields E. Data extracted for $E > 0$ from the upper branches of nine hysteresis loops measured at 10 kHz in 35 ˚C ≤ T≤ 280 ˚C. The EC effect is largest when absolute value of $\partial P/\partial T$ is maximized at the broad paraelectric to ferroelectric transition; the lines represent 4th order polynomial fits to the data [2].

Permittivity and tangent of dielectric loss have maximums at the boundary between ferroelectric to paraelectric phases T_c = 222˚C by cooling, and T_c = 215˚C by heating. During transition from antiferroelectric phase to ferroelectric no maximums were observed. It is connected with certain thin film macroscopic parameters, for instance with finite concentration coefficient. Electrocaloric adiabatic change of entropy S, energy U and temperature T for material with specific heat C and density ρ can be presented as:

$$\Delta S = -\frac{1}{\rho}\int_{E_1}^{E_2}\left(\frac{\partial P}{\partial T}\right)_E dE; \tag{4.25}$$

$$\Delta U = -\frac{1}{\rho}\int_{E_1}^{E_2} T\left(\frac{\partial P}{\partial T}\right)_E dE \tag{4.26}$$

$$\Delta T = -\frac{1}{\rho}\int_{E_1}^{E_2} \frac{T}{C}\left(\frac{\partial P}{\partial T}\right)_E dE; \tag{4.27}$$

Taking into account Maxwell equation $\partial P/\partial T = \partial S/\partial E$, $\partial P/\partial T$ values presented on fig.4.14 were measured for 4th polynomial degree $P(T)$. In observed temperature range

specific heat of Zr-rich PZT film is constant (330J · K^{-1} · kg^{-1}) and has maximum < 10% compared with other dependencies. It is connected with phase transition. In electrocaloric effect calculation for $Pb_{0.99}Nb_{0.02}(Zr_{0.75}Sn_{0.20}Ti_{0.05})_{0.98}O_3$ composition the value of specific heat was selected as 50% from its maximum value. Scientists used density value for following compound (Pb, Zr, Sn)TiO_3 as ρ = 8.3 g · cm^3 . Lower limit for voltage E = 295 kV cm^{-1} was selected to avoid the transition to antiferroelectric state. Upper limit E_2 = 776 kV cm^{-1} is maximal that can be obtained. Electrocaloric entropy change in the area of phase transition from ferroelectric to paraelectric phase is presented on fig.4.15:

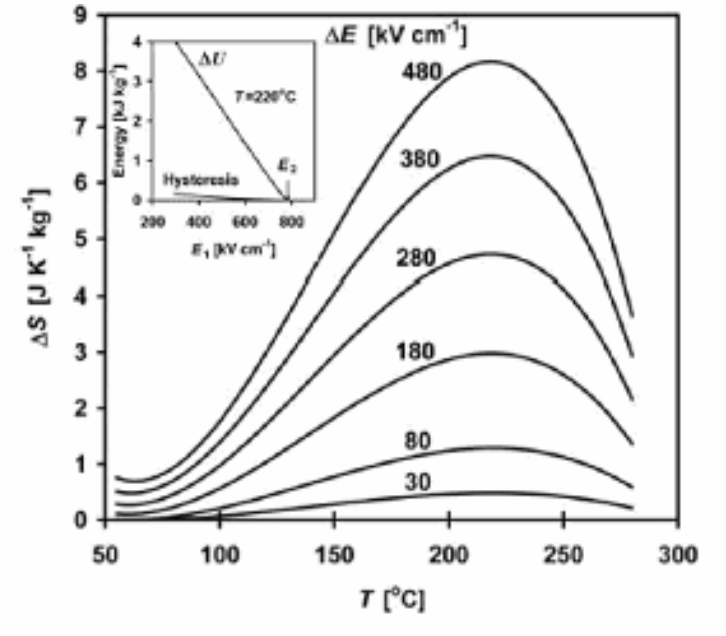

Figure 4.15 Electrocaloric entropy and energy changes. Main panel, entropy changes S were calculated from equation (4.25), using the fits presented on fig. at selected values of $E = E_2 - E_1$, where E_2 = 776 kVcm^{-1}. Inset, at T = 220˚C the EC energy U was similarly calculated from equation (4.26) as a function of $E = E_2$-E_1 with E_2 = 776 kVcm^{-1} . The corresponding hysteresis losses as determined from $P(E)$ loops are small. This justifies the indirect approach used to calculate the strength of the EC effect [2].

From above presented equation we see that in compound $Pb_{0.99}Nb_{0.02}(Zr_{0.75}Sn_{0.20}Ti_{0.05})_{0.98}O_3$ under applied field E = 30 kVcm^{-1} maximal entropy value is 0.6 $JK^{-1}kg^{-1}$. Under application of higher electric fields the entropy value increases.

Maximal obtained entropy change (15 $JK^{-1} \cdot kg^{-1}$) was preceded by magnetocaloric cooling with use of best magnetocaloric materials and under high magnetic fields of 5 T. Electrocaloric entropy change is shown below (see fig.4.16). [2]

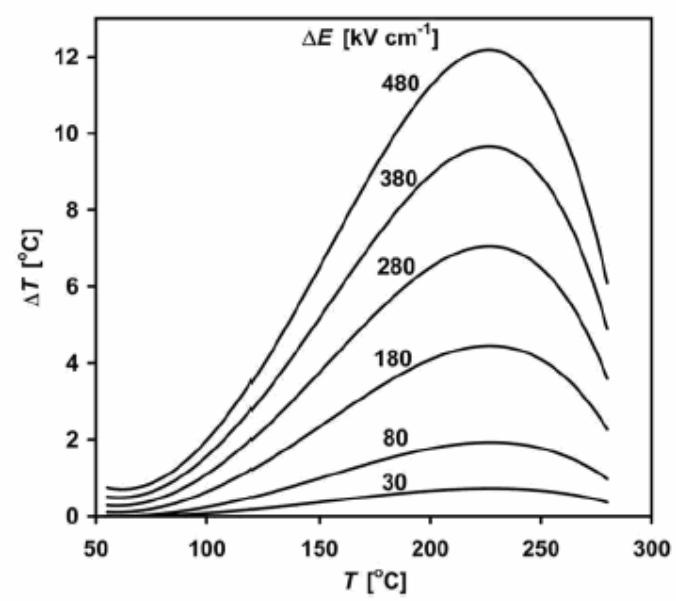

Figure 4.16 Electrocaloric temperature changes. *T* was calculated from the equation (4.27) using selected values $E = E_2 - E_1$ with $E_2 = 776$ $kVcm^{-1}$. The peak value of 12˚C occurs at $T_{ec} = 226$˚C with $E = 480$ $kVcm^{-1}$ [2].

Described electrocaloric effect in $Pb(Zr_{0.95}Ti_{0.05})O_3$ can be effectively used as solid state heat pump (refrigerating machine). To construct this refrigerator effective heat switches are needed, for instance, Peltier elements. When the switch is opened there is heat flow through it. When there is no heat flow switch operates as a passive thermal element. Electrocaloric elements can be separated by thermal switches to get maximal heat exchange [2], [58].

5 MATEMATICAL MODEL OF THE ELECTROCALORIC HEAT TRANSFORMER

Basic formula, describing the electrocaloric effect is

$$dQ = -T\varepsilon_0 \frac{d\chi}{dT} EdE = -\gamma(T)dE^2 . \quad (5.1)$$

It describes heat change dQ (heat per unit volume) induced by electric field change dE, $\gamma(T)$ is electrocaloric coefficient, namely temperature dependemce of permittivity derivative. Typical diagram for $\gamma(T)$ is presented on fig.5.1. If $T<T_c$ then electrocaloric coefficient $\gamma(T) > 0$, if $T > T_c$ then $\gamma(T) < 0$. In offered cycle there are two means of electric field change. According to first case, electrical field possesses sudden change from 0 to E. This process is characterized by time $\Delta\tau = 10^{-12}$ s. Temperature of electrocaloric element is kept unchanged during this time period. Typical time of heat process ~10^{-6} s. Induced heat can be expressed:

$$Q_1 = -\gamma \cdot T_i \cdot E^2 \quad . \quad (5.2)$$

Q_1 is induced heat and T_i is initial temperature of the electrocaloric element. The process of electrical field removal is relatively slow process, thus, heat is induced according to following equation:

$$Q_2 = -\int_{t_i}^{t_f} \gamma(T) E \frac{\partial E}{\partial T} dt = -\gamma \cdot T_{av} \cdot E^2 \quad . \quad (5.3)$$

Q_2 is absorbed heat, t_i is initial time and t_f is final time.

It is fundamentally important that $|Q_1| \neq |Q_2|$, i.e. heat induced and absorbed by electrocaloric effect is not equal. It happens because of $\gamma(T)$ nonlinearity. There are two possible constructions of electrocaloric refrigerator. First assumes that gaseous cooling medium can be added to provide effective heat exchange between different parts of cooling system. Second scheme is fully solid-state based construction where directed heat flow from cooled object to reservoir with big capacity is arranged. Even large electrocaloric effect itself doesn't mean that isolated element will work as a cooler. It is necessary to arrange thermodynamically effective cycle to reject the heat from cooled object. In order to construct an effective solid-state heat transformer the principles of Sterling cycle are discussed:

1) Electric field is applied. Heat Q_1 is induced;
2) Cooling-down to initial temperature;
3) Electric field is removed. Heat Q_2 is absorbed.

Further this process is repeated with a certain period A. If two electrocaloric elements are connected with each other, then elements work in antiphase. Analogy for that is instantaneous change of electric field, i.e. adiabatic process and slow change of electric field, i.e. isothermal process. Let us discuss in details physical processes in electrocaloric element under periodic electric field. In order to analyze interrelated thermal and electric processes in dielectric, we can choose temperature and electric field as variables. Thus, according to the second law of thermodynamics $dQ = TdS$ or

$$dQ = T\left(\frac{\partial S}{\partial T}\right)_E dT + T\left(\frac{\partial S}{\partial E}\right)_T dE \tag{5.4}$$

where S is entropy of observed unit volume in dielectric, Q is heat. Coefficient dT on the right side is ρC_E where ρ is density and C_E is specific heat under constant electric field, meaning

$$T\left(\frac{\partial S}{\partial T}\right)_E = \rho C_E . \tag{5.5}$$

It is possible to neglect volume change of dielectric by calculating change of free energy F. We also assume that polarization P is experimentally observed function of E and T.

$$dF = -SdT - PdE \tag{5.6}$$

From existed differential condition in 5.6 follows Maxwell equality:

$$\left(\frac{\partial S}{\partial E}\right)_T = \left(\frac{\partial P}{\partial T}\right)_E . \tag{5.7}$$

We substitute coefficients of differentials and finally:

$$dQ = \rho C_E dT + T\left(\frac{\partial P}{\partial T}\right)_E dE . \tag{5.8}$$

Let us consider that electric field E is given function of time t. Now we can derive equation describing time dependence of temperature. For that purpose, we need equation between heat power and current:

$$\frac{\partial Q}{\partial T} = -\operatorname{div}\mathbf{J} . \tag{5.9}$$

In linear approximation according to Fourier law:

$$\mathbf{J} = -\lambda \operatorname{grad} T \tag{5.10}$$

Finally, obtained equation:

$$\rho C_E \frac{\partial T}{\partial t} = \operatorname{div}\left(\lambda\left(\operatorname{grad} T\right)\right) - T\left(\frac{\partial P}{\partial T}\right)_E \frac{dE}{dt} \ . \qquad (5.11)$$

It differs from standard thermal conductivity equation by second term that we will consider as a heat source depending on time and temperature. To determine uniquely temperature, to this equation should be added initial and border conditions. By analogy with pyroelectric constant let us determine electrocaloric effect:

$$\gamma\left(E,T\right) = \frac{T}{2E}\left(\frac{\partial P}{\partial T}\right)_E . \qquad (5.12)$$

Let us rewrite equation in a form:

$$\rho C_E \frac{\partial T}{\partial t} = \operatorname{div}\left(\lambda\left(\operatorname{grad} T\right)\right) - \gamma\left(T,E\right)E\frac{dE}{dt} \ . \qquad (5.13)$$

For a particular case, when $P = \frac{1}{4\pi}\left(\varepsilon\left(T\right)-1\right)E$ (2.4.14), electrocaloric coefficient depends only on temperature (ε - permittivity):

$$\gamma\left(T\right) = \frac{T}{4\pi}\frac{\partial \varepsilon}{\partial T} . \qquad (5.14)$$

Electrocaloric effect coefficient $\gamma\left(T\right)$ can be either positive or negative, because heat can be induced or absorbed.

In general case equation (5.13) is non-linear ($\gamma\left(T\right)$ is arbitrary) and has analytical solution only if initial temperature is constant and dielectric is isolated (heat flow through its surface is equal to zero):

$$T\big|_{t=0} = T_0 = const \ . \qquad (5.15)$$

In this case temperature is equal at all points of dielectric and dependence of temperature is determined by integral solution of following equation:

$$2\int_{T_0}^{T} \frac{\rho(x)C_E(x)}{\gamma(x)}dx = E^2\left(0\right) - E^2\left(t\right). \qquad (5.16)$$

For negative $\gamma\left(T\right)$ values equation (5.16) gives:

1) Temperature change by application or removal of electric field is determined only by electric field intensity value at initial and final time;
2) If $E\left(t\right) > E\left(0\right)$ then $T\left(t\right) > T_0$, and vice versa, if $E\left(t\right) < E\left(0\right)$ then $T\left(t\right) < T_0$.

Under other initial or border conditions solution can be derived only numerically or approximately (needed to consider space distribution of temperature). [60]

Typical $\gamma(T)$ dependence is shown on fig.5.1.

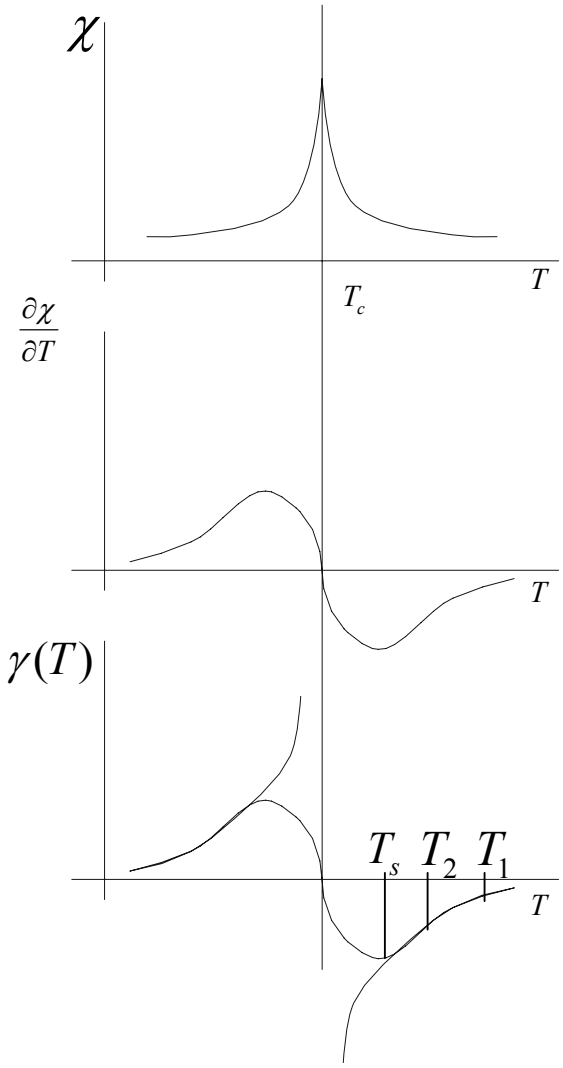

Figure 5.1 Electrocaloric ciefficient $\gamma(T)$ typical dependence [60].

6 FINITE ELEMENTS METHOD

All processes inside heat transformer are a nonlinear dependence dynamic problem. At that electric and thermal fields are connected. Therefore, we need to solve differential equations with partial derivatives for both electric and thermal field in geometrically complicated systems. For this modeling and optimization the finite elements analysis can be applied. Finite elements analysis is engineering simulation technique using finite element method in physics and mathematics [6], [61]. Finite element method (FEM) approximates solution of partial differential equation (PDE) or system of differential equations, for instance, equation describing heat transport processes. Solution is proceeded either by steady state conditions, i.e. fully eliminating the differential equation, or reproducing the PDE into an equivalent ordinary differential equation, that can be solved by standard techniques such as finite differences, etc. By finding solution of partial differential equations, the main difficulty is to produce a proper approximation of the studied equation, but at the same time to keep it numerically stable. There are many possibilities to do this, each including its advantages and disadvantages. The Finite Element Method can be applied for solving partial differential equations in complex systems, like cars and oil pipelines, in simulating the weather on Earth, where accurate predictions are needed. Method was successfully applied to hydromechanics, in particular to liquid flow in porous medium. Great and important contribution to development of FEM was made by two pioneers Alexander Hrennikoff (1941) and Richard Courant (1942). Development of the finite element method is also connected with names of Rayleigh, Ritz, and Galerkin and their results for solved partial differential equation. During the long time FEM was developed as one of the approach applied in structural mechanics. This approach is based on physical conception of minimum in total potential energy. FEM can be illustrated in the following way (1D case):

$$P_1 : \begin{cases} U'' = f\_in\_(0,1) \\ U(0) = U(1) = 0 \end{cases} \tag{6.1}$$

where f is given function of x, U is an unknown function of x, and U'' is the second derivative of U with respect to x. Dirichlet problem is a two dimensional problem.

Solution of P_1 assumes, firstly, its conversion to variation equivalents.

$$\int_0^1 f(x)v(x)dx = \int_0^1 U''(x)v(x)dx \tag{6.2}$$

Above shown equation is true for any smooth function, if U solves P_1. Integration by parts is used on the right side:

$$\begin{aligned}\int_0^1 f(x)v(x)dx &= \int_0^1 U''(x)v(x)dx \\ &= U'(x)v(x)\Big|_0^1 - \int_0^1 U'(x)v'(x)dx \\ &= -\int_0^1 U'(x)v(x)dx = -\phi(U,v)\end{aligned} \tag{6.3}$$

,

here we assume that $v(0) = v(1) = 0$. Let us assume that $H_0^1(0,1)$ is a function of (0,1) boundary variation. Now we need to replace the infinite dimensional linear problem with:

$$\text{Find } U \in H_0^1 \text{ such that } \forall v \in H_0^1, -\phi(U,v) = \int fv \tag{6.4}$$

In case of finite dimension:

$$\text{Find } U \in V \text{ such that } \forall v \in V, -\phi(U,v) = \int fv \tag{6.5}$$

where V is finite dimensional subspace $H_0^1(0,1)$. For problem $P1$, we take n x values in the interval $(0,1)$ $0 = x_0 < x_1 < ... < x_n < x_{n+1} = 1$ and V is defined as:

$$V = \left\{U : [0,1] \to R : U \text{ is continuous, } U\big|_{|x_k, x_{k+1}|} \text{ is linear, } k = 0,...,n \text{ and U(0)=U(1)} = 0\right\}, \tag{6.6}$$

where $x_0 = 0$ and $x_{n+1} = 1$. If $v \in V$ then the derivative is typically not defined at any $x = x_k$, $k = 1,...,n$. However, at every other value of x the derivative exists and one can derive it by means of integration by parts.

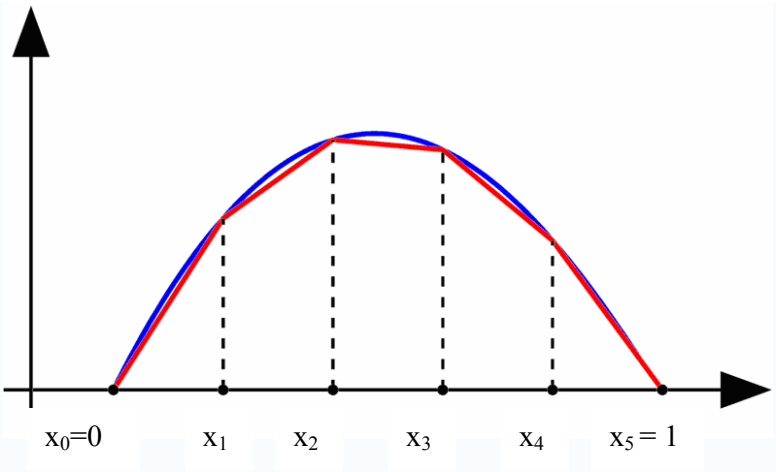

Figure 6.1 A function in H^1_0, with zero values at the endpoints (blue), and a piecewise linear approximation (red) [61].

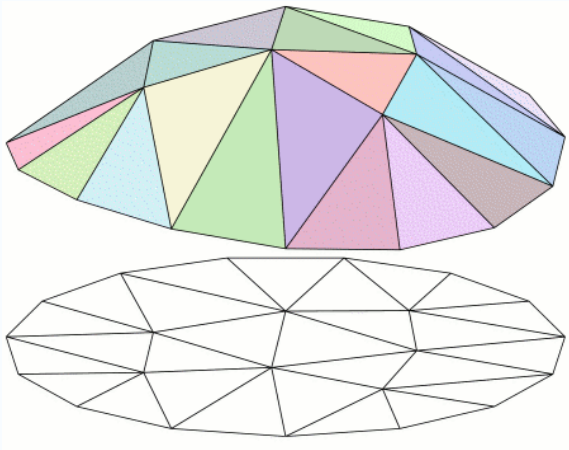

Figure 6.2 A piecewise linear function in two dimensions [61].

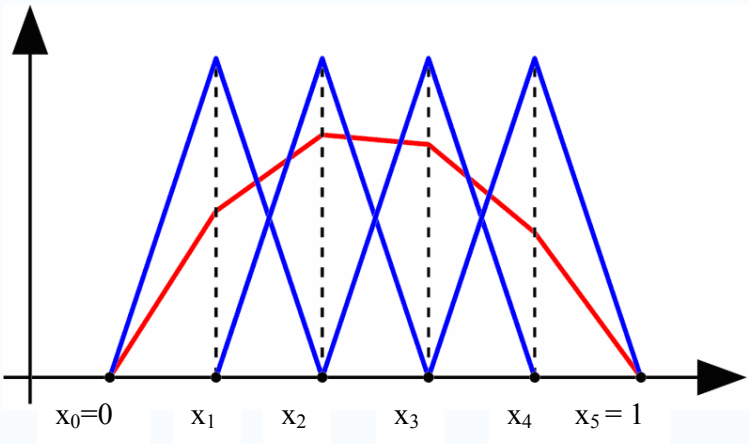

Figure 6.3 Basis functions v_k (blue) and a linear combination of them, which is piecewise linear (red) [61].

Generally, idea of FEA (Finite Element Analysis) consists in fact that any continuous function, such as temperature, pressure and shift is possible to approximate by discrete model including great number of piecewise continuous functions determined on finite number of areas. Piecewise continuous functions are determined by values of continuous quantity within finite number of points of a certain area. In general case this continuous variable is unknown and it is needed to find values of this quantity in some inner points of area. One should follow certain steps during construction of discrete model for continuous quantity:

1) Within concerned area we determine finite number of points;
2) Value of continuous variable is what we need to define;
3) Definitional domain of continuous quantity is divided into finite number of sub-domains called elements. These elements have common node points and in aggregate approximate domain form;
4) For each element is determined polynom, however polynoms are selected in order to keep continuity along borders of element [6], [23], [61].

7 COMSOL MULTIPHYSICS (FEMLAB)

Comsol Multiphysics is powerful and interactive media that speed up simulation and calculation of all kind of engineering problems based on PDE and FEM. Using this program package it is possible to extend standard models with one differential equation to multiphysical models and calculate interrelated physical effects. Coefficients of PDE are specified as understandable physical parameters such thermal conductivity, specific heat, heat-transfer coefficient, etc. Conversion of these parameters into coefficients of PDE is automatically preceded. Interaction with program occurred by means of standard method – through user's graphical interface or by programming with use of Comsol Scripts or MATLAB. Program is based on FEM as it has been already mentioned.
There are three mathematical methods of system determination:

1) Coefficient form (for linear and close to linear models);
2) General form (for non-linear models);
3) Weak form (for models with PDE on borders or in case of mixed and time derivatives).

Using these methods one can choose analysis type:

1) Stationary and transitional analysis;
2) Linear and non-linear analysis;
3) Model and intrinsic frequency analysis.

Software starts FEA with grid that considers element's configuration and errors control. Since many physical effects are determined in a form of PDE one can simulate wide range of scientific and engineering phenomenon in acoustics, chemical reactions, diffusion, electromagnetism, hydrodynamics, filtering, heat-and-mass transfer, optics, quantum mechanics, semiconductor devices, etc. Moreover, owing to coupling variables program allows us to connect models in different geometries and interrelate non-equidimensional models.

To construction and calculation of a certain problem it is needed to follow these steps:

1) Choose dimension of model, physical section in Model Navigator (each section has a certain differential equation), stationary/non-stationary temperature field analysis;
2) Determine workspace and element geometry;
3) Set initial data, time dependences and coordinate for our variables;
4) Indicate initial conditions, thermal and physical characteristics;

5) Indicate boundary condition;
6) Specify calculation parameters and build a grid;
7) Start calculation;
8) Tune representation mode;
9) Obtain results. [62]

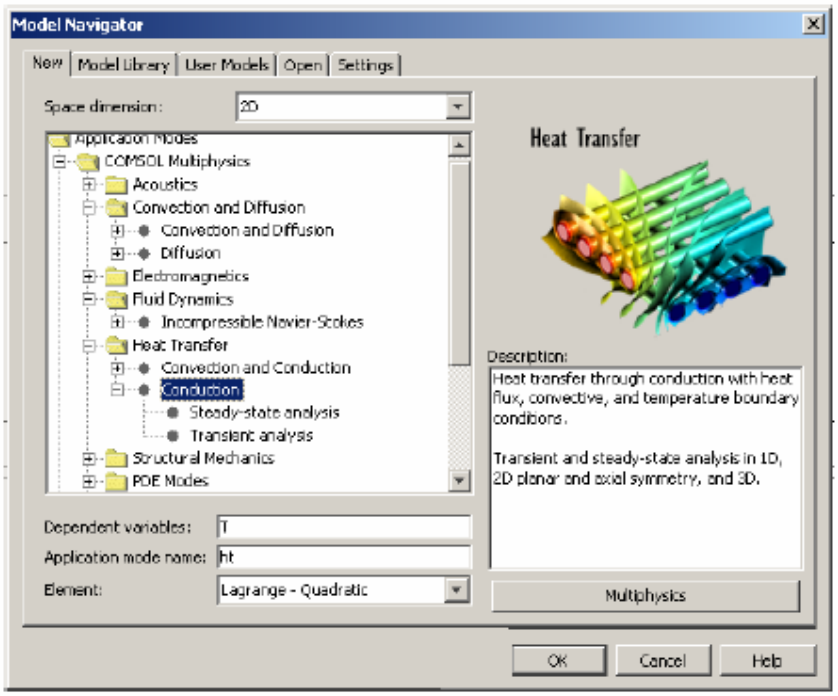

Figure 7.1 Model Navigator window [62].

In block map form a succession of task solution in FEMLAB can be presented as on fig. 7.2.

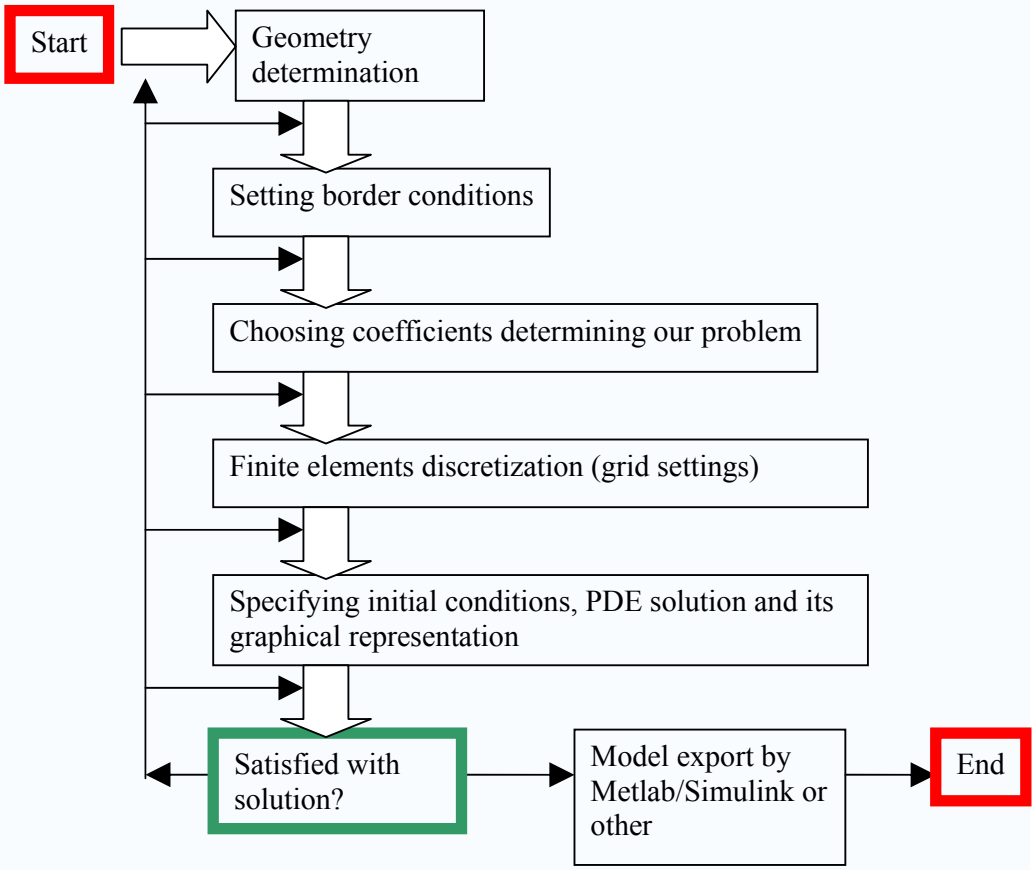

Figure 7.2 Block map of task solution process in FEMLAB [6].

8 ELECTROCALORIC EFFECT SIMULATIONS

Computer simulation helps us to estimate numerically the electrocaloric effect. As an example let us consider temperature dependencies of permittivity and its derivative for $Ba_{0.6}Sr_{0.4}TiO_3$. From the point of view of better temperature response there is an important point on the right side (see fig.8.1) regard to Curie temperature, i.e. in paraelectric phase, marked with T_o. Appropriate choice of x in $Ba_xSr_{1-x}TiO_3$ allows us to shift working temperature range of device. On the picture shown below (see fig.8.1) working point is T_o = 275 K. Cooling device will work more effectively in the range 270 – 280 K. However, it is needed to emphasize once again that large value of the electrocaloric effect doesn't mean that cooler will provide effective heat rejection from cooled body. Thermodynamically effective cooling cycle must be arranged.

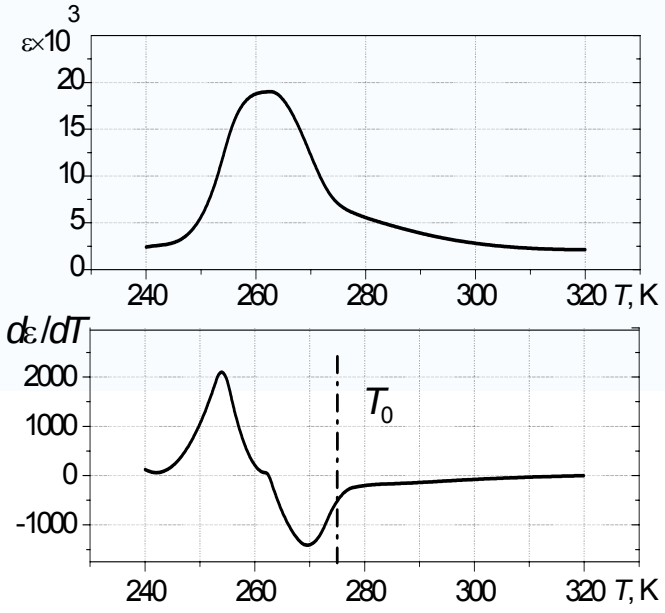

Figure 8.1 Temperature dependence of permittivity and its derivative [63].

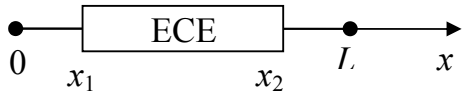

Figure 8.2 Cooling line model of one electrocaloric element [6].

Fig.8.2 has shown the electrocaloric cooling line consisting from one element. Electrocaloric element is separated from the environment by thermal-conduction layers *[0 ÷ x_1]* and *[x_2– L]*. We consider 1D model and, thus, temperature changes only along axis *x*. One border, namely, *x* = 0, is thermally isolated. On the other border at point *L* kept temperature T_o, that is accepted as an initial. Point *x* = 0 will be cooled as result of electrocaloric effect in element and point *L* is kept under constant temperature. We also assume that thermal conductivity and thermal capacity are constant within the layer. $T(x,\tau)$ is solution of following equation:

$$C(x)\frac{\partial T}{\partial x} = \frac{\partial}{\partial x}\lambda(x)\frac{\partial T}{\partial x} + P(x,t,T) \tag{8.1}$$

Border conditions are:

$$\lambda_0 \left.\frac{\partial T}{\partial x}\right|_{x=0} = 0 \ , \ T\big|_{x=L} = T_0 \tag{8.2}$$

Initial condition is: $T(x,\ 0) = T_0$

Function *P(x, t, T)* determines heat source (electrocaloric element):

$$P(x,t,T) = -T\varepsilon_0 \frac{\partial \varepsilon}{\partial T}\frac{\partial E^2}{\partial t}, \tag{8.3}$$

where *E* is electric field intensity, *P(x, τ, T)* is not equal to zero only on the electrocaloric element. E depends periodically on time with period *A* (see electric pulses applied to structure on fig.8.3).

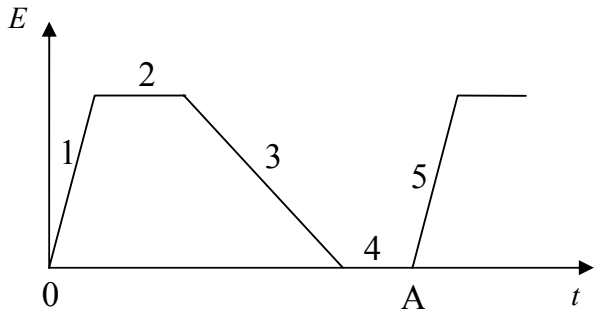

Figure 8.3 Periodical dependence of electrical field [63].

By applying pulses to ferroelectric structure we realize cycle on the fig. 8.4.

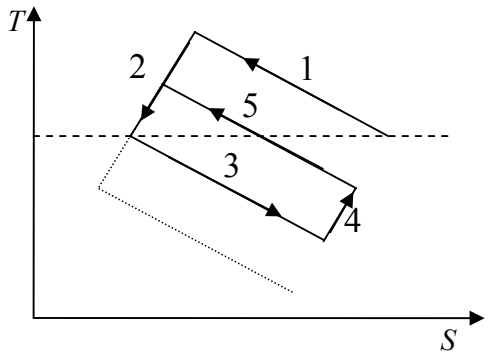

Figure 8.4 T-S diagram of thermodynamic cycle [63].

1 – Charge of ferroelectric capacitor and its polarization, that leads entropy decrease;

2 – Heat, resulting from electrocaloric effect, goes trough the structure keeping capacitor charged and cooled;

3 – Discharge of capacitor resulting in depolarization processes and cooling;

4 – Capacitor can absorb heat from cooled body;

5 – Heating process started and in order to avoid transition to initial state next pulse 5 is applied. The cycle is repeated further. It is necessary to note, that due to non-linearity of temperature dependence of permittivity derivative and proper selection of working point, heat amount that electrocaloric effect can absorb during discharge process is more than heat induced during charging. This distinctive feature is the main reason for cooling process on one end of the electrocaloric line.

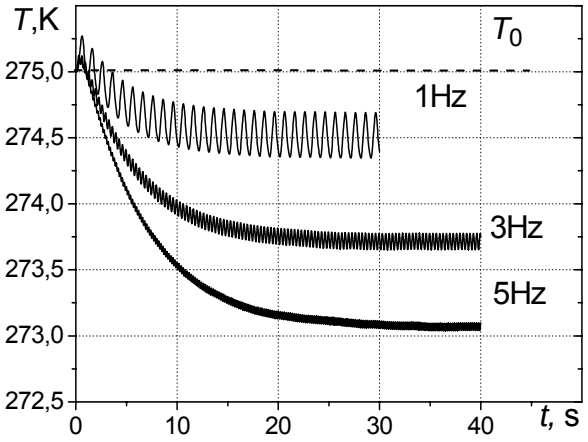

Figure 8.5 Electrocaloric cooling on one end of the cooling line comprising one electrocaloric element [6], [63].

The same approach can be applied to electrocaloric cooling line consisting from two electrocaloric elements (Fig.8.6). Here advantage of using second electrocaloric element results in more effective cooling that is clearly seen by comparison of pictures below (see fig.8.7).

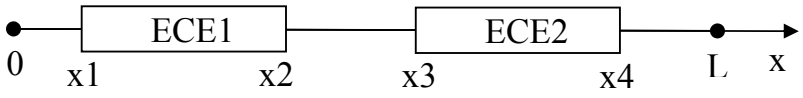

Figure 8.6 Electrocaloric cooling line based on two elements [6].

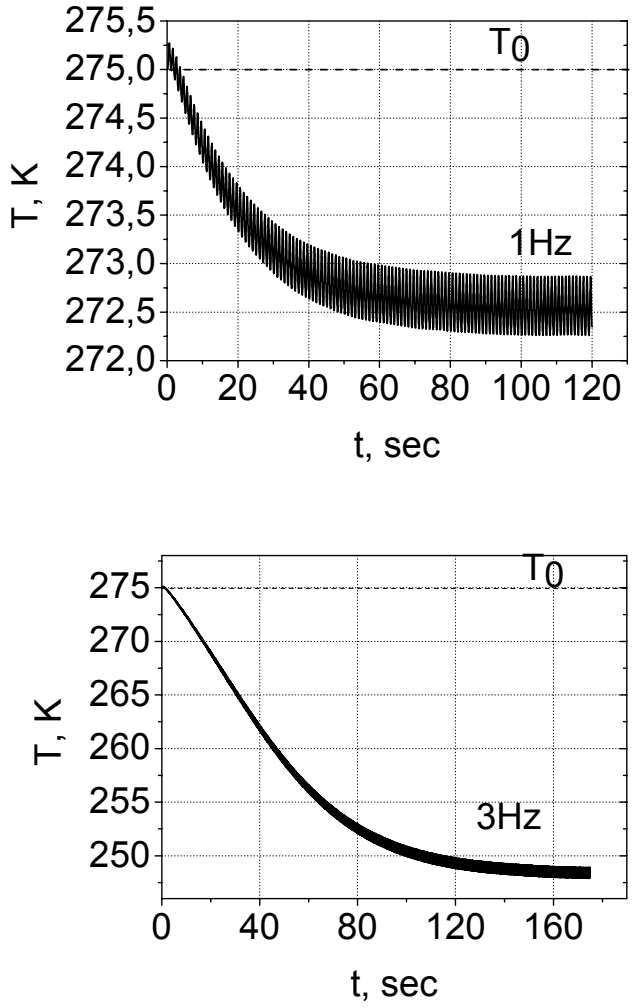

Figure 8.7 Electrocaloric cooling on one end of the cooling line comprising two elements. By 1 Hz temperature change is 2.5K and by 3Hz already 25 K [63].

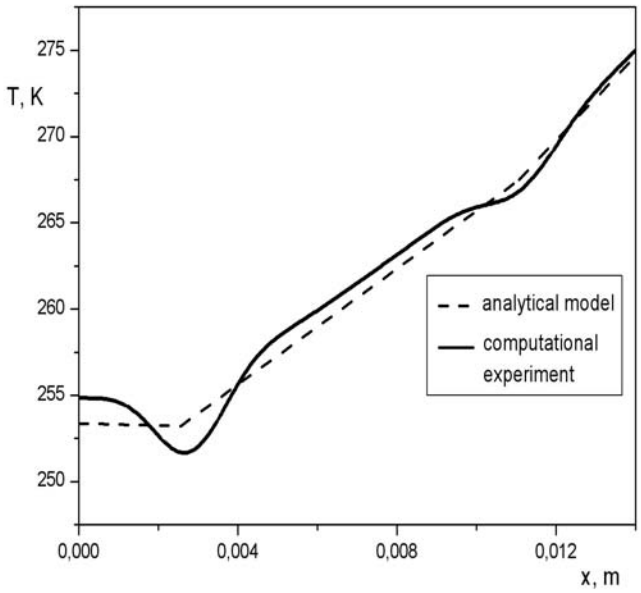

Figure 8.8 Temperature distribution across the structure [63],[64].

From fig.8.8 is clear that linear parts of dependence are for thermal elements. Drops on dependence are due to field switching. Analytical methods allow us only estimate temperature change character in steady state [63], [64].

9 EXPERIMENT AND RESULTS

9.1 Experimental detection of EC temperature change in capacitors

Experimental part contained series of measurements on thin film and bulk capacitor samples of $Ba_{1-x}Sr_xTiO_3$ (BSTO) of different composition. The exact composition can not be provided for all samples because of technological "know how". However, it is possible to define at least approximetely value of *x* in formula, but it would not be so helpful, because other technological parameters, temperatures, for instance, are not defined.

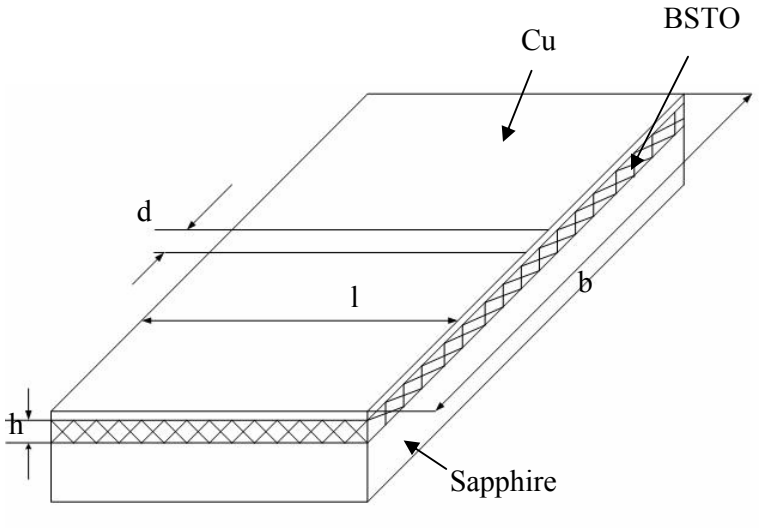

Figure 9.1 Thin film capacitor.

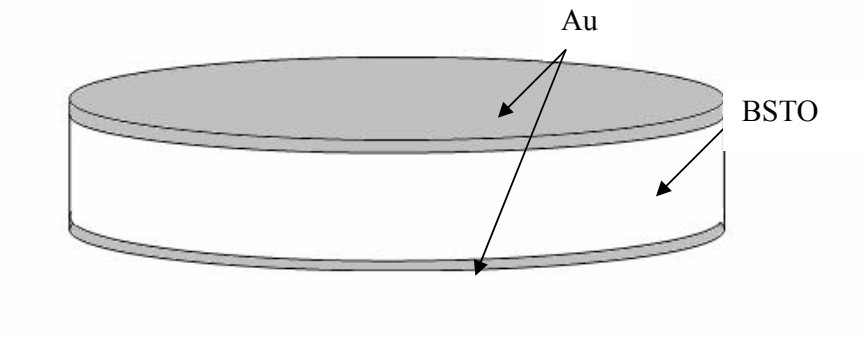

Figure 9.2 Bulk ceramic capacitor.

The origin of ceramic capacitors is not defined. Thin film capacitors were produced by magnetron sputtering. Magnetron sputtering technology presented on fig.9.3 is widely

used for thin film deposition on substrate. Plasma is created by applying high voltage to a low-pressure gas, for example argon. There is colourful light is produced therefore sometimes effect is called “glow discharge”. Ions of plasma strike a “target” made from desired material. Thus, atoms of “target” leave it with sufficient energy and velocity to be deposited on substrate. [65]

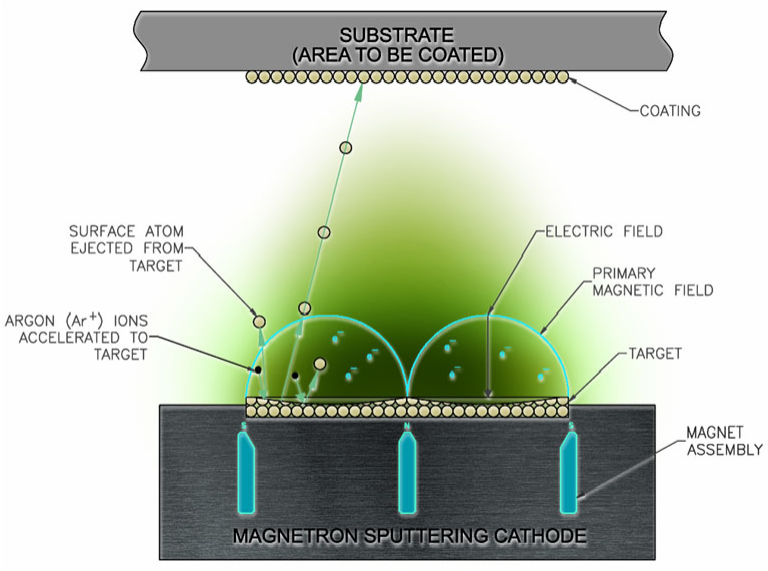

Figure 9.3 Magnetron sputtering technology [65].

Detailed information about capacitors can be found in tables 9.1 and 9.2.

Table 9.1 Linear sizes of bulk ceramic capacitors.

	C6	C12
Thickness, mm	0.5	0.3
Diameter, mm	0.65	0.65

The idea was to measure temperature dependence of capacitance from which we can derive temperature dependence of permittivity and its derivative. Temperature derivative of permittivity represents electrocaloric coefficient in our considerations.

Table 9.2 Linear sizes of thin film capacitors.

	KR7	268
Thickness , μm	0.45	0.4
Height, μm	0.3	0.3
Lenght , μm	820	286
Actuation width between electrodes, μm	8	4.5

Therefore, this is enough at first stage to estimate how large effect in our samples is by defining permittivity derivative vs temperature. In experiment was used pricisious LCR-meter. Additionally was important to arrange effective cooling of sample. For this purpose we used liquid nitrogen (77 K), i.e. standard method used in cryogenics. We moved sample mechanically into box with liquid nitrogen giving a temperature gradient. There are several requirements needed to meet: box with liquid nitrogen must be thermally isolated material, thus, temperature inside has reliable value; the box has to be long enough so that sample can be put down and indeed cooled down to 77 K. We needed to get fast temperature response from cooling system. There are many standard methods in thermal effects measurements. For example, there are following thermocouple types: chromel-alumel, chromel-constantan, iron-constantan, platinum-rhodium, etc. Each is better in different practices. However, during this experiment we used thermocouple Cu-Constantan since its easy and cheap method in arrangement.

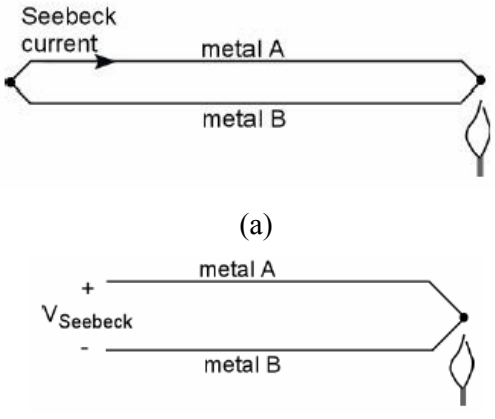

Figure 9.4 (a) Thermocouple (b) Presence of Seebeck voltage in opened circuit [66].

Thermocouple is universal device for obtaining temperature response from observed object. It was discovered by Thomas Seebeck in 1821. Temperature difference between the ends of connected dissimilar metals produces current through this circuit. If the circuit is opened voltage appears at the ends, so called Seebeck voltage, which is function of two metalic materials and temperature at junction. This temperature sensor is very simple in use [66].

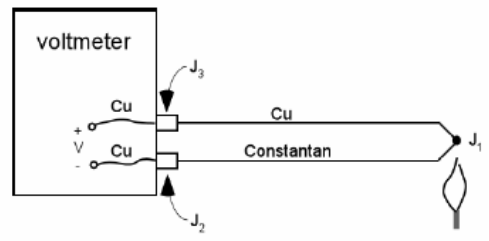

Figure 9.5 Measuring the voltage [66].

It is enough to know type of junction (Cu-Co) and voltage at junction (*V1*) to define temperature at *J1*. Thermocouple measures a temperature difference, thus there is needed a reference temperature. This is described on fig.9.6 where we use ice temperature as reference one.

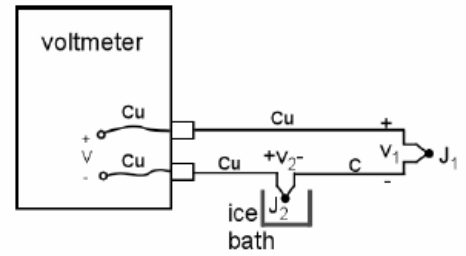

Figure 9.6 Use of ice bath [66].

To define unknown parameters, for instance *J2* temperature can be used ice bath or other reference temperature (liquied nitrogen or room). Thermocouple is applied in many experiments because of certain reasons such:

1) Wide temperature range;
2) Ruggedness (can be easily welded to a metal or clamped to a screw). It worth to mention problems connected with use of thermocouples:

1) Connection. Unappropriate connection may lead to appearance of unexpected junctions; junction is caused by any junction of two different metals, it is especially important if we need long wires;
2) Lead resistance. Thin wire is a way to reduce resistance, minimize thermal loading and increase response times; in our experiment used thermocouple 0.25 mm dimeter with a resistance of approximetely 15 Ω/m;
3) Decalibration. Altering of thermocouple wires is generally cased by influence of athmospheric particles on wires as well as by diffused impurities and chemicals from insulation;
4) Noise. Output of thermocouple is affected by electric noise, however, in our experiment there is not so extreme environment [66].

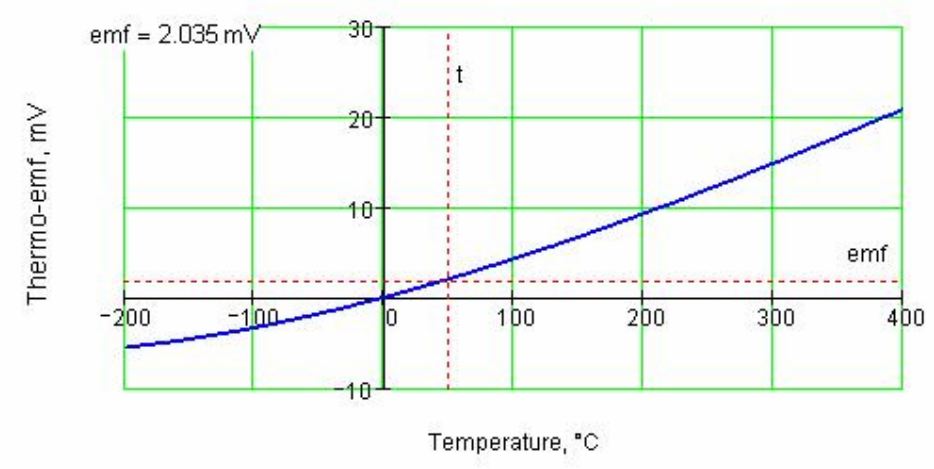

Figure 9.7 Typical curve for Cu-Co thermocouple (50˚C gives 2.035 mV).

Picture above represents standard calibration curve for Cu-Co thermocouple. We tested the calibration curve by measuring three points 0˚C, 20˚C and -196˚C (77 K), meaning ice, room and liquid nitrogen temperatures. Temperature could be obtained by usual resistive detector. We also tried to adapt this method. However, this temperature transducer reacts with a certain delay that makes experiment unconvinient. Moreover, it is not easy to find one with required temperature range. Our aim was to estimate approximately electrocaloric effect in samples; therefore, it is useful to apply thermocouple. One additional problem in connection with thermal effect measurements that we have met is how to make thermally isolated contact to the sample in order to obtain reliable temperature results. This problem can not be completely solved by use of thermocouple.

After desirable data were collected followed simulations by Comsol Multiphysics. This computational analysis gives possibility to estimate how large effect would be in cooling line consisting from one and electrocaloric capacitor. During simulation preceding the following coefficents were used for approximation (see tables 9.3 and 9.4). Approximation functions are $\varepsilon = C_k / \sqrt{A(T-T_c)/2+B} - C$ and

$$d\varepsilon = -C_k \cdot \frac{A}{2} \cdot \frac{T-T_c}{3A \cdot \frac{T-T_c}{2+B}}$$

Table 9.3 Coefficients of approximation function for bulk ceramic capacitors.

Capacitor	C6	C12
Temperature range ΔT, K	70..340	70..340
Ck	$5.292 \cdot 10^4$	$6.3 \cdot 10^4$
Tc, K	195.8	197
A	0.75	0.75
B	220	300
C	150	320

Table 9.4 Coefficients of approximation function for thin film capacitors.

Capacitor	268				KR7			
	0V	5V	20V	40V	0V	5V	20V	40V
Temperature range ΔT, K	70..360	70..360	70..360	70..360	70..360	70..360	70..360	70..360
Ck	$5.292 \cdot 10^4$	$5.24 \cdot 10^4$	$4.7 \cdot 10^4$	$4.45 \cdot 10^4$	$5 \cdot 10^4$	$4.75 \cdot 10^4$	$4.25 \cdot 10^4$	$3.3 \cdot 10^4$
Tc, K	183	183	183	183	250	250	250	250
A	0.13	0.128	0.11	0.1	0.3	0.32	0.32	0.23
B	220	220	220	220	220	220	220	220
C	960	960	960	960	1500	1500	1500	1500

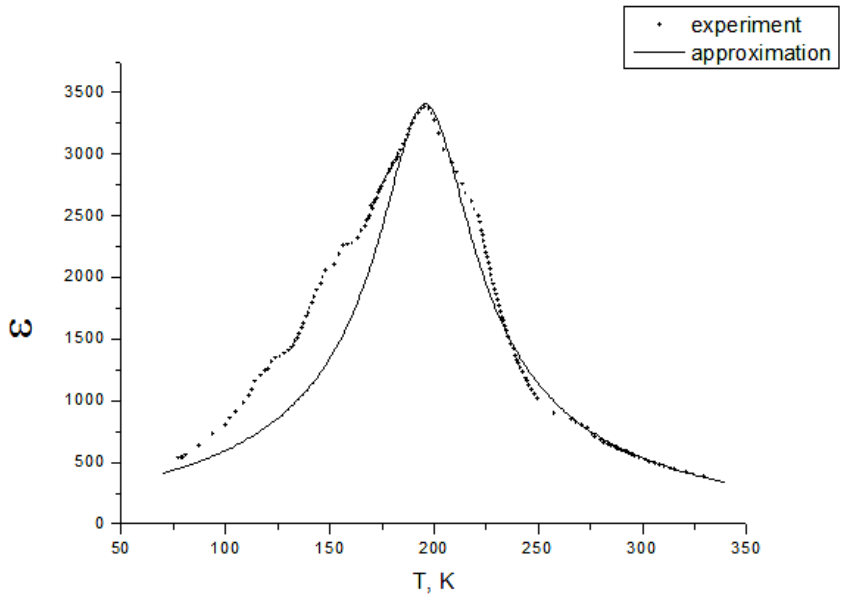

Figure 9.8 Temperature dependence of permittivity for ceramic capacitor C6.

Fig.9.8 shows temperature dependence of permittivity for bulk ceramic capacitor C6. Phase transition occures at about 184 K. Expermentally obtained data were appoximated and after that temperature dependence of permittivity derivative was obtained (see fig.9.9).

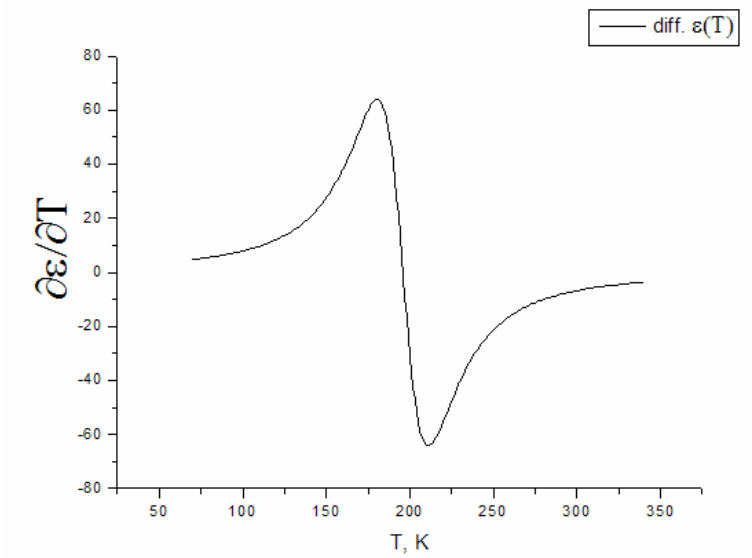

Figure 9.9 Temperature dependence of permittivity derivative for ceramic capacitor C6.

The same mesurements were carried out for second type of bulk ceramic capacitors C12 (see fig.9.10 and fig.9.11). Here should be mentioned that dielectric permittivity didn't

show strong field dependence in ceramic samples because applied fields are not enough for that purpose.

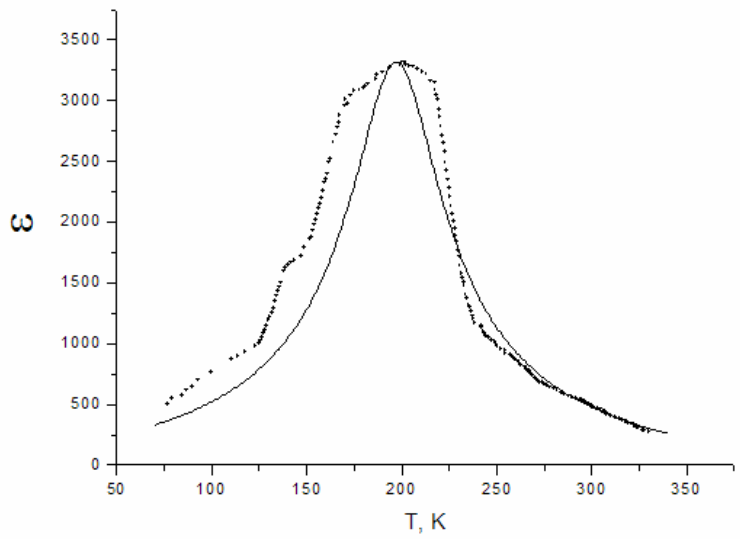

Figure 9.10 Temperature dependence of permittivity for ceramic capacitor C12.

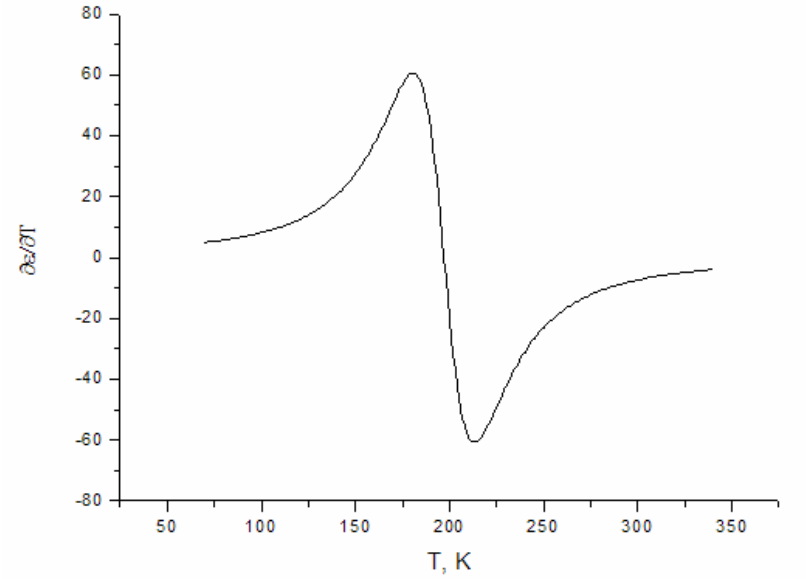

Figure 9.11 Temperature dependence of permittivity derivative for ceramic capacitor C12.

In thin film samples there is stronger field dependence in comparison to bulk capacitors. This is shown on fig.9.12 and fig.9.13.

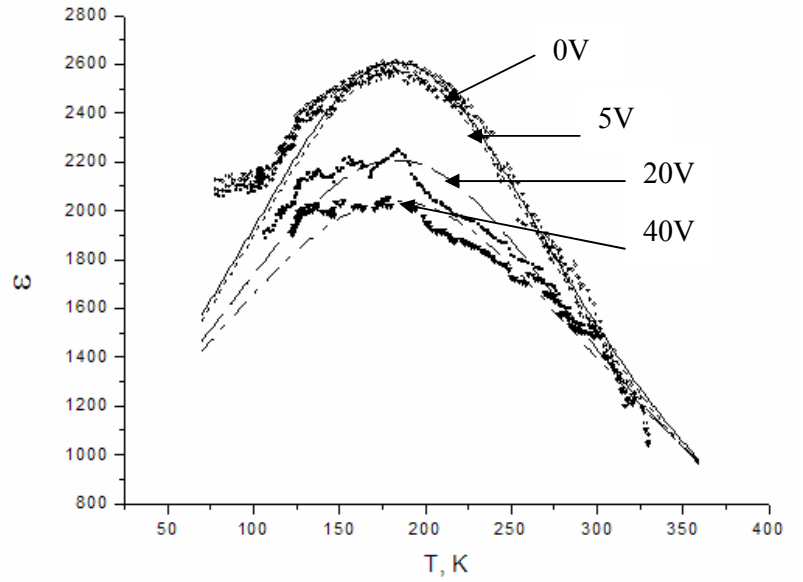

Figure 9.12 Temperature dependence of permittivity for film capacitor C268 under selected values of field $U = 0, 5, 20, 40$ V.

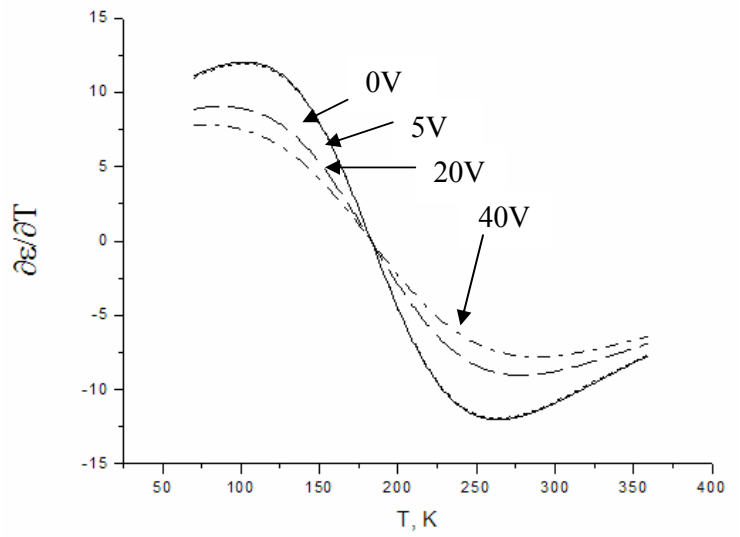

Figure 9.13 Temperature dependence of permittivity derivative for film capacitor C268 under selected values of field $U = 0, 5, 20, 40$ V.

By application of higher electric fields dependence goes down and maximum becomes smoother. This is presented on fig.9.14 and fig.9.15. Experimental results for second type of thin film capacitors are provided below.

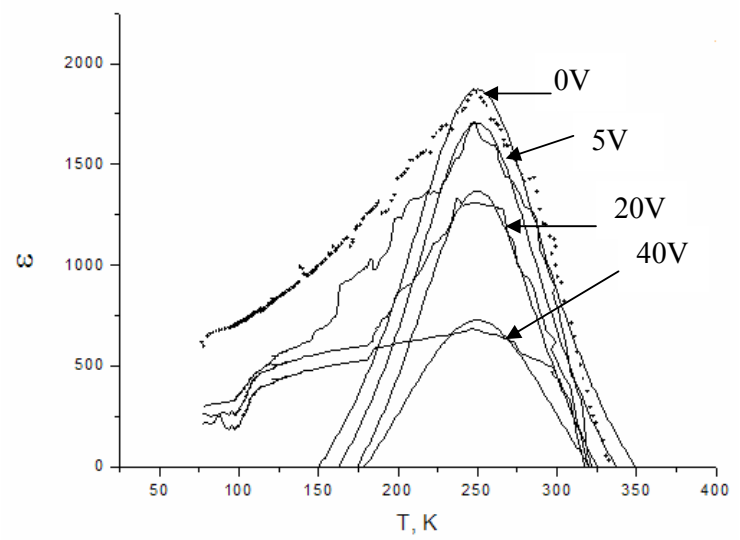

Figure 9.14 Temperature dependence of permittivity for film capacitor KR7 under selected values of field $U = 0, 5, 20, 40$ V.

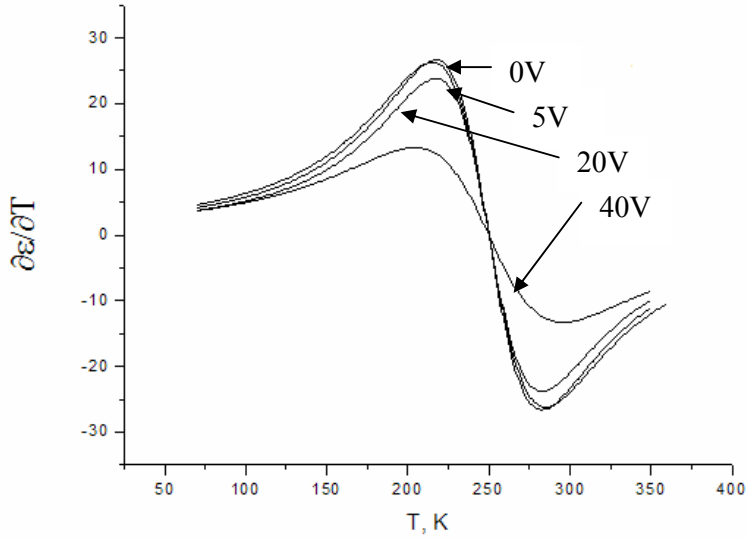

Figure 9.15 Temperature dependence of permittivity derivative for film capacitor KR7 under selected values of field $U = 0, 5, 20, 40$ V.

After simulation according to one electrocaloric element model can be obtained:

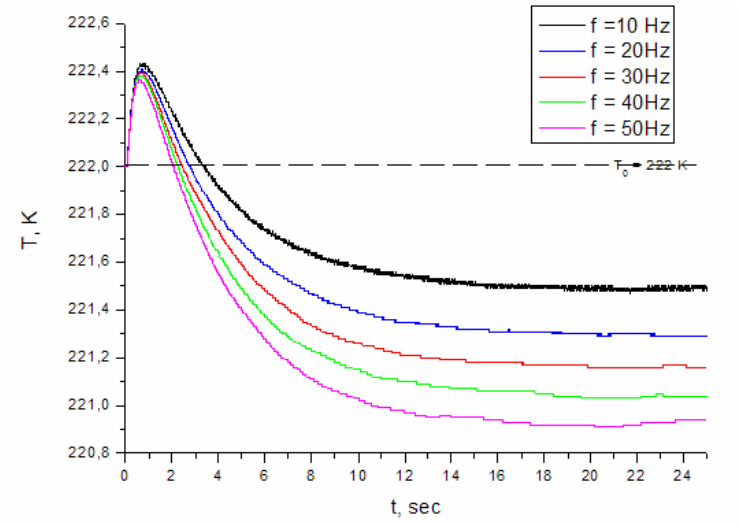

Figure 9.16 Electrocaloric temperature change in C6 capacitor for one EC element model under selected values of frequency f = 10, 20, 30, 40, 50 Hz.

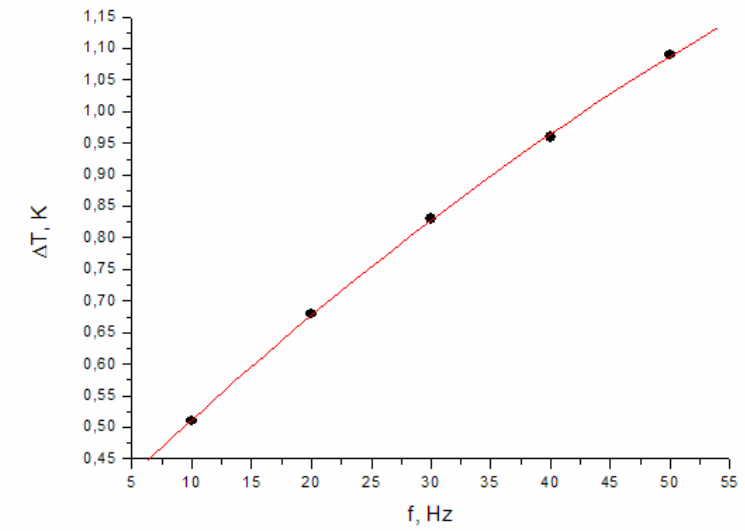

Figure 9.17 Frequency dependence of electrocaloric temperature change in C6 for one EC element model.

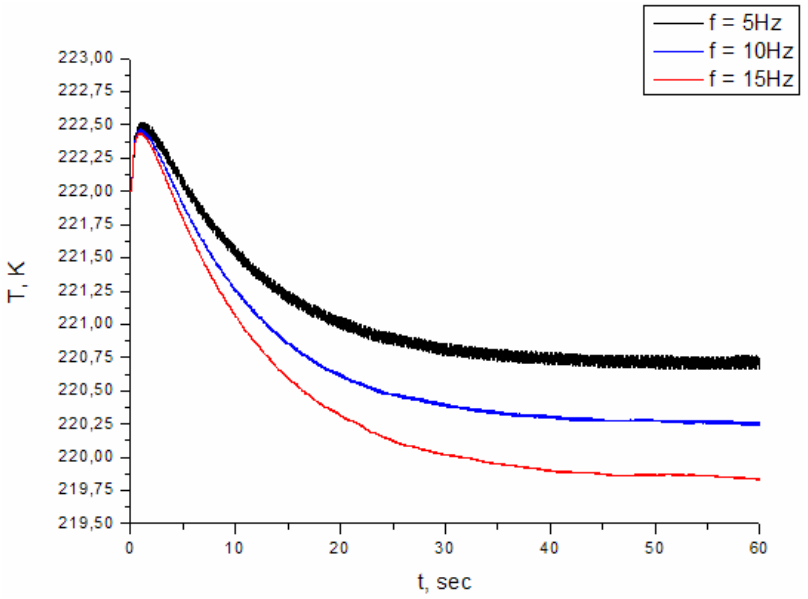

Figure 9.18 Electrocaloric temperature change in C6 capacitor for two EC elements model under selected values of frequency f = 5, 10, 15 Hz.

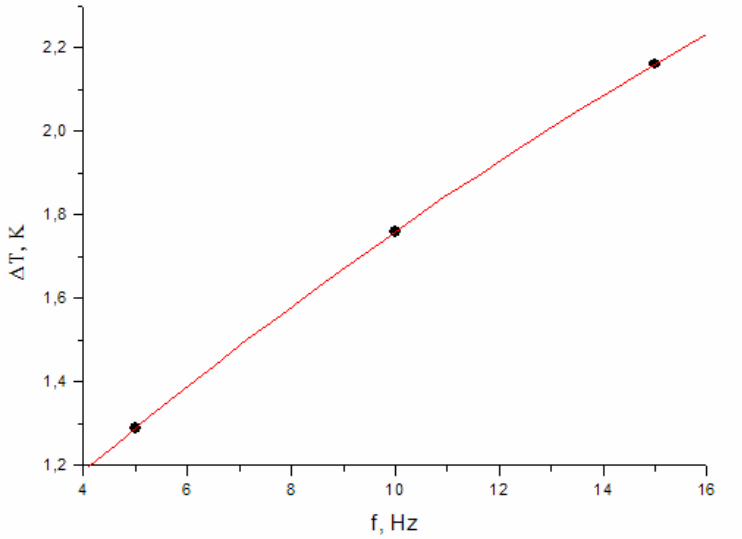

Figure 9.19 Frequency dependence of electrocaloric temperature change in C6 for two EC elements model.

Above presented dependence shows how effectively operates cooling device at a certain frequency.

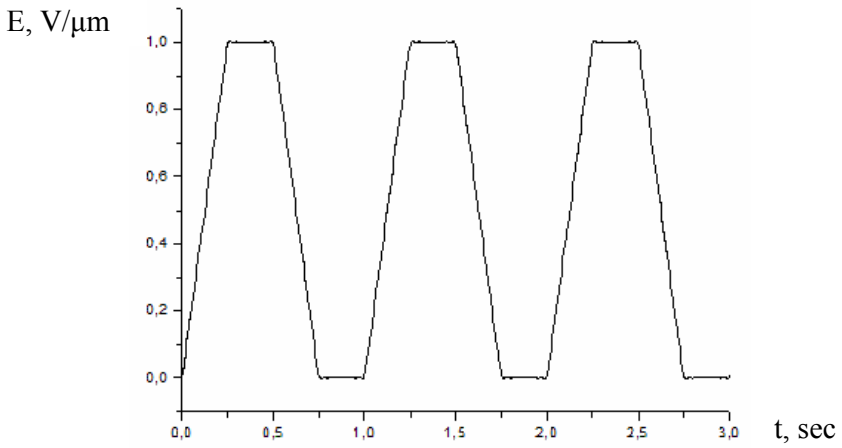

Figure 9.20 Electric field pulses applied to capacitor structure.

Obtained cooling is obviously not large, but in fact increase of frequency, proper choice of material and effective thermodynamic cycle realization can improve it. Moreover, temperature change is calculated in bulk samples where thermal effects are not expected to be large. Fot thin films there are certain difficulties with modeling, for instance, how to avoid capacitance of substrate and how to eliminate cross impact of electric field vs permittivity. But it is believed that in thin film cooling efficiency would be much higher.

Since planar tehnology is expected to be widely applied to production of film capacitors, new methods of temperature control in material should be found. Thickness of films is around 0.1 - 1 μm. Thus, temperature changes obtained due to the electrocaloric effect can not be detected by means of common contact methods of temperature control. All existed methods are technologically complicated and unpractical. Therefore, Pt bridge method is proposed. Its resistance changes with temperature as in case of usual resistive detector. Before ferroelectric film sputtering must be sputtered a Pt meander with thickness 20 - 80nm. Total resistance of this structure is about several kΩ. Calibration of bridge is preceded by four-probe method measurements. After that thin film of ferroelectric material, i.e. electrocaloric capacitor, for instance BSTO is evaporated. Temperature of dielectric is changed due to electrocaloric effect under applied field to capacitor plates. It can be detected by Pt bridge since it reacts on temperature change in capacitor and changes its resistance.

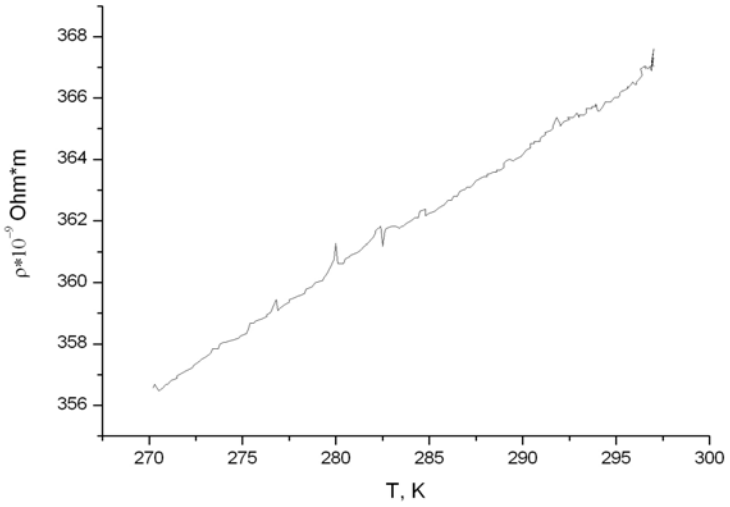

Figure 9.21 Pt film resistance vs remparature with linear parameters: width = 200 μm, length = 430 μm, thickness = 40 nm).

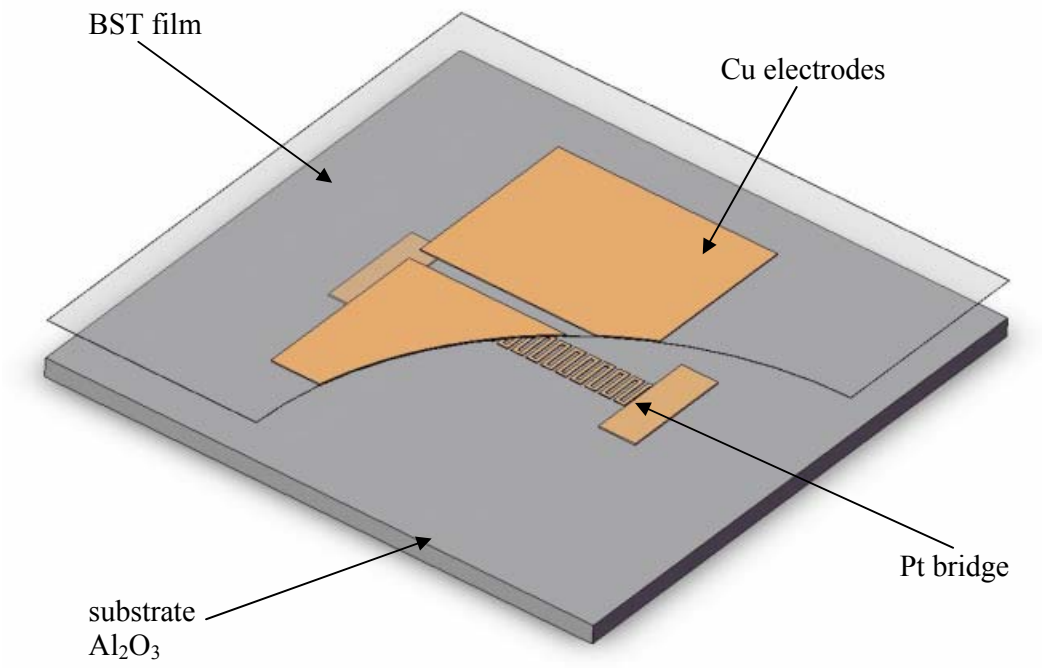

(b)

Figure 9.22 Pt bridge assembling.

9.2 Overview on existed methodics of EC effect measurements

Nowdays measurements of electrocaloric effect are all about electric polarization. In the future we also assume to measure polarization vs electric field from which can be obtained electricaloric temperature change vs electric field. Difficulties to provide these experiments are connected with lack of equipment. For instance, there is needed electric pulse generator with special, complicated pulses form.

Polarization measurement itself is widely investigated process. Let us examine one classic example of the Sawyer-Tower circuit. Let us define polarization:

$$P = Q/A, \tag{9.1}$$

where P is polarization, Q is charge induced on capacitor plates and A is area of the plates. Polarization values for good ferroelectric vary 10 μC cm^{-2} < P < 100 μC cm^{-2} . The classical Sawyer-Tower circuit for polarization measurements is presented on fig.9.2.1.

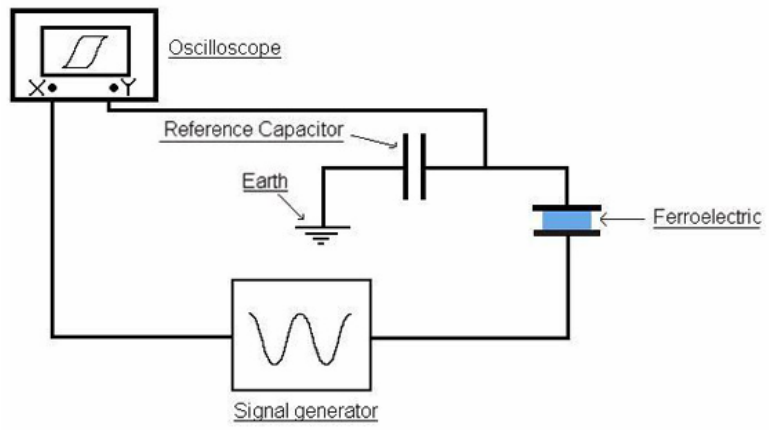

Figure 9.23 The Sawyer-Tower circuit [67].

There are ferroelectric and reference capacitors in series over which charge must be the same. Signal generator produces voltage signal. We measure voltage across the reference capacitor. The charge on ferroelectric is considered to be:

$$Q=C\cdot V, \tag{9.2}$$

where C is capacitance of reference capacitor, Q is charge and V is voltage that measured over reference capacitor. Then polarization of material is presented in an oscillating electric field. Applied voltage and charge on surface are plotted on x and y axes of oscilloscope respectively. Most voltage is found over ferroelectric due to rather big difference between capacitances of reference and ferroelectric capacitors. Thus, methos is

based on mearing polarization by cycling the voltage across ferroelectric structure. It is impossible to measure absolute values at instant moment. Therefore, we obtain it by measuring changes in ferroelectric parameters during cycling of polarization. [67] Modern methods of thermal effects detection are presented in literature. For instance, group of chienese scientists offered following sheme (see fig. 9.24). The samples are inside an airproof cover. It is needed to eliminate thermal contact of base and sample, therefore, heat insulation is used. SCIT noncontract IR detector indicates temperature change on the sample. DZ2672A current test apparatus supplies the direct electric current. Joule heat is completely avoided in this system because resistance of the sample is about TΩ and, thus, Joul heat is less than sensitivity of device. Other Chinese group [68] of researchers adopted another system for electrocaloric measurements (fig. 9.25). Investigated samples and clamp are in silicon oil. A voltage adjuster is used for adjusting appropriate temperature. Two platinum wire thermometers are used to measure temperature change of the sample by applied DC electric field. It is dislayed digitally.

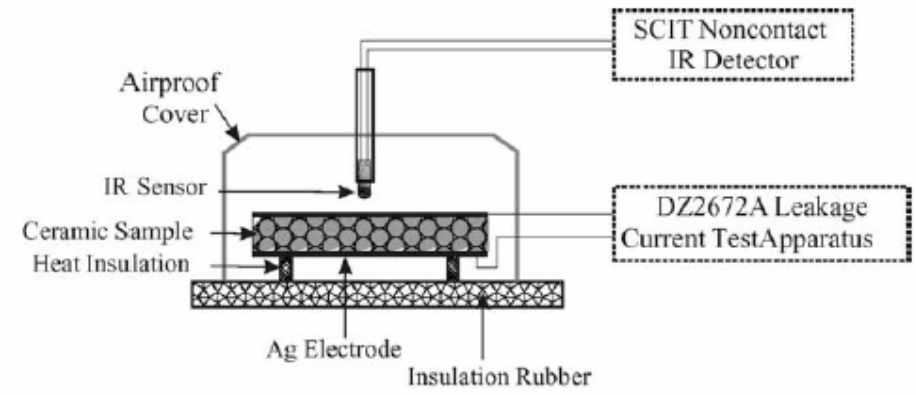

Figure 9.24 The sketch map of the EC effect measurement device [17].

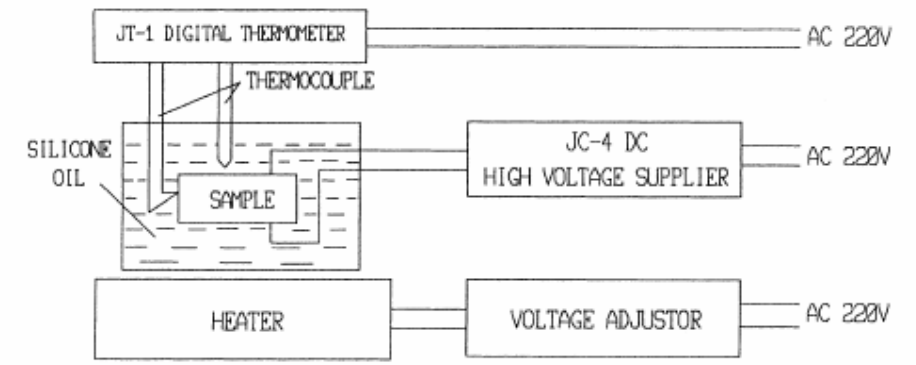

Figure 9.25 The measurement set up for electrocaloric effect [68].

One of the examples of successful applications of the electrocaloric effect is a radial planar cooler presented on fig. 9.26. On the sapphire substrate from both sides sputtered thin film of BSTO or other ferroelectric material. Electrodes are made in a form of interdigital transducer. There are two rings of interdigital transducer presented; however, design with higher amount of electrodes rings is also possible. Radiator provides effective heat rejection; hence a center of the structure or chip placed there is cooled. Heat flow in cooler is shown also. It is clear from that how temperature distributed in cross-section area.

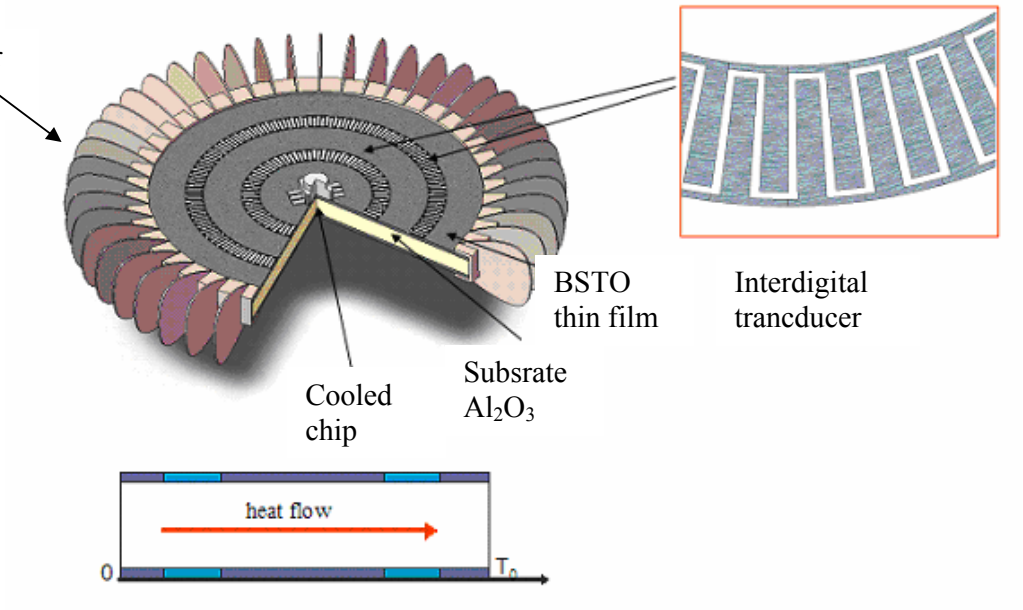

Figure 9.26 Prototype of planar radial cooler [6].

10 CONCLUSIONS

Based on analytical, computational and experimental results, it has been schown that directed heat flux induced by periodic electric field in electrocaloric capacitor results in cooling. Analysis has shown that temperature difference between two ends of cooling line can even reach 20 K in equilibrium regime.

Experiments were carried out on the BSTO ceramic and thin film capacitors. Each type of capacitor has indicated temperature change of several degrees. However, electrocaloric effect is greater in thin film capacitors that can be applied futher for construction of electrocaloric cooling line. Experimental results are in agreement with theory of effect and allow us to consider that obtained temperature change is sufficient for designing of effective and low-cost electrocaloric cooler.

Electrocaloric cooling is exremely effective method that causes no damage to environment. It is energetically advantagable as well. Realization doesn't require high costs. Those are not even the full list of profits. Example of cooler shown above proves that this method is not our imagination. We are faced with the fact that cryogenics is ready to adopt completely new technology. Reality is not what we used to think, i.e. all usual refrigerating technologies became outdated. This is a real chance for researchers to bring their knowledge for the common good. Present research is one step on a way to successful application of modern cryogenic technologies in our life.

REFERENCES

[1] http://en.wikipedia.org/wiki/Electrocaloric_effect

Wikipedia: Electrocaloric effect

[2] A. Mischenko, Q. Zhang, J.F. Scott, "Giant electrocaloric effect in thin film $PbZr_{0.95}Ti_{0.05}O_3$" (2005).

[3] A.Eskow, S.Karmanenko, "Investigation and calculation of heat transformers and cooling elements based on electrocaloric materials" (rus.), Izvestia vuzov (2006).

[4] J.F.Scott , "Application of modern ferroelectrics" (2005).

[5] Yu. V. Sinyavskii, "Electrocaloric refregerators: a promising alternative to current-low temperature apparatus" , J. Chemical and Petroleum Engineering, Vol. 31, Nos. 5-6(1995).

[6] A.Eskow Master Thesis "Investigation and calculation of heat transformers and cooling elements based on electrocaloric materials" (2006), Saint-Petersburg State Electrotechnical University "LETI", unpubl.

[7] http://en.wikipedia.org/wiki/Haloalkane

[8] Inventions & Innovation. Project fact sheet. "Electrocaloric materials for room temperature investigations", http://www.eere.energy.gov/inventions/pdfs/ceramphys.pdf

[9] http://www.xbitlabs.com/web/display/20050509032835.html

[10] http://www.learner.org/exhibits/dailymath/population.html

[11] G.G.Weiman, J.K. Kuebler, "Electrocaloric effect in ferroelectric Rochelle"
J.Physical Review, vol.131, №5 (1963).

[12] H.Mueller, "Properties of Rochelle Salt", J.Physical Review, vol.58 (1940).

[13] I.Shepherd, G.Feher, "Cooling by the adiabatic depolarization of OH^- molecules in KCl", J.Physical Review, vol.15, №5 (1965).

[14] R.O.Pohl, V.L.Taylor "Electrocaloric effect in dopped alkali halides",
J.Physical Review, vol.178, №3 (1968).

[15] W.N. Lawless, "Specific heat and electrocaloric properties of $KTaO_3$ at low temperatures",J.Physical Review, vol.16, №1 (1976).

[16] D.A.Payne, B.A.Tuttle, R.B.Olsen, W.F.Butler, "Observation of a polecoloric(electrocaloric effect) of 2˚C in lead zirconate modified with Sn^{+4} and Ti^{+4}", J.Physical Review, vol.45, №17 (1980).

[17] L.Shaobo, L.Yanqiu, "Research on the electrocaloric effect of PMN/PT solid solution for ferroelectrics MEMS microcooler",J. Materials Science and Engineering B 113 (2004) 46–49.

[18] http://www.memsnet.org/mems/what-is.html

[19]D.Guyomar, G.Sebald, B.Guiffard, L.Seveyrat, "Ferroelectric electrocaloric conversion in 0.75(PbMg1/3Nb2/3O3)–0.25(PbTiO3) ceramics", J. Phys. D: Appl. Phys. 39 (2006) 4491–4496.

[20] H.D. Young, R.A. Freedman, "University Physics" (2000).

[21] http://en.wikipedia.org/wiki/Laws_of_thermodynamics

[22] http://en.wikipedia.org/wiki/Carnot_heat_engine

[23] Master Thesis "Investigation of heat transformers and cooling elements based on electrocaloric materials" (2005), Saint-Petersburg State Electrotechnical University "LETI", unpubl.

[24] http://hyperphysics.phy-astr.gsu.edu/hbase/thermo/carnot.html

[25] B.M. Yavorskiy, A.A. Detlaf "Physics hand-book" 7th edition, "NAUKA" (1979)

[26] http://www.infrost.ru/

[27] http://en.wikipedia.org/wiki/Sorption

[28] http://en.wikipedia.org/wiki/Stirling_cycle

[29] http://en.wikipedia.org/wiki/Peltier-Seebeck_effect

[30] http://en.wikipedia.org/wiki/Magnetocaloric_effect

[31] A. Schuka, "Electronics", "Visshaya shkola " (2004)

[32] http://www.msm.cam.ac.uk/doitpoms/tlplib/ferroelectrics/dipole.php

[33] A.Safari, R.K.Panda ,V.F.Janas, "Ferroelectric Ceramics : Processing, Properties & Applications"

[34] J.F. Scott, "Physics of ferroelectrics", PBLittlewood (2002)

[35] http://www.msm.cam.ac.uk/doitpoms/tlplib/ferroelectrics/fabrication.php

[36] http://www.msm.cam.ac.uk/doitpoms/tlplib/ferroelectrics/switching2.php

[37] http://www.msm.cam.ac.uk/doitpoms/tlplib/ferroelectrics/switching1.php

[38]http://www.msm.cam.ac.uk/doitpoms/tlplib/ferroelectrics/temp_dependence.php

[39] http://www.msm.cam.ac.uk/doitpoms/tlplib/ferroelectrics/transitions.php

[40] Y.B.Tagantsev, "Ferroelectric materials for microwave applications" (2002)

[41] http://www.msm.cam.ac.uk/doitpoms/tlplib/ferroelectrics/polarisation.php

[42] J.Cowley, Phys.Rew.Lett. 9 159 (1962)

[43] A.Stirling, J.Phys. C5, 2711 (1972)

[44] http://www.msm.cam.ac.uk/doitpoms/tlplib/ferroelectrics/barium_titanate.php

[45] A.Bogdanov, "Physics of ferroelctrics" (1978)

[46] http://www.msm.cam.ac.uk/doitpoms/tlplib/ferroelectrics/phase_changes.php

[47] H. Kneipkamp, and W. Heywang, Z. Angew. Phys., 6, 385 (1954)

[48] D. Hennings, and G. Rosenstein, J. Am. Ceram. Soc., 67, 249 (1984)

[49] A. J. Bell, Proc. 1994 Int. Symp. Appl. Ferroelectrics, (1994)

[50] T. Yamamoto, M.Saho, K. Okazaki, and E. Goo, Jap. J. Appl. Phys., 26-2, 57 (1987)

[51] K. M. Rittenmyer, and R. Y. Ting, Ferroelectrics, 110, 171 (1990)

[52] K. Takeuchi, D. Damjanovic, T. R. Guraraja, S. L. Jang, and L. E. Cross, Proc. 1986 IEEE Symp. Appl. Ferroelectrics, 402 (1986)

[53] Y. Yamashita, K. Yokoyama, H. Honda, and T. Takahashi, Jap. J. Appl. Phys., 20-4, 183 (1981)

[54] G. H. Haertling, Ferroelectrics, 75, 25 (1987)

[55] L. E. Cross, Ferroelectric Ceramics-Tutorial Reviews, Theory, Processing and Applications, N. Setter, and E. L. Colla, ed., 1 (Birkhauser Verlag, Basel, 1993)

[56] Borisovski, K. E. and Prudan, A. M., Electrocaloric coefficients of strontium titanate at cryogenic temperatures. Solid State Phys., (1989), 31, 53–56.

[57] K.E.Borisovskiy, A.I.Dedyk, A.M.Prudan "Dimensional effect of electrocaloric cooling in BSTO samples"(rus.). Solid state physics.34, № 6. (1992)

[58] Vendik, O. G., ed., Ferroelectric at Microwaves. Soviet Radio, Moscow (1979)

[59] V.Ginzburg, "Theory of ferroelectric phenomenon" (1949)

[60] A.Starkov “Electrocaloric element in periodic electric field”, unpubl. (2006)

[61] http://en.wikipedia.org/wiki/Finite_element_analysis

[62] V.Egorov , “PC application for heat transfer problems” (2004)

[63] A.Eskow, S.Karmanenko, “Investigation and calculation of heat transformers and cooling elements based on electrocaloric materials” (rus.), Izvestia vuzov (2005).

[64] S. Karmanenko “Layered ceramic structure based on the electrocaloric elements working as a solid state cooling line”, Journal of European Ceramic society (2007)

[65] http://www.angstromsciences.com/technology/sputtering-technology/index.html

[66] RS datasheet “Thermocouples” (2001)

[67] http://www.msm.cam.ac.uk/doitpoms/tlplib/ferroelectrics/measuring_pol.php

[68] D.Q.Xiao, Y.C.Wang, R.L.Zhang “Electrocaloric properties of (1- x)Pb($Mg_{1/3}Nb_{2/3}$)O_3±xPbTiO3 ferroelectric ceramics near room temperature” , Materials Science Comunication (1998).